Identifying Functionally Distinct Neuronal Ensembles within the Memory Engram

By

Xiaochen Sun

B.S., Biological Sciences, Tsinghua University, 2014

Submitted to the Department of Brain and Cognitive Sciences
in Partial Fulfillment of the Requirements for the Degree of

DOCTOR OF PHILOSOPHY IN NEUROSCIENCE

at the

MASSACHUSETTS INSTITUTE OF TECHNOLOGY

May 2020

Signature of Author .....
Department of Brain and Cognitive Sciences
March 30, 2020

Certified by .....
Guoping Feng
Poitras Chair Professor of Neuroscience
Thesis Supervisor

Accepted by.....
Rebecca Saxe
John W. Jarve (1978) Professor of Brain and Cognitive Sciences
Associate Head, Department of Brain and Cognitive Sciences

Identifying Functionally Distinct Neuronal Ensembles within the Memory Engram

By

Xiaochen Sun

Submitted to the Department of Brain and Cognitive Sciences
on March 30, 2020 in Partial Fulfillment of the Requirements for the Degree of
Doctor of Philosophy in Neuroscience

Abstract

Memories in the brain are encoded by sparse ensembles of neurons within the memory engram. However, it remains unclear whether these neurons are functionally identical or can be divided into distinct subpopulations that encode distinct aspects of the memory and differently drive memory outputs. In this study, we found that contextual fear memory engrams in the mouse dentate gyrus (DG) contained functionally distinct neuronal ensembles, genetically defined by the *Fos*- or *Npas4*-dependent transcriptional pathways. The *Fos*-dependent ensemble promotes memory generalization and receives enhanced excitatory synaptic inputs from the medial entorhinal cortex. The *Npas4*-dependent ensemble mediates memory discrimination and receives enhanced inhibitory synaptic drive from local cholecystokinin-expressing interneurons. Moreover, acute deletion of *Npas4* disrupted inhibitory synaptic transmission and memory discrimination, suggesting that activity-dependent genes like *Npas4* and *Fos* play causal roles in the formation of memory engrams. Taken together, our findings support a working model in which neuronal ensembles within engrams undergo distinct learning-induced synaptic modifications and drive memory-guided behaviors differentially.

Table of Contents

Dedication

This thesis is dedicated to
my parents, Hanxu Sun and Ping Sun,
and my wife, Jianfei Guo.

Acknowledgements

My time at graduate school is a journey full of exciting moments and unforgettable lessons. However, it's only possible because of the people I share the journey with.

Thank you to my Ph.D. advisor, Dr. Yingxi Lin, for your unconditioned support and constant caring over the years. From you, I learned how to do rigorous science and how to become a good person. The journey that we went through together will definitely become part of my deepest memory.

Thank you to my thesis committee members, Dr. Mark Bear, Dr. Guoping Feng, and Dr. Leon Reijmers. The critics I received from my committee have become the most valuable lessons in my scientific career. It's from you that I learned how to form grounded hypotheses, how to approach a question progressively, and how to stay strong and humble in science.

Thank you to the entire Lin Laboratory, which has always been a warm family to me. I'd like to especially thank Max and Meizhen for working with me on my thesis project, thank Andreas and Eddie for being my mentors when I started in the lab, and thank Alex and Yuxiang for your accompany through the ups and downs.

Special thanks to Dheeraj Roy, who has been, and will always be, my scientific mentor.

Special thanks to Eugene Lee, for all the important moments we shared together during graduate school.

I owe everything I have achieved in my life to my parents, Hanxu Sun and Ping Sun. I'm extremely lucky to have you as my parents, and also as my friends.

Lastly, I'd like to thank my wife and my best friend, Jianfei Guo. The journey of life is short. However, being with you makes it nothing but wonderful.

Chapter 1

Introduction

Chapter 1 - Introduction

1.1. Understanding the Engram: Marr's Three Levels of Analysis

Memory refers to the ability to retain information of past experience (Eysenck, 2012; Gluck et al., 2016; Sherwood, 2015; Squire, 2009b). It is essential for all organisms to survive, because future actions are strongly influenced by memories for the past (Dudai, 2004; Kandel et al., 2014; Nairne and Pandeirada, 2016; Staddon, 2016; Thompson, 1986). The capacity to learn and memorize is also the basis for human intelligence, as it is indispensable for high-level cognitive functions such as language, decision making, and self-conscienceless (Eysenck, 2012; Griggs, 2010; Johnson and Hasher, 1987; Tulving, 1985). Therefore, studying the neurobiology of memory is key to our understanding of the brain. It is also critical for the development of potential therapeutic treatments for memory disorders such as amnesia (Cole et al., 2016; Ostergaard, 1987; Squire and Zola, 1998) and Alzheimer Diseases (Burns and Iliffe, 2009; Morris and Kopelman, 1986; Souchay and Moulin, 2009). Besides, recent years witnessed a growing interest in neuroscience-inspired artificial intelligence (Bell, 1999; Cox and Dean, 2014; Hassabis et al., 2017). Understanding how the biological memory system learns would shed light on the development of advanced machine learning algorithms (Kumaran et al., 2016; Marblestone et al., 2016; Richards et al., 2019).

In order to understand the memory system, an essential question needs to be asked first: *where and how are memories stored in the brain*? Identifying the neural substrate of memories, the so-called *memory engram* (Semon, 1921), is therefore the very first step to understand memory processing in the brain. It's believed that memories are stored as biophysical or biochemical changes elicited by learning (Josselyn and Tonegawa, 2020; Semon, 1921), and decades of research have been trying to locate engrams in the brain. Early studies in rodents found that ablating different parts of the brain all resulted in disrupted spatial memories,

suggesting that engrams were distributed in a large-scale brain network (Bruce, 2001; Lashley, 1950b). Later studies further pinpointed key brain regions, such as the hippocampus, that are involved in the storage of long-term episodic memories (Milner, 1972; Scoville and Milner, 1957; Squire, 2009a). It was found that patients with hippocampal lesion were able to acquire motor skills, but failed to form new episodic memories (Penfield and Milner, 1958). To understand how memories are stored in individual neurons, Donald Hebb proposed the influential idea that memories are formed through the synaptic potentiation among ensembles of neurons that fire together during learning (Hebb, 1949). In support of this idea, learning-induced synaptic plasticity has been found essential for forming long-term memories (Andersen et al., 2017; Bear and Abraham, 1996; Bliss and Lømo, 1973; Martin et al., 2000). Recent studies further identified the sparse populations of neurons within the engram (Han et al., 2007; Josselyn and Tonegawa, 2020; Mayford, 2014; Reijmers et al., 2007). These neurons are shown to be activated by the learning experience (Deng et al., 2013; Guenthner et al., 2013b; Reijmers et al., 2007), undergo long-lasting synaptic modifications (Choi et al., 2018; Ryan et al., 2015), and mediate the expression of encoded memories (Cai et al., 2016; Han et al., 2009; Liu et al., 2012; Yokose et al., 2017). Taken together, it's generally believed now that an engram comprises sparse populations of neurons across the memory-related circuits, and these engram neurons encode individual episodes of memories (Josselyn and Tonegawa, 2020; Tonegawa et al., 2015a).

Although significant progress has been made to localize the engram into specific neuronal populations, many aspects of the engram remain enigmatic (Denny et al., 2017; Josselyn and Tonegawa, 2020). How is an engram formed? Why certain neurons, but not others, are recruited into the engram? How does an engram guide our future behaviors? Substantial works are needed to further understand the neural substrates of memories. David Marr argued that a complex system, such as the brain or a computer, should be understood at three levels: *computational theories*, *representation and algorithm*, and *hardware implementation* (Marr, 1982). Here we suggest that memory engrams should also be analyzed according to Marr's

tripartite view. The memory engram may be better understood by studying it at the computational, representation/algorithm, and implementation levels.

1) At the first level, the *computational goals* of engrams need to be understood. Why do we need a memory system? What does an engram do? From an evolution perspective, the primary goal of an engram is to store past information for the purpose of guiding future actions (Johnson and Hasher, 1987; Pavlov, 1926; Robinson et al., 2013; Rubin et al., 2014). Importantly, in real-life situations, the same memories often need to drive various kinds of memory-guided actions based on the particular situation (Ghirlanda and Enquist, 2003; Staddon, 2016). Therefore, it's critical to understand how an engram supports different forms of adaptive behaviors (Nairne and Pandeirada, 2016; Pavlov, 1926).

2) At the *representation/algorithm* level, how does the engram accomplish its functions, for example, driving adaptive behaviors? Questions at this level are often difficult to address due to the complexity of the engram (Josselyn et al., 2015; Lashley, 1950a; Thompson, 2005). Episodic memories involve various forms of information including time, space, events, knowledge, and relationships, which are all represented together in a single engram (Eichenbaum, 2004; Josselyn et al., 2015; Lashley, 1950b; Vetere et al., 2017). It's therefore necessary, from a reductionist point of view, to dissect the engram into individual functional components (Mallory and Giocomo, 2018; Tanaka and McHugh, 2018b). An exciting direction of the field is to understand how individual neurons within the engram encode information and drive memory outputs.

3) Lastly, What are the biological *implementations* that are needed to form an engram? What are the cellular and synaptic processes that store long-lasting memories? There have been two learning-related processes that are mostly studied: synaptic plasticity and activity-dependent gene expression. Synaptic plasticity has been suggested to be the primary mechanism underlying memory formation (Bliss and Lømo, 1973; Nakazawa et al., 2004; Whitlock et al., 2006), but the specific synaptic modifications onto the memory engram remain largely unclear. Besides,

forming long-term memories requires *de novo* activity-dependent gene expression (Alberini and Kandel, 2015; Bear et al., 2007; Schafe and LeDoux, 2000). However, the molecular processes underlying the emergence of engram neurons are yet to be understood. Questions at this level are particularly important from a translational perspective, as identifying the molecular and synaptic mechanisms of memory may lead to the discoveries of new therapeutic targets for memory-related disorders (Iaccarino et al., 2016; Roy et al., 2016; Ryan et al., 2015).

1.2. The Computational Level: Flexible Memory Expression

In contrast to computer memory whose primary goal is to faithfully encode and retrieve the original information, one unique objective of biological memory is to flexibly drive behavioral output in novel situations (Eichenbaum, 2004; Gluck et al., 2016; Staddon, 2016). As natural stimuli in an ever-changing environment rarely reoccur in identical forms, it is more critical for us to apply past knowledge to new situations rather than to remember the exact original scene (Ghirlanda and Enquist, 2003; Pearce, 1994; Robinson et al., 2013). For example, if an animal forms a fear memory through encountering a predator (Figure 1.1), the chance that the animal would run into the same predator at the same place again is very low. Therefore, an adaptive memory system should be able to function flexibly and inform the animal to run away when it encounters a similar, even though not the same, predator (e.g., another lion). This example demonstrates the flexible nature of biological memory. Generating situation-dependent behaviors based on past memories is one of the fundamental goals of our memory systems (Eichenbaum, 2004; Gluck et al., 2016; Pavlov, 1926).

However, flexibly memory expression involves trade-offs. For example, expression of encoded memories is constantly challenged by a fundamental dilemma: the need to apply the learned knowledge under similar circumstances (memory generalization), and the necessity to differentiate non-identical stimuli based on the original experience (memory discrimination)

(Dunsmoor and Paz, 2015; Dymond et al., 2015; Ghirlanda and Enquist, 2003; Pearce, 1994). For example, an animal learned that the lion is dangerous needs to generalize the fear memory to a similar predator, such as a cheetah or a tiger; but also be able to tell the difference between these predators with a cat (Figure 1.1). Discrimination and generalization are like the two sides of the same coin, and they need to be delicately balanced during memory expression (Dunsmoor and Paz, 2015; Ghirlanda and Enquist, 2003; Johnston et al., 2016; Pearce, 1994). A similar discussion can be found in Pavlov's early studies on conditioned reflexes: "*generalization* of stimuli can be interpreted from a biological point of view…(but) now the question can now be discussed as to how the *discrimination* of external agencies arise" (Pavlov, 1926). The imbalance between the two, for example, maladaptive generalization, could lead to brain disorders such as posttraumatic stress disorder (PTSD) and panic disorders (Bonne et al., 2004; Dunsmoor and Paz, 2015; Kheirbek et al., 2012a).

What are the internal and external factors that influence an animal's memory discrimination and generalization? Like other memory-related processes, the discrimination-generalization balance is strongly modulated by internal factors including emotional state (Jasnow et al., 2017; Kuhn et al., 2016), circadian rhythms (Koch et al., 2017), genetic background (Temme et al., 2014), and gender (Keiser et al., 2017; Lynch et al., 2013). These factors affect memory expression likely through the close interaction between the memory system (e.g., hippocampus, amygdala) and non-memory systems that control motivation, homeostasis, and decision-making (e.g., thalamus, hypothalamus, and prefrontal cortex). As for external factors, either stronger conditioning or the passage of time can lead to stronger memory generalization and/or weaker memory discrimination (Poulos et al., 2016; Wiltgen and Silva, 2007). It's therefore conceivable that, in order to drive memory output in a situation-dependent manner, it's critical to integrate multiple external and internal factors together to determine the discrimination-generalization balance.

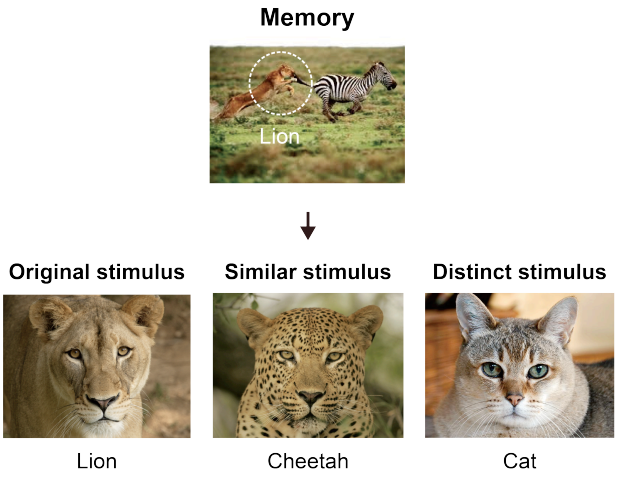

Figure 1.1. Flexible Memory Expression: the Balance between Discrimination and Generalization.

During learning, the zebra forms a fear memory towards the predator, a lion. An adaptive memory system allows the zebra to generalize the fear memory to a similar predator, a cheetah (memory generalization), but also differentiate a cat from potential predators (memory discrimination).

In summary, a computational goal of the memory system is to generate flexible memory outputs. Maintaining the balance between discrimination and generalization is critical for adaptive memory expression and avoiding maladaptive conditions, but the underlying neural processes remain largely unclear.

1.3. The Representation Level: Heterogeneity within a Memory Engram

At the *representation* level, how does the memory representation support adaptive memory expression? Memories are believed to be represented by sparse populations of neurons within the memory engram (Josselyn et al., 2017; Mayford, 2014; Tonegawa et al., 2015a), but it remains unclear how individual neurons within the engram contribute to flexible memory expression. Memory engrams are generally assumed to be homogenous entities, as in most of the studies, neurons within engrams are characterized and manipulated together as homogenous populations (Cai et al., 2016; Garner et al., 2012; Han et al., 2009; Liu et al., 2012; Ryan et al., 2015). However, theoretical studies suggest that functional heterogeneity within a single engram could be advantageous for efficient information encoding (Mejias and Longtin, 2012; Meyers et al., 2008; Osborne et al., 2008). More importantly, functionally distinct subunits within an engram are postulated to favor flexible memory expression, as these subunits would allow memory output to be fine-tuned by individual modules (discrimination vs. generalization) (Eichenbaum, 2017; Mallory and Giocomo, 2018; Tanaka and McHugh, 2018b). Nevertheless, experimental evidence that supports functional heterogeneity within the engram has been lacking.

Recent studies using large-scale electrical recordings and calcium imaging found that neurons showed heterogeneous activity patterns during learning (Grewe et al., 2017; Karlsson and Frank, 2008; Tanaka and McHugh, 2018a). During spatial memory formation, neurons in the medial entorhinal cortex (MEC) exhibited different spatial firing patterns and could be subdivided into grid cells, head direction cells, and border cells (Hardcastle et al., 2017; Moser et al., 2008).

Furthermore, neurons in the amygdala form distinct subgroups that were preferentially activated during either the expression or the extinction of the associative fear memory (Herry et al., 2008). These results together support the existence of functionally distinct neuronal subpopulations within an engram.

In addition to exhibiting distinct firing patterns, engram neurons are differentially modulated by learning (Grewe et al., 2017; Suvrathan and Raymond, 2018). In a tone fear conditioning task, neurons initially responding to the conditioned tone underwent "bi-directional plasticity": they showed either enhanced or reduced response towards the tone after learning (Grewe et al., 2017). In the hippocampus, neurons encoding the spatial memory can be classified as "rigid cells", whose activity did not change much before or after learning, and "plastic cells", which gained substantial firing specificity in their place fields (Grosmark and Buzsáki, 2016). It's conceivable that the roles played by these neuronal subpopulations are likely to be different. However, the functional significance of them in driving memory-guided adaptive behaviors remains unclear.

Taken together, recent findings support an emerging view that the memory engram is not a homogeneous entity. Instead, a single engram may contain neural subpopulations with distinct properties, activity patterns, and functions (Ghandour et al., 2019; Grewe et al., 2017; Mallory and Giocomo, 2018). Nevertheless, causal evidence for functional heterogeneity within a single engram is still lacking. It's yet to be examined whether the observed heterogeneity is an epiphenomenon. Besides, it is also unknown how individual neuronal ensembles can be distinguished within an engram, and how they engage different neural mechanisms to modulate memory-guided adaptive behaviors.

1.4. The Implementation Level: Diversity of Activity-dependent Pathways

If there are indeed functionally distinct neuronal ensembles, what are the differences between them at the cellular and synaptic levels? At the *implementation* level, how is the memory system designed in a way to support heterogeneous engram populations and flexible memory expression?

The existence of functionally distinct neuronal ensembles is strongly implied by the diversity of activity-dependent pathways, which have been individually used to tag neuronal ensembles (Figure 1.2). Neuronal ensembles within memory engrams are typically identified with genetically encoded activity reporters based on activity-dependent pathways (e.g. *Fos*, *Arc*, *Egr1*) (Barth et al., 2004; Deng et al., 2013; Guenthner et al., 2013a; Kawashima et al., 2013; Reijmers et al., 2007; Sørensen et al., 2016), which have traditionally been used as proxies of neuronal activity (Guzowski et al., 2005; Hunt et al., 1987). Importantly, these activity-dependent pathways are known to be functionally diverse, implying that the neurons defined by them may be different (Flavell and Greenberg, 2008; Renier et al., 2016; Sun and Lin, 2016).

First, the cellular functions of individual activity-dependent pathways are very different. *Fos*, *Npas4*, and *Egr1* are transcription factors that activate large-scale downstream gene networks (Flavell and Greenberg, 2008; Kim et al., 2010). *Arc* and *Homer* are synaptic proteins that directly regulate synaptic transmission (Diering et al., 2017; Shepherd and Bear, 2011). Other activity-dependent genes encode secreted proteins, such as *BDNF*, *IGF*, and *Nptx2,* which mediate the communication between neurons (Bambah-Mukku et al., 2014; Chang et al., 2010; Mardinly et al., 2016). Given these diverse cellular functions, it's conceivable the roles of activity-dependent genes in learning and memory may not be identical.

Next, activity-dependent pathways are induced differently by extracellular and sensory stimuli. While activity-dependent genes such as *Fos* and *Arc* are broadly induced by various extracellular stimuli such as neurotrophic factors and PKA-dependent pathways, other genes like *Npas4* are selectively induced by neuronal activity (Lin et al., 2008; Ramamoorthi et al., 2011). Besides, each activity-dependent gene is induced by stimulation with specific temporal patterns (Fields et al., 1997; Tyssowski et al., 2018). For example, activity-regulated genes such *Pcsk1*

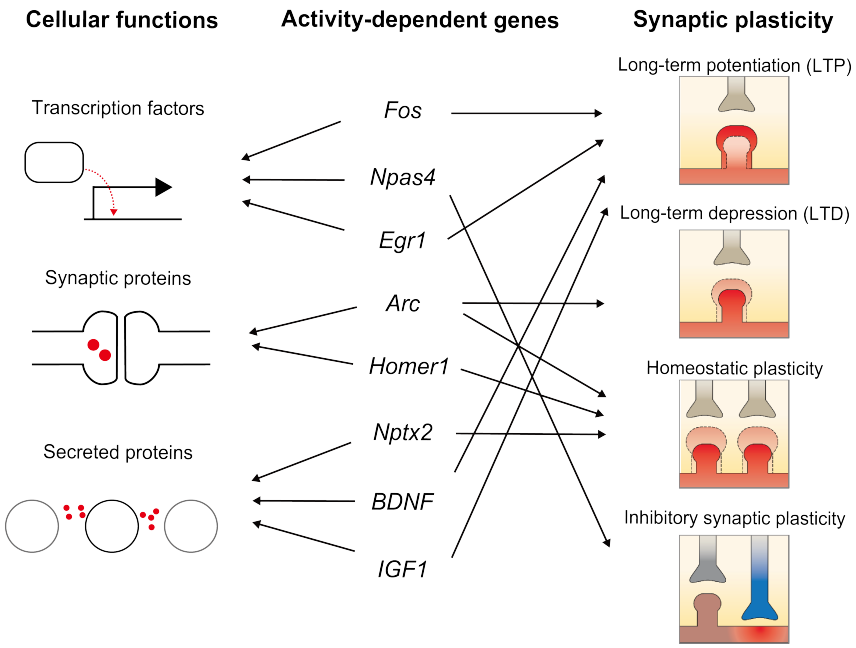

Figure 1.2. Activity-dependent Pathways Have Diverse Cellular and Synaptic Functions.

Some of the well-known activity-dependent genes along with their cellular and synaptic functions are listed. At the cellular level, activity-dependent genes function as transcription factors, synaptic proteins, or secreted proteins. At the synaptic level, they regulate various forms of synaptic plasticity, including LTP, LTD, homeostatic plasticity, and inhibitory synaptic plasticity.

and *Crem* are selectively induced by sustained, but not brief, visual stimulation (Tyssowski et al., 2018). Furthermore, rewarding and aversive experiences differentially triggered the expression of individual activity-dependent genes, and the expression patterns of them could be used to robustly decode the experience (Mukherjee et al., 2018). Sensory stimulation induced *Fos* and *Npas4* expression in distinct populations of neurons in the somatosensory cortex (Renier et al., 2016). *Npas4* in the nucleus accumbens was induced in a subset of Fos^{+} neurons during cocaine-context learning (Taniguchi et al., 2017). These diverse induction patterns of activity-dependent pathways may due to their different upstream signaling cascades related to activity regulators like CREB, MEF2, and SRP (Flavell and Greenberg, 2008; Kuzniewska et al., 2016). Overall, these findings together suggest that the diverse activity-dependent pathways may define different neuronal ensembles. Nevertheless, it's also known that in some cases activity-dependent genes are highly co-expressed in the same neurons (Lonergan et al., 2010; Stone et al., 2011).

Lastly, activity-dependent pathways have diverse synaptic functions. Activity-dependent genes have been extensively studied for their roles in synaptic plasticity such as long-term potentiation (LTP), long-term depression (LTD), and homeostatic plasticity (Figure 1.2) (Bear and Abraham, 1996; Bliss and Lømo, 1973; Turrigiano and Nelson, 2004). *Fos*, *Egr1, BDNF,* and *IGF1* have all been suggested to mediate LTP at excitatory synapses (Bozdagi et al., 2013; Fleischmann et al., 2003; Korte et al., 1995; Penke et al., 2014). *Homer1* and *Nptx2* are required for homeostatic regulation of excitatory synapses in response to activity perturbation (Chang et al., 2010; Diering et al., 2017). *Arc* is required for homeostatic plasticity (Béïque et al., 2011), but it also mediates mGluR-dependent LTD through long-term increases in AMPA receptor endocytosis rate (Park et al., 2008; Waung et al., 2008). *Npas4*, on the other hand, preferentially regulates inhibitory synapses (Bloodgood et al., 2013; Lin et al., 2008). The diverse synaptic functions of activity-dependent genes imply that these genes may initiate various forms of synaptic modifications onto the neuronal subpopulations defined by them.

1.5. The Overarching Hypothesis: Functionally Distinct Ensembles within the Engram

Based on the existing evidence at the computational, representation, and implementation levels, we reason that there may be functional heterogeneity within a single memory engram. Functionally distinct neuronal subpopulations within the memory representation would favor flexible memory expression, and may be implemented through the diverse activity-dependent pathways induced in individual ensembles of neurons. Therefore, we decided to directly test the following two hypotheses in this study:

1) **The memory engram is heterogeneous and can be dissected into functionally distinct neuronal ensembles.**
2) **Distinct synaptic and circuit modifications associated with individual neuronal ensembles support their differential roles in flexible memory expression.**

Taking advantage of the diverse activity-dependent pathways, we first aim to develop different activity-dependent reporters to tag multiple neuronal ensembles and study their causal roles in flexible memory expression (Chapter 2) (Sun et al., 2020). To understand how these ensembles differentially drive memory outputs, we subsequently study the synaptic and circuit properties of each ensemble (Chapter 3). Lastly, at the molecular level, we investigate the causal roles of activity-dependent pathways in the formation of memory engram (Chapter 4). In the end, a working model is proposed to provide insights on how neuronal ensembles within the memory trace emerge and support memory-guided adaptive behaviors (Chapter 5).

Chapter 2

Distinct Neuronal Ensembles within the Memory Engram

Chapter 2 - Distinct Neuronal Ensembles within the Memory Engram

2.1 Abstract

Memories are believed to be encoded by sparse ensembles of neurons within the memory engram. Although individual memory engrams are generally assumed to be homogeneous entities, theoretical studies suggest that functional heterogeneity within each engram could be advantageous for efficient information encoding and flexible memory expression. In this study, we directly investigated the functional heterogeneity within contextual fear memory engrams in the mouse dentate gyrus (DG). We engineered activity-dependent reporters to identify two neuronal ensembles that are genetically defined by the *Fos*- or *Npas4*-dependent transcriptional pathways, respectively. The *Fos*-dependent ensemble exhibits comparable activity levels in similar contexts and promotes memory generalization. The *Npas4*-dependent ensemble shows differential activity between similar contexts and is required for memory discrimination. These findings provide causal evidence for functional heterogeneity within the memory engram, and reveal neuronal mechanisms regulating the discrimination-generalization balance.

2.2. Introduction

Memory engrams, representing individual memories, are the long-lasting biological changes that take place in the brain to encode specific experiences (Josselyn et al., 2015; Lashley, 1950a; Semon, 1921; Thompson, 2005). Recent studies suggest that a memory engram contains a sparse population of neurons that are activated by the specific learning experience (Josselyn et al., 2015; Tonegawa et al., 2015a). These neurons undergo long-lasting synaptic modifications (Choi et al., 2018; Ryan et al., 2015) and play causal roles in the expression of encoded memories (Cai et al., 2016; Han et al., 2009; Liu et al., 2012; Yokose et al., 2017). However, a fundamental question remains unclear: whether neurons within a single memory engram are functionally homogeneous, as generally assumed, or heterogeneous, as hypothesized to allow different aspects of a memory to be individually represented and regulated (Ghandour et al., 2019; Mallory and Giocomo, 2018; Richter et al., 2016; Tanaka and McHugh, 2018b), which would favor flexible memory expression in an ever-changing environment (Eichenbaum, 2004; Xu and Sudhof, 2013). Interestingly, heterogeneous firing patterns among active neurons have been observed during learning by electrical recording and calcium imaging (Ghandour et al., 2019; Grewe et al., 2017; Grosmark and Buzsáki, 2016; Hardcastle et al., 2017). Nevertheless, it remains unknown whether individual memory engrams can be dissected into discrete neuronal ensembles that are functionally distinct. To answer this question, we first need to develop methods to define these neuronal ensembles, and then determine if they play different roles in the behavioral outputs associated with the encoded memory.

Active neuronal ensembles in memory engrams have been identified using genetically encoded activity reporters based on activity-dependent pathways (e.g. *Fos*, *Arc*, *Egr1*) (Barth et al., 2004; Guenthner et al., 2013a; Reijmers et al., 2007). Here we directly examine the functionalities of neuronal ensembles defined by two transcriptional pathways downstream of the IEGs *Fos* and *Npas4*, both of which are highly induced by learning but likely trigger distinct

synaptic changes in activated neurons (Flavell and Greenberg, 2008; Sun and Lin, 2016). The widely used activity marker *F*os mediates long-term potentiation of excitatory synapses (Fleischmann et al., 2003). *Npas4*, a neuron-specific IEG that is selectively activated by neuronal activity, differs from *Fos* in that it preferentially recruits inhibitory synapses, or sometimes diminishes excitatory synapses, onto excitatory neurons (Lin et al., 2008; Weng et al., 2018). These different synaptic functions of *Fos* and *Npas4* strongly suggest that the ensembles they define may be functionally distinct.

To investigate the functionalities of the *Fos*- and *Npas4*-dependent ensembles, we focus on the dentate gyrus (DG) of the hippocampus and the roles of these ensembles in memory discrimination and generalization, opposed processes that must be balanced appropriately to differentiate between different stimuli (Frankland et al., 1998; Grosso et al., 2018; van Dijk and Fenton, 2018) yet also allow recognition of shared features (Dunsmoor and Paz, 2015; Wiltgen and Silva, 2007). The discrimination-generalization balance is critical to adaptive learning and avoiding maladaptive conditions such as post-traumatic stress disorder (PTSD) (Mahan and Ressler, 2012) and panic disorder (Kheirbek et al., 2012b). The DG has traditionally been believed to mediate memory discrimination (Leutgeb et al., 2007; McHugh et al., 2007; Treves and Rolls, 1994), but recent studies suggest that this region can also promote memory generalization (Hainmueller and Bartos, 2018; Nakashiba et al., 2012). Very little is known about whether and how neuronal ensembles in the DG are involved in these processes. Here we show that the *Fos*- and *Npas4*-dependent neuronal ensembles within the DG contextual fear memory engram regulate memory generalization and discrimination, respectively, by engaging distinct synaptic and circuit mechanisms.

2.3. Results

2.3.1. Developing *Fos*- and *Npas4*-dependent RAM Reporters

To identify *Fos*- and *Npas4*-dependent ensembles, we took advantage of our previously developed Robust Activity Marking (RAM) reporter system (Sørensen et al., 2016) and created *Fos*-dependent RAM (*F*-RAM) and *Npas4*-dependent RAM (*N*-RAM) reporters. As transcription factors, FOS and NPAS4 exert their functions via their downstream transcriptional targets, expression of which requires other cellular signals and co-activators in addition to the action of the transcription factors. For this reason, we designed reporters that reflected the transcriptional outputs of FOS and NPAS4 instead of their expression. Unlike conventional activity reporters that use the upstream promoter region of IEGs to drive reporter genes(Barth et al., 2004; Reijmers et al., 2007; Wang et al., 2006), the promoters in *F*-RAM and *N*-RAM ($P_{F\text{-RAM}}$ and $P_{N\text{-RAM}}$) consist of the consensus DNA binding sequences of FOS and NPAS4 (Figure 2.1A). Both promoters drive the expression of reporter genes under the temporal control of a modified doxycycline (Dox)-dependent Tet-Off system that we developed for the RAM system (Sørensen et al., 2016) (Figure 2.2A).

$P_{F\text{-RAM}}$ and $P_{N\text{-RAM}}$ were first validated in primary mouse hippocampal neurons using luciferase assays. Both $P_{F\text{-RAM}}$ and $P_{N\text{-RAM}}$ were robustly activated by membrane depolarization (Figure 2.2B), suggesting that they are regulated by neuronal activity. $P_{F\text{-RAM}}$ was activated by various extracellular stimuli that are known to activate *Fos*, including neurotrophic factors (e.g. BDNF, NT4)(Gaiddon et al., 1996; Ginty et al., 1994) and the protein kinase A activator, Forskolin(Simpson and Mcginty, 1994). $P_{N\text{-RAM}}$, on the other hand, was selectively activated by neuronal activity, recapitulating this unique properties of *Npas4* (Lin et al., 2008; Ramamoorthi et al., 2011). Overexpression of *Fos*, but not *Npas4*, drives $P_{F\text{-RAM}}$ activity, whereas overexpression of *Npas4*, but not *Fos*, activates $P_{N\text{-RAM}}$ (Figure 2.2B), indicating that $P_{F\text{-RAM}}$ and $P_{N\text{-RAM}}$ are selectively activated by the *Fos*- and *Npas4*-dependent pathways, respectively.

Like the original RAM reporter (Sørensen et al., 2016), the *F*-RAM and *N*-RAM reporters are compact enough to be packaged into a single adeno-associated virus (AAV). Cultured

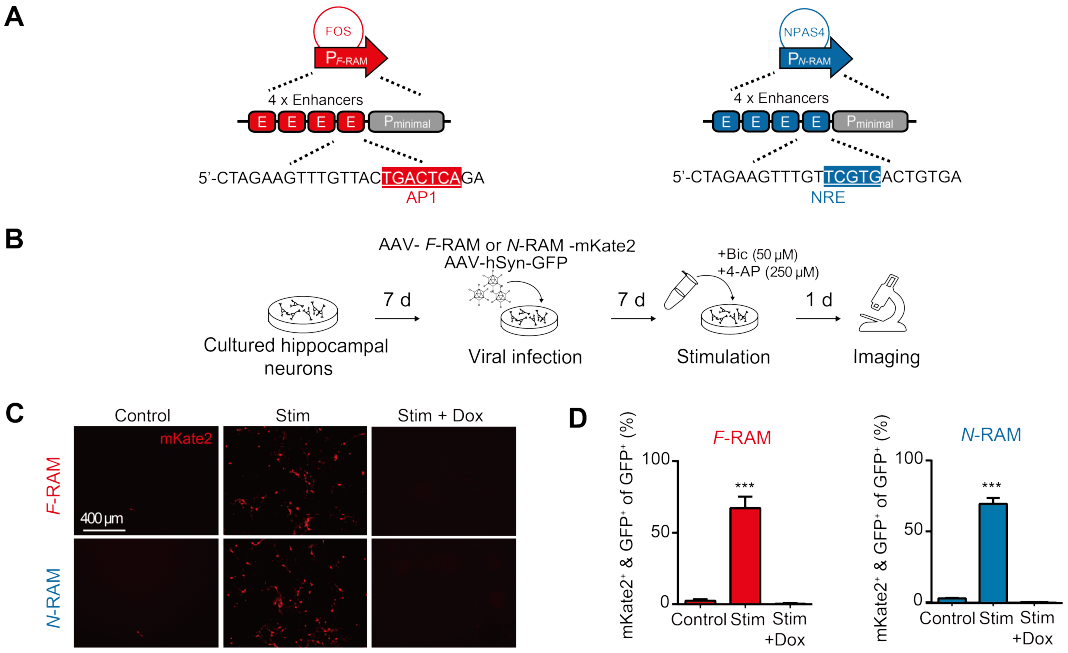

Figure 2.1. Characterization of the *F*-RAM and *N*-RAM Reporters *in vitro*.

(A) The promoters of the two reporters, $P_{F\text{-RAM}}$ and $P_{N\text{-RAM}}$, were based on the existing RAM system. Both promoters contain 4 tandem repeats of 24-bp enhancer modules and a minimal promoter from the human *FOS* gene. The enhancer module in $P_{F\text{-RAM}}$ contains the Activator Protein 1 (AP1) site (TGANTCA), a consensus binding sequence for FOS/JUN family transcription factors. The enhancer module in $P_{N\text{-RAM}}$ contains the NPAS4 Responsive Element (NRE) (TCGTG), a consensus binding motif for NPAS4.

(B) Experimental scheme. Cultured mouse hippocampal neurons were infected with AAVs carrying either the *F*-RAM or *N*-RAM reporter and a control virus (AAV-hSyn-GFP) at 7 days *in vitro* (DIV), stimulated with bicuculline (Bic, 50 µM) and 4-aminopyridine (4-AP, 250 µM) at 14 DIV and harvested for immunocytochemistry and imaging at 15 DIV.

(C) Representative images showing expression of the reporters under three conditions: Stim, stimulated with Bic and 4-AP as described above; Control, without stimulation; Stim + Dox, same as Stim but in the presence of Dox (40 ng/mL).

(D) Quantification of the percentage of $mKate2^+$ neurons among infected neurons (AAV-hSyn-GFP^+). Both *F*-RAM and *N*-RAM were substantially induced by stimulation and inhibited by Dox. One-way ANOVA, Dunnett's test, n = 6 per condition.

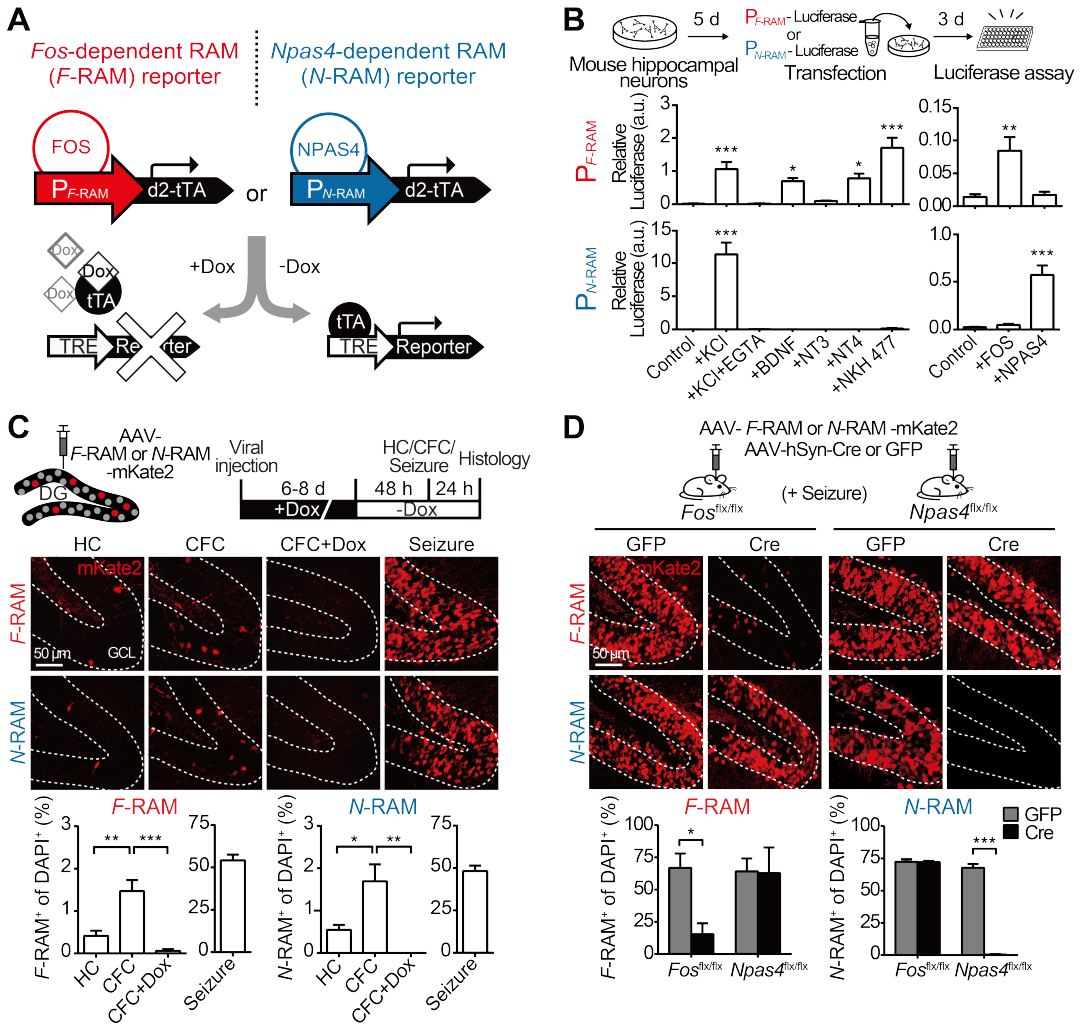

Figure 2.2. The *F*-RAM and *N*-RAM Reporters Selectively Capture *Fos*- and *Npas4*-dependent Neuronal Ensembles.

(A) Design of the *F*-RAM and *N*-RAM reporters.

(B) Characterization of $P_{F\text{-RAM}}$ and $P_{N\text{-RAM}}$. Cultured hippocampal neurons were transfected with luciferase expression plasmids and treated with various extracellular stimuli. The induction of $P_{F\text{-RAM}}$ or $P_{N\text{-RAM}}$ by various extracellular stimuli was measured by luciferase assay. One-way ANOVA, Dunnett's test, n = 8-9.

(C) *F*-RAM and *N*-RAM label experience-activated neuronal ensembles *in vivo*. Representative images of the dorsal DG granule cell layers (GCL, dashed lines) and quantifications showing ensembles labeled under the home cage (HC), contextual fear conditioning (CFC), CFC but on Dox (CFC+Dox), and seizure conditions. One-way ANOVA, Tukey's test, n = 4 per condition.

(D) *F*-RAM and *N*-RAM are dependent on endogenous *Fos* and *Npas4*, respectively. Representative images and quantifications showing seizure-induced reporter activation in *Fos* and *Npas4* conditional knockout animals. Two-way ANOVA, Sidak's test, n = 3-4.

Data are shown as mean ± SEM. *p < 0.05, **p < 0.01, ***p < 0.001.

hippocampal neurons were infected with either AAV-*F*-RAM-mKate2 or AAV-*N*-RAM-mKate2, expressing the red fluorescence protein, mKate2, as the reporter gene. Both the *F*-RAM and *N*-RAM reporters showed low background activation, and were robustly induced by neuronal activity in a Dox-dependent manner (Figure 2.1D). We next used AAV-*F*-RAM-mKate2 or AAV-*N*-RAM-mKate2 to label active neuronal ensembles *in vivo* in the mouse dorsal DG following CFC (see Methods for the detailed experimental procedure). Sparsely labeled cells were primarily located in the granule cell layer of the DG (Figure 2.2C), suggesting that they are mostly granule cells, the principal neurons in the DG. On average, both the *F*-RAM and *N*-RAM reporters labeled 1-2% of the granule cells, consistent with sparse activities reported in the DG during contextual learning (Chawla et al., 2005; Jung and Mcnaughton, 1993). Both the *F*-RAM and *N*-RAM reporters showed low background activation in the home cage, were robustly activated by neuronal activity induced by seizure, and were completely inhibited in the presence of Dox (Figure 2.2C). Both reporters also labeled small populations of cells, mostly mossy cells, in the dentate hilus regions. The number of labeled hilar cells was similar in the HC and CFC conditions, suggesting that contextual fear learning didn't significantly activate these reporters in the hilus (Figure 2.3A-D).

Finally, we used *Fos* and *Npas4* conditional knockout mice ($Fos^{f/f}$ and $Npas4^{f/f}$) to verify that the activation of *F*-RAM and *N*-RAM specifically required *Fos* and *Npas4*, respectively. The *Fos* and *Npas4* genes were deleted in the DG (Figure 2.3F-G) by delivering AAVs expressing DNA recombinase Cre (AAV-hSyn-Cre). *F*-RAM activity was largely abolished in the absence of *Fos*, but not with the removal of *Npas4* (Figure 2.2D). The small remaining activity of *F*-RAM might be due to the recruitment of other *Fos* family members such as *c-Jun* and *FosB*, which can also bind the AP1 sites in $P_{F\text{-RAM}}$ (Hess et al., 2004). *Npas4* deletion, but not *Fos* deletion, eliminated *N*-RAM activity. These results suggest that the *F*-RAM and *N*-RAM reporters specifically label *Fos*- and *Npas4*-dependent active neuronal ensembles, respectively.

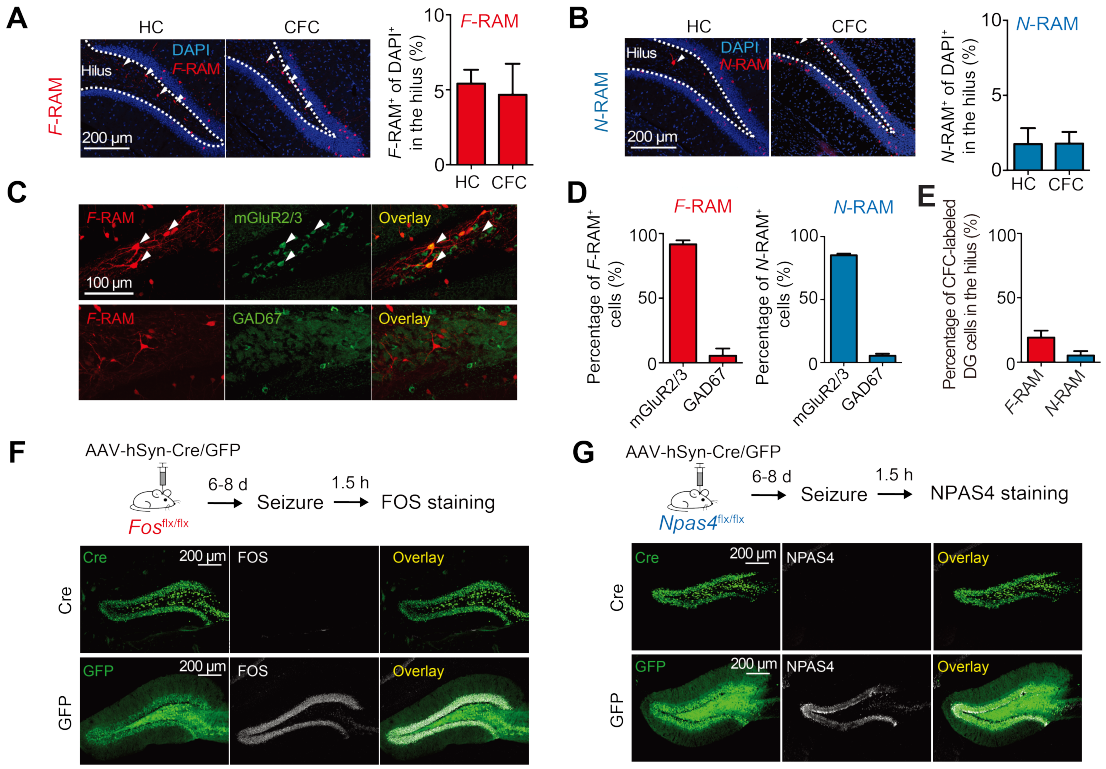

Figure 2.3. Characterization of the *F*-RAM and *N*-RAM Reporters in the dentate hilus.

(A) *F*-RAM labeled comparable numbers of hilar cells under home cage (HC) and contextual fear conditioning (CFC) conditions (Mann-Whitney test, n = 3 per group). White arrows indicate *F*-RAM$^+$ cells in the hilus and dashed lines outline the hilus region.

(B) *N*-RAM labeled comparable numbers of hilar cells under HC and CFC conditions (Mann-Whitney test, n = 4 per group). White arrows indicate *N*-RAM$^+$ cells in the hilus and dashed lines outline the hilus region.

(C) Representative images showing that *F*-RAM$^+$ cells co-localize with the mossy cell marker mGluR2/3 (white arrows) but not the GABAergic interneuron marker GAD67.

(D) The majority of CFC-induced *F*-RAM$^+$ and *N*-RAM$^+$ cells in the hilus were mossy cells (mGluR2/3$^+$, n = 3 per group).

(E) Percentage of DG cells labeled with *F*-RAM or *N*-RAM under the CFC condition that were in the hilus (n = 3-4).

(F) *Fos*$^{flx/flx}$ animals were injected with AAVs expressing Cre or GFP (control) into the DG. Seizures were induced by kainic acid (18 mg/kg) via i.p. injection and animals sacrificed 1.5 hours later to stain for FOS or NPAS4. *Fos* expression was abolished in *Fos*$^{flx/flx}$ animals infected with Cre-expressing virus, indicating effective *Fos* deletion.

(G) Same as **(F)**, but with *Npas4*$^{flx/flx}$ animals. *Npas4* expression was abolished in *Npas4*$^{flx/flx}$ animals infected with Cre-expressing virus, indicating effective *Npas4* deletion.

Data are shown as mean ± SEM. ***p < 0.001.

2.3.2. The *F*-RAM and *N*-RAM Reporters Define Distinct Neuronal Ensembles within the Memory Engram

We next measured co-localization between each ensemble and the *Fos*-expressing neurons that have been postulated to be memory engram cells (Garner et al., 2012; Tanaka et al., 2014; Tonegawa et al., 2015a). We used the FosTRAP mouse (Guenthner et al., 2013a), in which the endogenous *Fos* promoter drives the expression of Cre^{ER} to label *Fos*-expressing ensemble in green via a Cre-dependent EYFP reporter (Figure 2.4A). The *F*-RAM or *N*-RAM ensemble was labeled red with mKate2 (Figure 2.4B). The *F*-RAM and Fos-Cre^{ER} ensembles, both of which should correlate with *Fos* expression, showed substantial (49.902 ± 5.053%) co-localization (Figure 2.4C). These data further indicate that the *F*-RAM and *N*-RAM reporters likely capture two distinct neuronal populations.

2.3.3. The *F*-RAM and *N*-RAM Ensembles Display Distinct Activity Patterns during Memory Recall

The distinct synaptic properties of the *F*-RAM and *N*-RAM ensembles suggested that they may play different roles in memory expression. We therefore investigated their functions in contextual fear memory discrimination and generalization, which are known to be mediated by the DG (Danielson et al., 2017; Guo et al., 2018; Knierim and Neunuebel, 2016; Senzai and Buzsaki, 2017). In an adopted memory discrimination-generalization assay (Huckleberry et al., 2016; Rozeske et al., 2018), mice were fear conditioned in context A, and exposed 24 hours later to either the conditioned context A, an unconditioned context B very similar to A, or a highly distinct context C (Figure 2.5A and Figure 2.6A). Strong fear responses (freezing) were observed in the conditioned context A (Figure 2.5B). Clear fear responses were also observed in context B, suggesting a degree of memory generalization due to the similarity of the two contexts. Memory discrimination also occurred, however, as freezing levels in context B were significantly lower

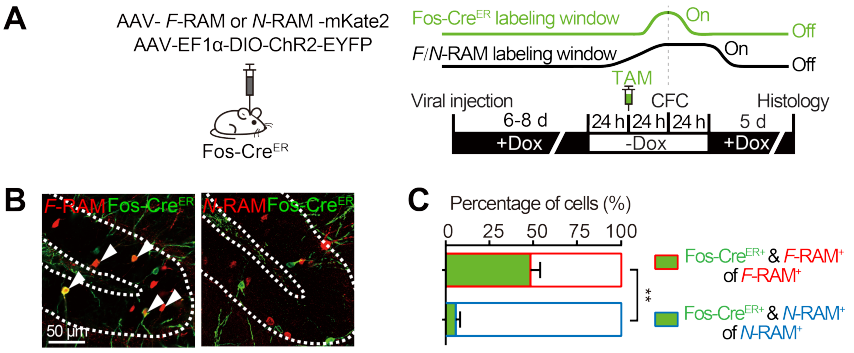

Figure 2.4. The *F*-RAM and *N*-RAM Ensembles are Distinct Neuronal Populations.

(A) Experimental scheme to co-label the *F*-RAM or *N*-RAM and Fos-Cre^{ER} ensembles in Fos-Cre^{ER} mice. Dox was removed 48 hours before CFC to label the *F*-RAM or *N*-RAM ensemble (black line). Tamoxifen (TAM) was injected i.p. 24 hours before CFC to label the Fos-Cre^{ER} ensemble (green line).

(B and C) Representative images (B) and quantification (C) showing overlap between the *F*-RAM or *N*-RAM and Fos-Cre^{ER} ensembles. Mann-Whitney test, n = 5 per group.

Data are shown as mean ± SEM. **p < 0.01.

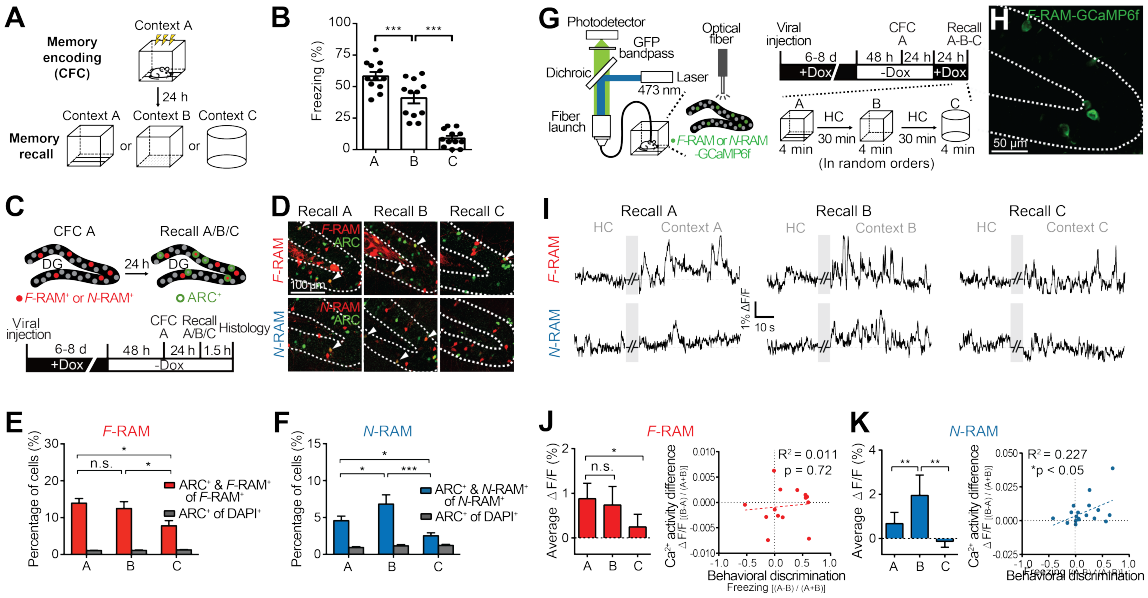

Figure 2.5. The *F*-RAM and *N*-RAM Ensembles Show Distinct Activity Patterns During the Contextual Fear Memory Discrimination-Generalization Assay.

(A) Schematic of the behavioral assay.

(B) Freezing levels during memory recall in the three contexts. One-way ANOVA, Tukey's test, n = 12 per group.

(C) Experimental scheme to identify recall-activated *F*-RAM and *N*-RAM ensemble neurons using *Arc* expression (ARC$^+$).

(D) Representative images showing overlap (white arrows) of the labeled *F*-RAM$^+$ or *N*-RAM$^+$ neurons and ARC$^+$ neurons.

(E and F) Percentages of the *F*-RAM$^+$ (E) and *N*-RAM$^+$ neurons (F) reactivated during memory recall. Two-way mixed ANOVA, Tukey's test, n = 7-9.

(G) Schematic and timeline for examination of Ca^{2+} activity in ensemble neurons using fiber photometry.

(H) Representative image showing the expression of GCaMP6f in the *F*-RAM ensemble after CFC.

(I) Representative traces showing Ca^{2+} activity in *F*-RAM$^+$ and *N*-RAM$^+$ neurons.

(J) Left, *F*-RAM ensemble activity (ΔF/F) during memory recall in different contexts (Friedman's one-way repeated measures ANOVA, Dunn's test, n = 14). Right, correlation between animal's ability to discriminate contexts A and B ($Freezing_{[(A-B)/(A+B)]}$) and the difference in *F*-RAM ensemble activities in these two contexts ($\Delta F/F_{[(B-A)/(A+B)]}$; linear regression, n = 14).

(K) The same as (J), except for *N*-RAM (n = 19).

Data are shown as mean ± SEM. *p < 0.05, **p < 0.01, ***p < 0.001.

than in A. In context C mice displayed the basal level of freezing expected for a novel context, indicating strong memory discrimination and minimal generalization.

To understand the roles of the *F*-RAM and *N*-RAM ensembles, we first examined their reactivation during memory recall in the different contexts using expression of the IEG ARC (Figures 2.5C-D). The *F*-RAM ensemble showed similar rates of reactivation in contexts A and B but less in context C (Figure 2.5E), suggesting that the activity of *F*-RAM$^+$ neurons is not sensitive to small differences between contexts and thus favors memory generalization. *N*-RAM$^+$ neurons, however, were differentially reactivated, and, interestingly, significantly less in context A than in B (Figure 2.5F). The higher reactivation rate of *N*-RAM$^+$ neurons in context B was not an effect of novelty, because a lower rate of reactivation was observed in the entirely novel context C. *N*-RAM$^+$ neurons therefore may be involved in mediating differential memory expression in similar contexts. Similar results were obtained using FOS instead of ARC as the activity marker (Figure 2.6C).

To confirm that the *F*-RAM and *N*-RAM ensembles were reactivated differently *in vivo*, we measured their calcium (Ca^{2+}) activity during memory recall using fiber photometry (Figure 2.5G). GCaMP6f, a genetically encoded Ca^{2+} indicator, was expressed in *F*-RAM$^+$ or *N*-RAM$^+$ neurons after CFC (Figure 2.5H), and GCaMP6f signals were measured when animals recalled memories in the three contexts in random orders (Figure 2.5I). Consistent with the IEG staining, the *F*-RAM ensemble showed strong and comparable Ca^{2+} activities during recall in contexts A and B, quantified by the averaged Ca^{2+} signals ($\Delta F/F$) during the entire recall session (Figure 2.5J). The *N*-RAM ensemble showed significantly less Ca^{2+} activity in context A than in B (Figure 2.5K). Remarkably, the difference in Ca^{2+} activity levels between contexts A and B ($\Delta F/F_{[(B-A)/(A+B)]}$) of the *N*-RAM, but not *F*-RAM, ensemble was significantly correlated with the performance of an animal in discriminating between these two contexts ($Freezing_{[(A-B)/(A+B)]}$, Figure 2.5K), indicating that the *N*-RAM ensemble is important for memory discrimination.

A

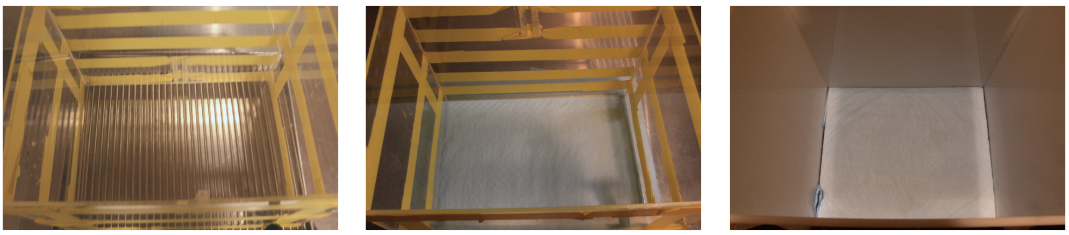

B

	Context A	Context B	Context C
Chamber (L × W × H)	24 cm × 19 cm × 17.5 cm	24 cm × 19 cm × 17.5 cm	32 cm × 25 cm × 32 cm
Floor	Steel grid	Soft pad	Soft pad
Wall	Transparent (w/ visual cue)	Transparent (w/ visual cue)	Opaque and white
Odor	Acetic acid (1%)	Acetic acid (1%)	Benzaldehyde (0.25%)
Lighting	Ambient light	Ambient light	Ambient light + lamp

C

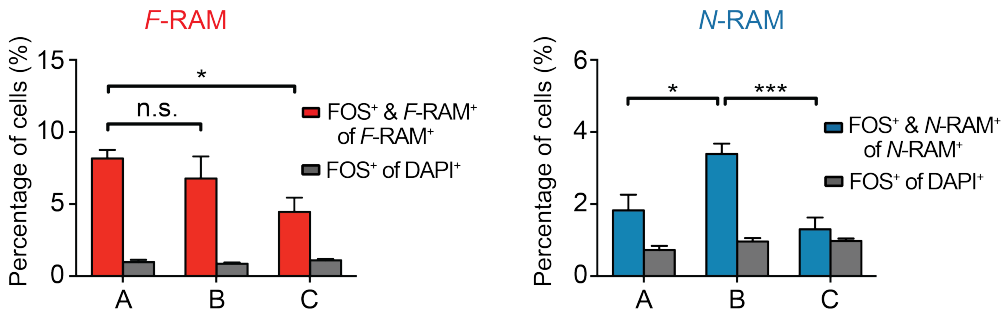

Figure 2.6. The Memory Discrimination-Generalization Assay and the Activity Patterns of the *F*-RAM and *N*-RAM Ensembles Measured by *Fos* Induction During the Assay.

(A) Images of contexts A, B and C.

(B) Detailed features of the three contexts. Context A is made of transparent plastic walls with a steel grid floor for foot-shock delivery. Acetic acid (1%) is used as the odor cue. Context B shares all features with context A except for a different floor: a soft pad insert instead of the steel grid. Context C is a completely different chamber, with a soft padded floor and distinct odor cues (benzaldehyde, 0.25%) and lighting.

(C) Using FOS rather than ARC as the activity marker also showed that similar percentages of *F*-RAM$^+$ neurons were reactivated (FOS$^+$) in contexts A and B, while fewer *N*-RAM$^+$ neurons were reactivated during recall in context A than in B. Two-way mixed ANOVA, Tukey's test, n = 7-9.

These results suggest that the *F*-RAM and *N*-RAM ensembles play different roles in regulating the discrimination-generalization balance.

2.3.4. The *F*-RAM and *N*-RAM Ensembles Differentially Regulate the Memory Discrimination- Generalization Balance

Based upon the previous results, we hypothesized that the *F*-RAM ensemble promotes memory generalization, while the *N*-RAM ensemble mediates memory discrimination. To directly test this hypothesis, we chemogenetically manipulated the activity of *F*-RAM$^+$ and *N*-RAM$^+$ neurons during memory recall. By expressing the inhibitory (hM4Di) or the excitatory (hM3Dq) DREADDs (Designer Receptors Exclusively Activated by Designer Drugs) (Roth, 2016) in the ensemble neurons (Figure 2.6A-B), we were able to inhibit or activate their activity with the DREADD agonist clozapine *N*-oxide (CNO), delivered by intraperitoneal (i.p.) injection 30 minutes before memory recall (Figure 2.6C and Figure 2.7A). In addition to measuring the freezing levels in different contexts, we calculated discrimination indices (DIs) for contexts A and B and contexts A and C to detect bi-directional shifts in the discrimination-generalization balance. A larger DI indicates enhanced discrimination and/or reduced generalization, while a smaller DI indicates enhanced generalization and/or reduced discrimination.

We found that inhibiting the *F*-RAM ensemble enhanced discrimination between contexts A and B (Figure 2.6D-E), while inhibiting the *N*-RAM ensemble reduced memory discrimination (Figure 2.6F). These results suggest that the *F*-RAM and *N*-RAM ensembles shift the discrimination-generalization balance in opposite directions. Notably, these manipulations only affected discrimination between similar contexts (A and B), but not distinct contexts (A and C), consistent with previous reports that the DG is primarily involved in distinguishing similar patterns (Bernier et al., 2017; Kheirbek et al., 2013; Treves and Rolls, 1994). These behavioral effects were not due to any non-specific effects of CNO (Figure 2.8C) or altered general

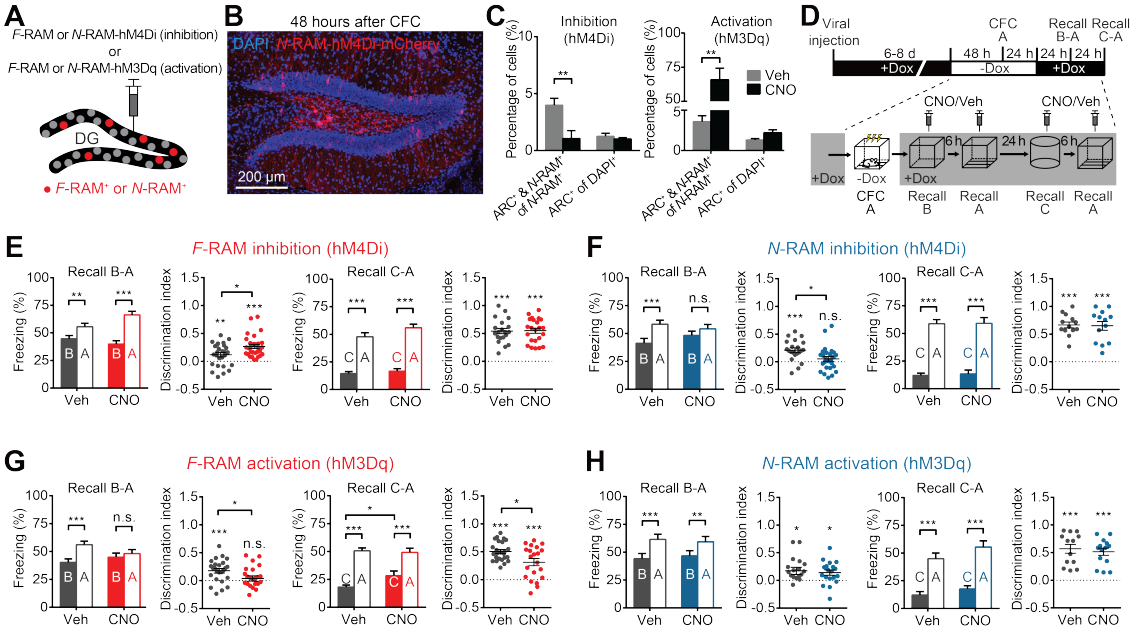

Figure 2.7. *F*-RAM and *N*-RAM Ensembles Oppositely Regulate the Memory Discrimination-Generalization Balance.

(A) Schematics for expression of hM4Di or hM3Dq in ensembles.

(B) Representative image showing expression of hM4Di-mCherry in the *N*-RAM ensemble.

(C) Percentages of ensemble neurons reactivated during memory recall, labeled by *Arc* expression (ARC^+), showing that hM4Di inhibited and hM3Dq activated ensemble neurons (two-way mixed ANOVA, Sidak's test, n = 5 per group).

(D) Experimental scheme to probe the functions of the *F*-RAM and *N*-RAM ensembles in memory discrimination-generalization.

(E) Inhibition of *F*-RAM ensembles enhanced discrimination between contexts A and B (Veh, n = 27; CNO, n = 29), but not A and C (n = 20, 23). Discrimination indices are calculated as $Freezing_{[(A-B)/(A+B)]}$ or $Freezing_{[(A-C)/(A+C)]}$.

(F) Inhibition of *N*-RAM ensembles reduced discrimination between contexts A and B (n = 21, 26), but not A and C (n = 13, 13).

(G) Activation of *F*-RAM ensembles reduced discrimination between contexts A and B (n = 25, 23), and between A and C (n = 21, 25).

(H) Activation of *N*-RAM ensembles did not affect discrimination between contexts A and B (n = 18, 19), or A and C (n = 13, 14).

Two-way mixed ANOVA with Sidak's test was used for freezing levels, Mann-Whitney test for comparing discrimination indices, and one-sample t-test to compare discrimination indices with zero. Data are shown as mean ± SEM. *p < 0.05, **p < 0.01, ***p < 0.001.

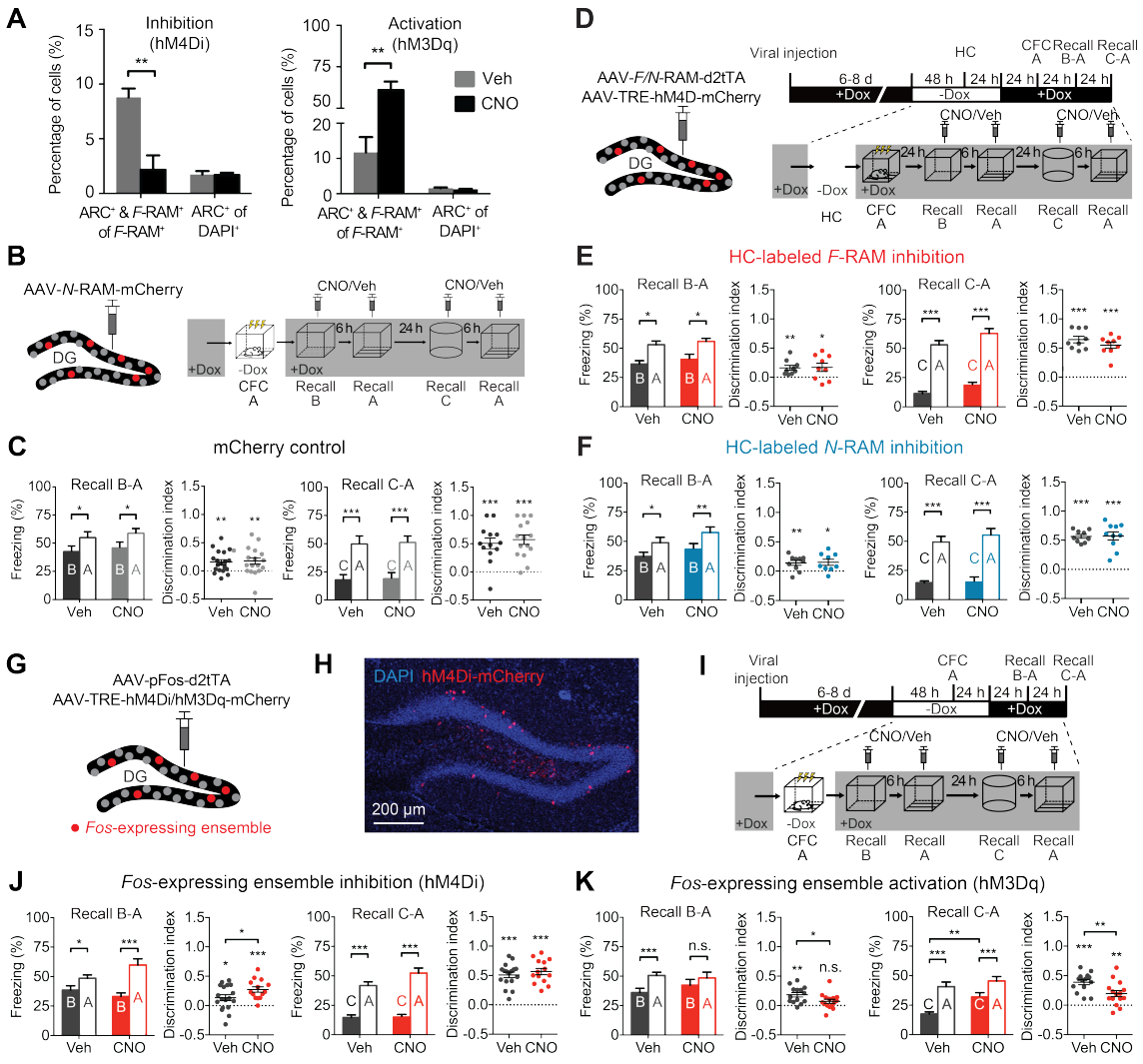

Figure 2.8. Control Experiments for Chemogenetic Manipulation of the Ensembles.

(A) Validation of DREADDs in *F*-RAM$^+$ cells. hM4Di inhibited and hM3Dq activated tagged *F*-RAM$^+$ cells. Animals were injected i.p. with CNO or vehicle (Veh) 30 minutes before recall in context A. Percentages of ensemble neurons that were reactivated (ARC$^+$) were quantified (two-way mixed ANOVA, Sidak's test, n = 4 per group).

(B) Experimental scheme to determine the effect of CNO injection alone on memory discrimination-generalization. AAVs expressing mCherry without DREADD (AAV-*N*-RAM-mCherry) were injected into the DG and mice were subjected to the contextual fear memory discrimination-generalization assay. CNO (4 mg/kg) and vehicle (Veh) were injected i.p. 30 minutes before memory recall.

(C) CNO and Veh groups showed similar discrimination between contexts A and B (Veh, n = 19; CNO, n = 18), as well as A and C (n = 13, 15). Two-way mixed ANOVA with Sidak's test was used for the freezing levels, Mann-Whitney test for comparing the discrimination indices, and one-sample t-test to compare discrimination indices with zero.

(D) Experimental scheme to inhibit cells that are labeled under the HC condition during memory discrimination-generalization. Animals remained in their home cages during the off-Dox window

to label cells activated by background activity, including hilar cells and other granule cells. Labeled cells (hM4Di$^+$) were inhibited during memory recall.

(E) Inhibiting HC-labeled *F*-RAM$^+$ cells did not affect discrimination between contexts A and B (Veh, n = 9; CNO, n = 9) or A and C (n = 9, 9).

(F) Inhibiting HC-labeled *N*-RAM$^+$ cells did not affect discrimination between contexts A and B (n = 10, 9) or A and C (n = 9, 10).

(G) Schematics for expression of the inhibitory DREADD hM4Di or excitatory DREADD hM3Dq in *Fos*-expressing ensembles after CFC. *Fos*-expressing ensembles were labeled by AAV-pFos-d2tTA, which uses an engineered *Fos* promoter to drive d2tTA.

(H) Representative image showing expression of hM4Di-mCherry in the *Fos*-expressing ensemble after CFC.

(I) Experimental scheme to probe the function of the *Fos*-expressing ensemble in memory discrimination-generalization.

(J) Inhibition of the *Fos*-expressing ensemble enhanced discrimination between contexts A and B (Veh, n = 18; CNO, n = 14), but not A and C (n = 17, 14).

(K) Activation of *Fos*-expressing ensembles reduced discrimination between contexts A and B (n = 14, 15) and between A and C (n = 14, 15).

Two-way mixed ANOVA with Sidak's test was used for freezing levels, Mann-Whitney test for comparing discrimination indices and one-sample t-test to compare discrimination indices with zero. Data are shown as mean ± SEM. *$p < 0.05$, **$p < 0.01$, ***$p < 0.001$.

locomotion or anxiety levels, as freezing levels in context C remained similar across all treatments. Furthermore, inhibiting the *F*-RAM or *N*-RAM ensembles labeled under the home cage condition did not affect memory discrimination-generalization either (Figures 2.8D-F). We also found that activation of the *F*-RAM ensemble by hM3Dq enhanced memory generalization and diminished discrimination between contexts (Figure 2.7G), consistent with the idea that this ensemble promotes memory generalization. Activation of the *N*-RAM ensemble, however, did not affect discrimination (Figure 2.7H), suggesting that it is required for, but does not actively drive, memory discrimination. Lastly, we compared the observed effects with the results of manipluating the *Fos*-expressing ensemble (Figure 2.8G-I), the mostly studied ensembles within the engram. Inhibiting the *Fos*-expressing ensemble enhanced discrimiation (Figure 2.8J), while activationg it redcuded discrimiation (Figure 2.8K). Therefore, similar to the *F*-RAM emseble, the *Fos*-expressing ensemble promotes memory generalization.

Taken together, our results indicate that the contextual fear memory engram consists of functionally distinct neuronal ensembles, and those labeled by *F*-RAM and *N*-RAM oppositely modulate the balance between memory discrimination and generalization.

2.4. Discussion

Here we provide direct experimental evidence for functional heterogeneity within individual memory engrams. It suggests that a single homogeneous neuronal ensemble, for example defined by a single IEG (Denny et al., 2014; Liu et al., 2012), likely gives an incomplete picture of a memory engram. We show that two distinct neuronal ensembles, the *F*-RAM and *N*-RAM ensembles, in the representations of the same memory promote opposing behavioral outputs: memory generalization and discrimination. While the present study focuses on contextual fear conditioning in the DG, heterogeneity of the memory engram could be a widespread phenomenon (Grewe et al., 2017; Jun et al., 2010; Mallory and Giocomo, 2018): memory engrams can be

composed of functional subcomponents that differentially modulate experience-dependent behavioral outputs.

Critical questions remain regarding how many distinct ensembles there are and how best to define them genetically. Here we have investigated ensembles associated with two pathways, but other activity-dependent pathways such as *Arc* and *CREB* may define additional functionally distinct subpopulations (Denny et al., 2014; Park et al., 2016). Many activity-dependent pathways partially share upstream signaling and may be co-activated in some neurons (Lonergan et al., 2010). Although multiple lines of evidence from our study (Figures 2.4, Figure 2.5, and Figure 2.6) indicate that the *F*-RAM and *N*-RAM ensembles in DG are distinct neuronal populations, our data cannot exclude the possibility of some potential overlap. A challenge for the future is to identify orthogonal sets of activity-dependent reporters that reveal distinct populations and provide a complete description of the memory engram.

Unlike most of the activity reporters currently being used, *F*-RAM and *N*-RAM report the transcriptional output rather than the expression of IEGs. It is conceivable that the *F*-RAM and *N*-RAM ensembles are not identical to those defined by the promoter of *Fos* and *Npas4*, which may partially explain the incomplete overlap between the *F*-RAM and Fos-Cre^{ER} ensembles (Figure 2.4). Since transcription factors exert their functions through their downstream transcriptional targets, reporters such as *F*-RAM and *N*-RAM monitoring transcriptional outputs may better capture functional populations that undergo learning-induced changes.

It is also currently unknown how neurons are recruited from the general population into the kinds of functionally distinct ensembles we describe here. Factors including intrinsic excitability (Yiu et al., 2014; Zhou et al., 2009), connectivity (Ryan et al., 2015) and firing patterns (Tanaka et al., 2018) have been suggested. Future work, for example using time-lapse Ca^{2+} imaging and single-cell sequencing, will determine whether extrinsic or intrinsic factors or a mixture of both contribute to the formation of functionally distinct neuronal ensembles.

In additional to the traditional role of the DG in mediating pattern separation and discrimination (Treves and Rolls, 1994), our results strongly support the emerging view that this region mediates both discrimination and generalization (Hainmueller and Bartos, 2018; Nakashiba et al., 2012), possibly through different groups of cells with place-modulated firing (Neunuebel and Knierim, 2012). It remains to be determined whether the *F*-RAM and/or *N*-RAM ensembles are related to place cells.

Both *F*-RAM and *N*-RAM reporters labeled small numbers of hilar mossy cells, which have been implicated by recent studies in pattern separation (Danielson et al., 2017; GoodSmith et al., 2017; Jinde et al., 2012; Senzai and Buzsaki, 2017). However, the numbers of mossy cells labeled, by either reporter, were similar between the HC and CFC conditions (Figure 2.3). Although other explanations exist, given that mice were treated identically throughout the 2-3 day window for reporter labeling except for the few minutes during which one group received CFC treatment, a parsimonious explanation is that the reporters captured mossy cells that were active in the home cage and CFC didn't activate additional mossy cells. In addition, memory discrimination-generalization was not affected when the mossy cells labeled in home cage were inhibited (Figures 2.8D-F). These results, though could not formally exclude their involvement, suggest that *F*-RAM$^+$ and *N*-RAM$^+$ mossy cells may not significantly affect memory discrimination-generalization. Genetic tools that can specifically capture mossy cells activated during contextual learning would be needed in the future to definitely define the roles mossy cells play in memory discrimination-generalization.

2.5. Methods

Mice

C57BL/6 male and female mice 7-11 weeks old were used for all experiments. Wildtype mice were purchased from the Charles River Laboratory. *Npas4*$^{flx/flx}$ (*Npas4* conditional knockout) mice were generated previously (Lin et al., 2008) and *Fos*$^{flx/flx}$ (*Fos* conditional knockout) mice were generously provided by Dr. Ming Xu at the University of Chicago. Gad2-Cre (*Gad2*$^{tm2(cre)Zjh}$/J), CCK-Cre (*Cck*$^{tm1.1(cre)Zjh}$/J), PV-Cre (*Pvalb*$^{tm1(cre)Arbr}$/J), SST-Cre (*Sst*$^{tm2.1(cre)Zjh}$/J) and Fos-Cre^{ER} (*Fos*$^{tm1.1(cre/ERT2)Luo}$/J) mice were purchased from the Jackson Laboratory. To produce Cre-expressing animals, heterozygous or homozygous mice carrying the Cre allele were bred with wildtype animals from the Charles River Laboratory. All mice were housed with a 12 hour light-dark cycle. Animal protocols were performed in accordance with NIH guidelines and approved by the Massachusetts Institute of Technology Committees on Animal Care and the Institutional Animal Care and Use Committee at SUNY Upstate Medical University.

Cell cultures for luciferase assays

Primary hippocampal neurons were prepared from mouse pups at postnatal day 0 as previously described (Ramamoorthi et al., 2011), and plated at 100,000 cells per well on coated 24-well plates. Cultures were kept in the dissection medium [Neurobasal A Medium (NBA, Invitrogen), 10% horse serum (Invitrogen), and GlutaMAX (Invitrogen)] for three hours before being switched to the culture medium [NBA supplemented, B27 (Invitrogen) and GlutaMAX]. Cultures were kept at 37 °C in humidified incubators supplemented with 5% CO_2 until use.

At 5 days *in vitro* (DIV), neurons were transfected with plasmids using lipofectamine 2000 (Life Technologies). Plasmid cocktails contained: luciferase reporter plasmids ($P_{F\text{-RAM}}$-Luc or $P_{N\text{-RAM}}$-Luc) expressing firefly luciferase under the control of $P_{F\text{-RAM}}$ or $P_{N\text{-RAM}}$, control plasmids (TK-Renilla) expressing renilla luciferase under the control of the constitutively active thymidine kinase promoter (Promega), and plasmids that overexpress *Fos* or *Npas4* under the control of a constitutive promoter (EF1α) in some cases.

At 8 DIV, cultures were blocked with tetrodotoxin (TTX, 1 μM, Tocris) and APV (100 μM, Tocris) for 1 hour prior to stimulation, and then stimulated for 6 hours with 34 mM KCl, or 34 mM KCl plus 5 mM EGTA (Sigma). Normal culture medium without a high concentration of KCl was used to treat the unstimulated control group. Neurotrophic factors and other drugs were directly added to the cultures in 10 μL culture medium, and the neurons were incubated for 6 hours. At the end of the experiment, neurons were rinsed briefly in phosphate buffered saline (PBS, Invitrogen) and lysed in passive lysis buffer (Promega) for 20 minutes at room temperature. Dual-Glo Luciferase Assay System (Promega) reagents were used, and luciferase levels measured using the SpectraMax Microplate Reader (Molecular Devices). For each experiment, relative luciferase value (a.u.) were calculated by normalizing the firefly luciferase level to the renilla luciferase level. Data were compiled from 3 separate batches of cultures, each conducted with 2 to 3 replicates.

Neurotrophic factors and other drugs were dissolved in water and used at the following final concentrations: recombinant human BDNF (50 ng/μL, PeproTech), recombinant human NT3 (50 ng/μL, PeproTech), recombinant human NT4 (50 ng/μL, PeproTech), NKH 477 (20 μM, Tocris), Bicuculline (50 μM, Sigma) and 4-aminopyridine (250 μM, Tocris).

Viral vectors

AAV1-hSyn-GFP, AAV1-hSyn-GFP-Cre, AAV1-EF1α-DIO-ChR2-EYFP were obtained from the University of Pennsylvania Vector Core via Addgene. All other AAVs were produced in house. AAVs were generated in HEK293T cells and purified using an adapted h gradient purification protocol as previously described (Sørensen et al., 2016). Viral dilutions were determined for individual experiments through pilot injections.

In experiments to label the *F*-RAM and *N*-RAM ensembles *in vitro* and *in vivo*, AAV2/AAV8-*F*-RAM-d2tTA-TRE-mKate2 or AAV2/AAV8-*N*-RAM-d2tTA-TRE-mKate2 virus was used. AAV2/AAV8s were mixtures of AAV2/2 (rep/cap) and AAV2/8 serotypes at a

1:1 ratio (Sørensen et al., 2016). In most experiments a control virus (AAV2/AAV8-EF1α-EGFP) was co-injected to determine the injection accuracy and infection efficiency. To determine whether the *F*-RAM and *N*-RAM reporters were dependent on endogenous *Fos* and *Npas4*, AAV9-*F*-RAM-d2tTA-TRE-mKate2 or AAV9-*N*-RAM-d2tTA-TRE-mKate2 virus was co-injected with AAV1-hSyn-GFP or AAV1-hSyn-GFP-Cre into *Npas4* or *Fos* conditional knockout mice. To examine the co-localization between the Fos-Cre^{ER} ensemble and either the *F*-RAM or *N*-RAM ensemble, AAV9-*F*-RAM-d2tTA-TRE-mKate2 or AAV9-*N*-RAM-d2tTA-TRE-mKate2 virus was co-injected with a Cre-dependent reporter virus, AAV1-EF1α-DIO-ChR2-EYFP. For the fiber photometry experiments, viral cocktails containing AAV9-TRE-GCaMP6f and either AAV9-*F*-RAM-d2tTA-TRE-mKate2 or AAV9-*N*-RAM-d2tTA-TRE-mKate2 were used.

To manipulate ensemble activity with DREADDs, viral cocktails containing AAV9-TRE-hM3Dq-mCherry or AAV9-TRE-hM4Di-mCherry and either AAV9-*F*-RAM-d2tTA-sEF1α-GFP or AAV9-*N*-RAM-d2tTA-sEF1α-GFP were used (the sEF1α-GFP component was used to determine injection accuracy and infection efficiency). For control experiments testing the effects of CNO injections alone, AAV9-TRE-mCherry was used instead of the DREADD-expressing viruses, and was co-injected with AAV9-*N*-RAM-d2tTA-sEF1α-GFP. In experiments to manipulate the activity of *Fos*-expressing ensembles, AAV9-pFos-d2tTA was co-injected with the DREADD viruses. pFos is an engineered *Fos* promoter similar to that used in previous studies (Liu et al., 2012; Reijmers et al., 2007).

C57BL/6 mice 7-11 weeks old were anesthetized with 1.5-2% isoflurane in O_2. To label and manipulate the *F*-RAM and *N*-RAM ensembles in the DG, stereotaxic injections were performed bilaterally into the dorsal hippocampal dentate gyrus with the following coordinates (relative to bregma) and volumes: DG (AP -1.90 mm, ML ±1.30 mm, DV -2.00 mm, 150-200 nL per hemisphere). Viruses were infused at a rate of 100 nL per minute, and needles were kept at the injection site for 5 minutes. The same coordinates and volumes were used to manipulate the

interneurons in the DG. To manipulate the activities of MEC and LEC projection neurons, the following coordinates and volumes were used: MEC (AP -4.75 mm, ML ±3.25 mm, DV -3.60 mm, 250-300 nL per hemisphere), LEC (AP -3.40 mm, ML ±4.35 mm, DV -4.10 mm, 250-300 nL per hemisphere). Mice were typically allowed to recover for 6-8 days following surgery. For experiments with Dox-dependent ensemble labeling, animals were put on Dox diet (40 mg/kg, Bio-Serv) after surgery.

For fiber photometry experiments, DG injections were performed unilaterally, followed by fiber implantation in the same procedure. The left or right hemisphere was randomly chosen for unilateral surgeries. Fiber implants were made of multimode fiber (400 μm core, 0.48 NA, Thorlabs) with plastic ferrules (2.5 mm, Thorlabs). Implants were placed unilaterally in the DG 0.20 mm above the injection site (AP -1.90 mm, ML ±1.30 mm, DV -1.80 mm).

For optogenetics experiments, viral injections into the MEC were followed by fiber implantation in the DG. Fiber implants were made of multimode fiber (200 μm core, 0.22 NA, Thorlabs) with plastic ferrules (1.25 mm, Thorlabs). Implants were placed bilaterally in the DG (AP -1.90 mm, ML ±1.30 mm, DV -1.80 mm).

For DG injections, only animals with viral infection of more than 80% of the dorsal DG and less than 20% of the CA3 were included in behavioral analyses. For MEC or LEC injections, only animals with selective infection of MEC or LEC axonal terminals in either the middle (MML) or outer (OML) third of the DG molecular layers were included. These histological analyses were performed in a blinded manner by investigators that were unaware of the genotypes or conditions.

Drug injections

To induce seizure, kainic acid (KA, Sigma) was dissolved in saline (1 mg/mL, Teleflex Medical) and injected intraperitoneally at 18 mg/kg. Animals were sacrificed 1.5 hours later to check immediate early gene expression, or 24 hours later to check *F*-RAM and *N*-RAM expression.

In experiments using Fos-Cre^{ER} mice, tamoxifen (Sigma) was dissolved in corn oil (Sigma) overnight at 37 °C (15 mg/mL) and injected (i.p) at 150 mg/kg 24 hours prior to the behavioral experiments. Tamoxifen solution was stored at 4 °C for no more than 24 hours before use.

Clozapine *N*-oxide (CNO, Tocris) was dissolved in DMSO (Sigma) at 20 mM and stored at -20 °C. Before experiments, stock CNO was diluted in saline to the desired concentration, 0.4 mg/mL (for hM4Di) or 0.05 mg/mL (for hM3Dq). The same amount of DMSO was diluted in saline as vehicle (Veh) control. Fresh CNO was injected (i.p.) at the dose of 4 mg/kg (for hM4Di) or 0.5 mg/kg (for hM3Dq) 30 minutes before memory recall. The doses of CNO were determined by pilot experiments, and are similar to published studies. For the control experiment testing the effects of CNO injection alone (without DREADD expression), a dose of 4 mg/kg was used. Diluted CNO solution was kept at 4 °C for up to 24 hours before use.

Contextual fear conditioning (CFC)

Prior to CFC, mice were handled daily in a holding room for 3 days. For experiments with Dox-dependent ensemble labeling, on the third handling day Dox diet was replaced by regular diet (off Dox) after the last handling session. In the control experiments testing reporter expression in the presence of Dox (CFC + Dox), animals were kept on Dox diet throughout the experiments. The behavioral training was typically carried out 48 hours after the last handling session.

On the training day, mice were first transported into the holding room and allowed to acclimatize for at least 30 minutes. Mice were then transported into the behavioral room and placed in context A: 24 cm (L) × 19 cm (W) × 17.5 cm (H), with steel grid floors and 1% acetic acid (Sigma). Mice were conditioned with the following protocol: animals were allowed to explore the conditioned chamber freely for 4 minutes and received 2 second 0.55 mA foot shock at 1 minute intervals 3 times, starting at the 58th second. After each experiment, the chamber was cleaned with 70% ethanol and then with water. In experiments to examine whether synaptic features of ensemble neurons depend on memory strength, no foot shock, weak foot shocks (0.35 mA), or strong foot shocks (0.55 mA, the same as other CFC experiments) were delivered. For experiments with Dox-dependent ensemble labeling, animals were switched back to Dox diet 24 hours after CFC if subsequent behavioral experiments were needed.

To test contextual fear memory discrimination-generalization, 24-48 hours after CFC fear conditioned mice were brought back to the same behavioral room and placed in the conditioned context (A), a similar context (B) or a distinct context (C) for memory recall for 4 minutes. Context B shares all features with context A except that a soft pad insert is used as the floor. Context C uses a different chamber that has white opaque walls, 32 cm (L) × 25 cm (W) × 32 cm (H), a soft padded floor, and is scented with 0.25% benzaldehyde (Sigma). In some of the experiments, animals were tested for memory recall in only one context, either A, B or C, and sacrificed 1.5 hours later for immunohistochemistry. In chemogenetics and fiber photometry experiments, the same animals were tested in multiple contexts in order to examine their discrimination between contexts. In those cases, fear conditioned animals were tested in contexts B and A on the first day (with at least 6 hours in between), and contexts C and A on the following day.

Contextual fear memory expression was measured by manually scoring freezing behavior over the 4 minute recall period, sampling every 5 seconds, with freezing defined as absence of

movement for at least 1 second. Discrimination indices (DIs) are calculated as $Freezing_{[(A-B)/(A+B)]}$ when comparing freezing levels in contexts A and B, or $Freezing_{[(A-C)/(A+C)]}$ when comparing freezing levels in contexts A and C. Scorers were blind to the experimental conditions. For example, for chemogenetics experiments researcher 1 would randomly assign CNO or Veh conditions to the animals and perform the drug injection; researcher 2 would carry out the behavioral testing and quantify the freezing behaviors without knowing the conditions.

Immunohistochemistry and confocal imaging

Animals were either perfused or drop fixed with 4% paraformaldehyde (PFA, Sigma) in PBS. For experiments examining immediate-early gene expression, animals were sacrificed 1.5 hours after the last behavioral test. Coronal sections were cut at 50 μm thickness. For typical immunohistochemistry experiments, brain slices were washed in PBS for 10 minutes 3 times, and blocked for 2 hours at room temperature with blocking solution: 1% Triton X-100 (Sigma) and 10% goat serum (Invitrogen) in PBS. Slices were then incubated with the primary antibodies overnight at 4 °C in the antibody solution: 0.1% Triton X-100 and 5% goat serum in PBS. Next day slices were washed in PBS for 10 minutes 3 times and then incubated with the secondary antibodies for 2 hours at room temperature in the antibody solution. Finally, slices were washed in PBS for 10 minutes another 3 times and mounted with DAPI Fluoromount-G (Southern Biotech). Note that for experiments staining for GAD67, a minimum-detergent protocol was adopted from a previous study (Dimidschstein et al., 2016): after initial washing with PBS following PFA fixation, brain slices were permeabilized with 0.1% Triton X-100 for 30 minutes. Slices were then blocked and stained in a detergent-free solution: 3% bovine serum albumin (Sigma) and 5% goat serum in PBS. In this case slices were incubated with anti-GAD67 primary antibody for 48 hours at room temperature.

Antibodies used and dilutions are as follows: rabbit anti-Npas4 (1:10,000, homemade), rabbit anti-Fos (1:1,000, Santa Cruz), rabbit anti-Fos (1:1,000, Synaptic Systems), guinea pig anti-Arc (1:1,000, Synaptic Systems), rabbit anti-mGluR2/3(1:500, Millipore), mouse IgG2a anti-GAD67 (1:500, Millipore) and Alexa 488, 555, 647 secondary antibodies (1:500, Invitrogen).

All images were acquired using an Olympus Fluoview FV1000 confocal microscope. For most of the cell counting experiments, high-resolution z-stack images of the DG were acquired using either a 20× or a 60× oil-immersion objective. Numbers of positive cells were determined manually from 6-12 images per animal as previously described (Sørensen et al., 2016). Analyses were performed in a blind manner by investigators who were unaware of the experimental conditions.

Fiber photometry

A customized fiber photometry system was used. A 473 nm diode laser (OEM Laser Systems) was controlled by a function generator (Agilent, 33599B Series, 400 Hz, square wave). The light was coupled to a 400 μm 0.48 NA optical fiber (Thorlabs) using a 40× 0.65 NA microscope objective (Olympus) and a fiber launch (Thorlabs). Optical fiber with the same diameter was glued to a ceramic ferrule (Thorlabs) and implanted into the mice. Before experiments, implants were connected to the laser setup with ceramic split mating sleeves (Thorlabs). The laser intensity was set to a level that generates fluorescence signals around 50% of the maximum detectable values. The GCaMP6f fluorescence signal was collected by the implanted optical fiber and passed through the objective and dichroic mirror. The signal was then transmitted through a longpass filter (Semrock) onto a NewFocus 2151 femtowatt silicon photoreceiver (Newport, DC High mode). The photoreceiver was connected to a lock-in amplifier (SR830 DSP, Stanford Research Systems, 8 ms time constant) and recorded by customized LabVIEW software (National Instruments).

Fear conditioned animals were subjected to fiber photometry experiments 48 hours after training. On the testing day, after connecting the fiber implants to the fiber photometry rig, animals were allowed 10-20 minutes to recover in their home cages. Animals were then gently transferred from the home cage to context A, B or C and allowed free exploration for 4 minutes. Animals were then transferred back to the home cage and allowed to recover for 30 minutes before being transferred to the next context. The order of context exposure was randomized. The GCaMP6f signal was collected throughout the experiments.

Fiber photometry data were analyzed with a custom MATLAB (MathWorks) program. Average $\Delta F/F$ signals over the entire 4-minute recall session were used to reflect neural activity. Signals were calculated as $\Delta F/F$ by normalizing the measured values during recall to the baseline fluorescence values. Baseline values were calculated as the median of the signals during the 60 seconds in the home cage prior to each context exposure. The signals recorded during physical transfer from the home cage to the contexts (30 seconds) were removed from the analysis.

Chapter 3

Synaptic and Circuit Changes Associated with Distinct Ensembles

Chapter 3 - Synaptic and Circuit Changes Associated with Distinct Ensembles

3.1. Abstract

Synaptic plasticity is thought to underlie the formation of long-term memories. However, how neurons within the engram undergo experience-dependent synaptic modifications remains unclear. Here, we test the hypothesis that functionally distinct neuronal ensembles undergo different synaptic and circuit changes after contextual fear conditioning. We found that the *Fos*-dependent ensemble in the mouse dentate gyrus (DG) received enhanced excitatory synaptic inputs selectively from the medial entorhinal cortex (MEC). On the contrary, the *Npas4*-dependent ensemble recruited stronger inhibitory synaptic inputs from the local cholecystokinin–expressing (CCK^+) interneurons. Importantly, optogenetic inhibition of the MEC-DG pathway impaired memory generalization, recapitulating the effects of inhibiting the *Fos*-dependent ensemble; chemogenetic inhibition of the CCK^+ interneurons abolished memory discrimination, recapitulating the phenotype when the *Npas4*-dependent ensemble was silenced. These suggest that MEC and DG CCK^+ interneurons respectively promote generalization and discrimination, likely through *Fos*- and *Npas4*-dependent ensembles. Taken together, our findings reveal synaptic and circuit mechanisms associated with *Fos*- and *Npas4*-dependent ensembles that regulate the discrimination-generalization balance.

3.2. Introduction

How are memories encoded in the engram? It has been postulated that modifications of synaptic connections between neurons underlying the formation of long-term memories, known as the *synaptic plasticity and memory hypothesis* (Lynch, 2004; Martin et al., 2000; Morris, 2003). Long-term potentiation (LTP), arguably best-known form of synaptic plasticity, is believed to a key mechanism for memory formation (Bliss and Lømo, 1973; Morris, 2003). LTP in the hippocampal circuits was found to be correlated with hippocampus-dependent learning (Bliss and Lømo, 1973; Whitlock et al., 2006). Moreover, preventing LTP by blocking the NMDA-dependent signaling pathway impaired memory formation (Cain et al., 1996; Nakazawa et al., 2004). Recent studies further demonstrate the causal links between synaptic plasticity and memory: encoded associative memories can be artificially inactivated and reactivated by optogenetic potentiation (optical LTP) and depression (optical LTD) of synapses, respectively (Nabavi et al., 2014). These results strongly support that learning-induced synaptic plasticity is crucial for the formation of new memories.

However, how synaptic plasticity shapes the neurons within the memory engram remains largely unknown. Most of the previous studies on synaptic plasticity focused on drastic learning-induced synaptic changes that were detectable at the population level, but not the fine changes specifically occurred onto the engram populations (Bear and Abraham, 1996; Bliss and Lømo, 1973; Whitlock et al., 2006). This is largely due to the lack of approach to pin down the engram-specific neuronal and synaptic sites. Recent studies using activity-dependent genetic reporters, however, were able to tag engram neurons and reveal synaptic changes associated with them (Choi et al., 2018; Ryan et al., 2015; Sun et al., 2020; Zhou et al., 2019). Neuronal ensembles identified by *Fos*-dependent reporters in both the DG and CA1 received stronger excitatory synaptic inputs compared with the unlabeled neighboring neurons (Choi et al., 2018; Ryan et al., 2015). *Arc*-expressing cells in the basolateral amygdala (BLA) showed enhanced learning-

induced presynaptic potentiation (Nonaka et al., 2014). Moreover, engram neurons between upstream and downstream regions are found to be preferentially connected. *Fos*-dependent ensembles between CA3 and CA1, and between ventral CA1 and nucleus accumbens, are strongly connected after aversive and reward learning, respectively (Choi et al., 2018; Ryan et al., 2015; Zhou et al., 2019). These findings together indicate that synapses between neurons within the engram undergo LTP-like potentiation, consistent with the essential roles of LTP in memory formation (Lynch, 2004; Morris, 2003).

Besides plasticity at the excitatory synapses, recent studies also suggest underappreciated roles of inhibitory synaptic plasticity in learning and memory (Barron et al., 2017; Hennequin et al., 2017). Correlated changes of excitatory and inhibitory synapses in the circuit are needed to maintain the excitatory-inhibitory balance of the network and prevent run-away activity (Vogels et al., 2011; Xue et al., 2014a). Besides, the strengthening of inhibitory synapses is believed to increases the specificity of memory by suppressing unspecific activities (Ball et al., 2012; Ruediger et al., 2011). Perturbing inhibitory interneurons, or even particular subtypes of interneurons, disrupted the engram (Stefanelli et al., 2016) and memory expression (Lovett-Barron et al., 2014; Turi et al., 2019). These results together support the emerging view that the inhibitory circuit plays essential roles in long-term memories (Barron et al., 2017). Nevertheless, how inhibitory plasticity modifies neurons in the memory engram remains unstudied. It's yet to know how the inhibitory interneurons interact with the engram to support memory-guided adaptive behaviors.

Here, we systematically examine the synaptic changes onto two functionally distinct neuronal ensembles within the memory engram: *F*-RAM and *N*-RAM. We have previously shown that the *F*-RAM and *N*-RAM ensembles oppositely regulate the balance between memory discrimination and generalization (Chapter 2), which implies their distinct cellular and synaptic features. Besides, *F*os has been shown to mediate long-term potentiation of excitatory synapses (Fleischmann et al., 2003), whereas *Npas4* preferentially recruits inhibitory synapses (Lin et al.,

2008; Weng et al., 2018). It's thus conceivable that *F*os and *Npas4* may lead to different synaptic changes onto the *F*-RAM and *N*-RAM ensembles, respectively. Therefore, we hypothesize that the *F*-RAM and *N*-RAM ensembles undergo different learning-induced synaptic modifications, which potentially give rise to the distinct functions of these two ensembles.

3.3. Results

3.3.1. Distinct Synaptic Properties of *F*-RAM$^+$ and *N*-RAM$^+$ Cells

To understand the synaptic and circuit mechanisms underlying the distinct functions of *F*-RAM and *N*-RAM ensembles, we first compared the synaptic properties of dentate granule cells (DGCs) in each ensemble. Whole-cell patch-clamp recordings were carried out on *F*-RAM$^+$ or *N*-RAM$^+$ cells 24 hours after CFC (Figure 3.1A), measuring spontaneous miniature excitatory and inhibitory postsynaptic currents (mEPSCs and mIPSCs). Compared to their neighboring unlabeled (*F*-RAM$^-$ or *N*-RAM$^-$) neurons, *F*-RAM$^+$ neurons received stronger excitatory inputs, specifically higher mEPSC frequencies (Figure 3.1B), while *N*-RAM$^+$ neurons received stronger inhibitory inputs, with increased mIPSC frequencies (Figure 3.1C). mIPSCs of *F*-RAM$^+$ neurons and mEPSCs of *N*-RAM$^+$ neurons were indistinguishable from those of their unlabeled neighbors. *F*-RAM$^+$ and *N*-RAM$^+$ neurons were rarely seen in the inner granule cell layer, and did not show the high intrinsic excitability typical of adult new-born DGCs (Kuhn et al., 1996; Mongiat et al., 2009) (Figure 3.2A-C), suggesting that they are mature granule cells. Together these data indicate that the *F*-RAM and *N*-RAM ensembles are mostly composed of two groups of mature granule cells with distinct synaptic properties.

In addition, DGCs labeled by either *F*-RAM or Fos-Cre^{ER} alone, or both, all had similar electrophysiological properties: increased mEPSC frequencies compared to unlabeled neurons (Figure 3.2D). In contrast, the *N*-RAM and Fos-Cre^{ER} ensembles were electrophysiologically distinct: DGCs labeled by *N*-RAM, including the small population labeled by both *N*-RAM and Fos-Cre^{ER}, had higher mIPSC frequencies than unlabeled DGCs and those labeled only by Fos-

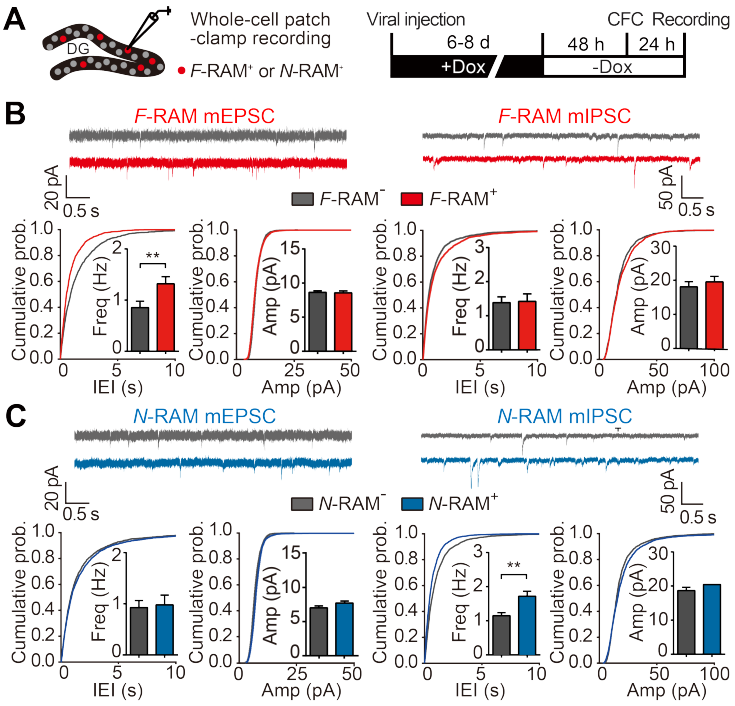

Figure 3.1. The *F*-RAM and *N*-RAM Ensembles Show Distinct Synaptic Properties.

(A) Experimental scheme to measure mEPSCs and mIPSCs on labeled *F*-RAM$^+$ or *N*-RAM$^+$ neurons and unlabeled neighboring neurons.

(B) *F*-RAM$^+$ neurons showed increased mEPSC frequency (Mann-Whitney test; *F*-RAM$^-$, n = 17; *F*-RAM$^+$, n = 17) but unchanged mIPSCs (n = 18, 19).

(C) *N*-RAM$^+$ neurons showed unchanged mEPSCs (*N*-RAM$^-$, n = 20; *N*-RAM$^+$, n = 20), but increased mIPSC frequency (n = 25, 26).

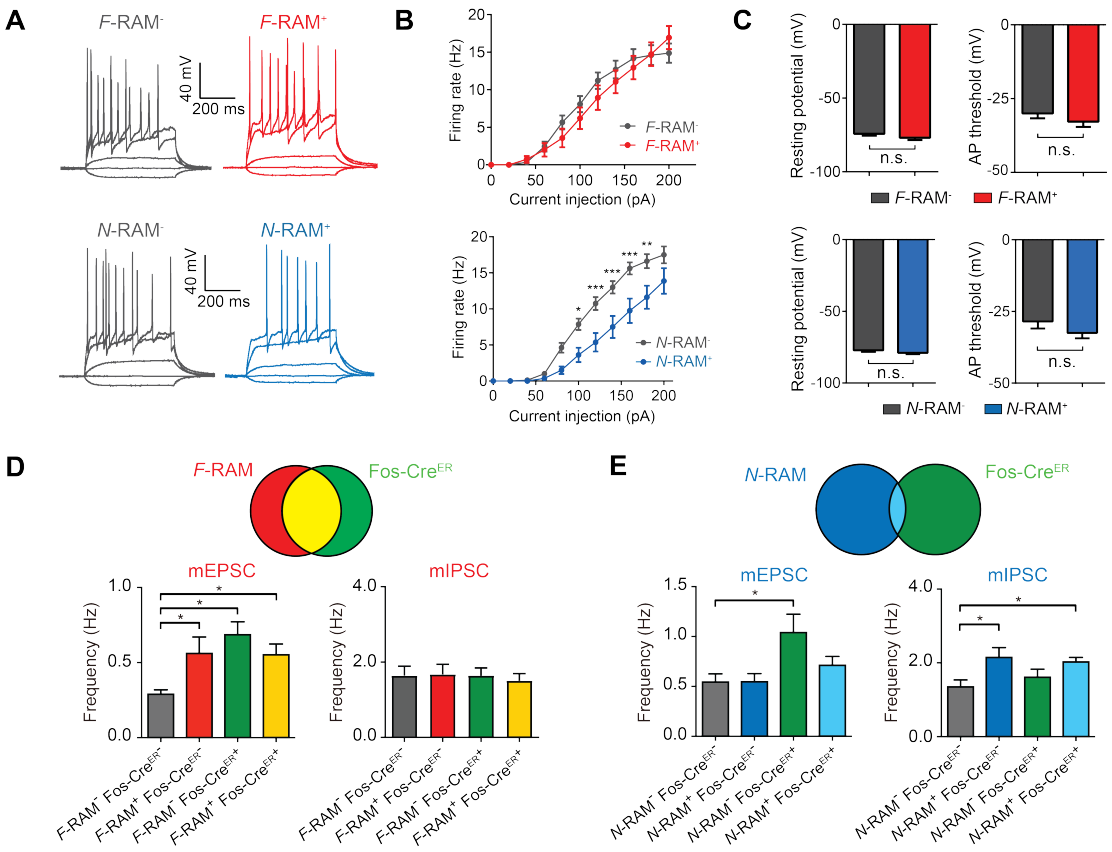

Figure 3.2. Intrinsic Excitability of *F*-RAM$^+$ and *N*-RAM$^+$ Neurons.

(A) Example traces showing membrane potentials of *F*-RAM$^+$ and *N*-RAM$^+$ neurons compared to their unlabeled neighbors, in response to -20, 0, 20, 100 and 200 pA current injections.

(B) Input-output curves of firing rates versus injected currents for *F*-RAM$^+$ and *F*-RAM$^-$ neurons (left), or *N*-RAM$^+$ and *N*-RAM$^-$ neurons (right). *F*-RAM$^+$ neurons show comparable excitability to *F*-RAM$^-$ neurons (*F*-RAM$^-$, n = 19; *F*-RAM$^+$, n = 23). *N*-RAM$^+$ neurons show decreased excitability compared to *N*-RAM$^-$ neurons (n = 16, 16). Two-way mixed ANOVA, Sidak's test.

(C) *F*-RAM$^+$ neurons *(F*-RAM$^-$, n = 19; *F*-RAM$^+$, n = 23) and *N*-RAM$^+$ neurons (n = 16, 16) show similar resting membrane potentials and action potential (AP) thresholds to their neighboring unlabeled cells. Mann-Whitney test.

(D) Whole-cell patch-clamp recordings were carried out on hippocampal slices from animals in which the *F*-RAM and Fos-Cre^{ER} ensembles were co-labeled. Neurons labeled by *F*-RAM, Fos-Cre^{ER} or both showed increased mEPSC frequencies. One-way ANOVA, Dunnett's test comparing to the *F*-RAM$^-$ Fos-CreER$^-$ group, n = 17, 15, 11, 16 (from left to right). mIPSC frequencies were similar for all groups (n = 13, 12, 12, 10, from left to right).

(E) Whole-cell patch-clamp recordings were carried out on hippocampal slices from animals in which the *N*-RAM and Fos-Cre^{ER} ensembles were co-labeled. Neurons labeled by Fos-Cre^{ER}, but not those labeled by *N*-RAM, showed increased mEPSC frequencies (n = 12, 11, 13, 17 from left to right). Neurons labeled by *N*-RAM, including the small population labeled by both *N*-RAM and Fos-Cre^{ER}, showed increased mIPSC frequencies (n = 19, 17, 14, 25 from left to right).

Data are shown as mean ± SEM. *p < 0.05, **p < 0.01, ***p < 0.001.

Cre^{ER} (Figure 3.2E). These data further indicate that the *F*-RAM and *N*-RAM reporters likely capture distinct neuronal populations.

3.3.2. The *F*-RAM Ensemble Receives Increased Excitatory Inputs from the MEC

How might two ensembles within the same memory engram mediate distinct functions? We hypothesized that each neuronal ensemble undergoes distinct circuit modifications that allow them to differentially modulate memory expression. Since *F*-RAM^+ DGCs receive stronger excitatory inputs than neighboring neurons (Figure 3.3B), we asked which of the three major afferent pathways of the DG provide this increased excitatory drive: the lateral perforant path (LPP) from the lateral entorhinal cortex (LEC), the medial perforant path (MPP) from the medial entorhinal cortex (MEC), or the mossy cell fibers (MCF) from the dentate hilus (Amaral and Witter, 1989) (Figure 3.3A). We electrically stimulated the axonal fibers of the LPP, MPP or MCF, which respectively target the outer, middle or inner molecular layers (OML, MML, IML) of the DG (Scharfman and Myers, 2013; Witter, 2007), and simultaneously measured evoked excitatory postsynaptic currents (eEPSCs) of *F*-RAM^+ and unlabeled neighboring neurons in pairs. Selective stimulation of the input pathways was confirmed by observation of their characteristic short-term plasticity: paired-pulse facilitation for the LPP and MCF and paired-pulse depression for the MPP (Hashimotodani et al., 2017; Petersen et al., 2013), and by selective reduction of the MPP response in the presence of the mGluR2/3 agonist DCG-IV (Macek et al., 1996) (Figure 3.3B). We found that the amplitude of eEPSCs originating from the MPP only was significantly larger on *F*-RAM^+ than *F*-RAM^- cells (Figure 3.3C). In contrast, eEPSCs from all three pathways were similar in *N*-RAM^+ neurons and their unlabeled neighbors (Figure 3.3F). Additionally, paired-pulse ratios (PPRs) and AMPA/NMDA ratios were comparable in *F*-RAM^+ and *F*-RAM^- neurons (Figure 3.3D-E). We confirmed these findings using optogenetic stimulation, which confirmed that inputs to *F*-RAM^+ neurons from the MPP, but not the LPP or

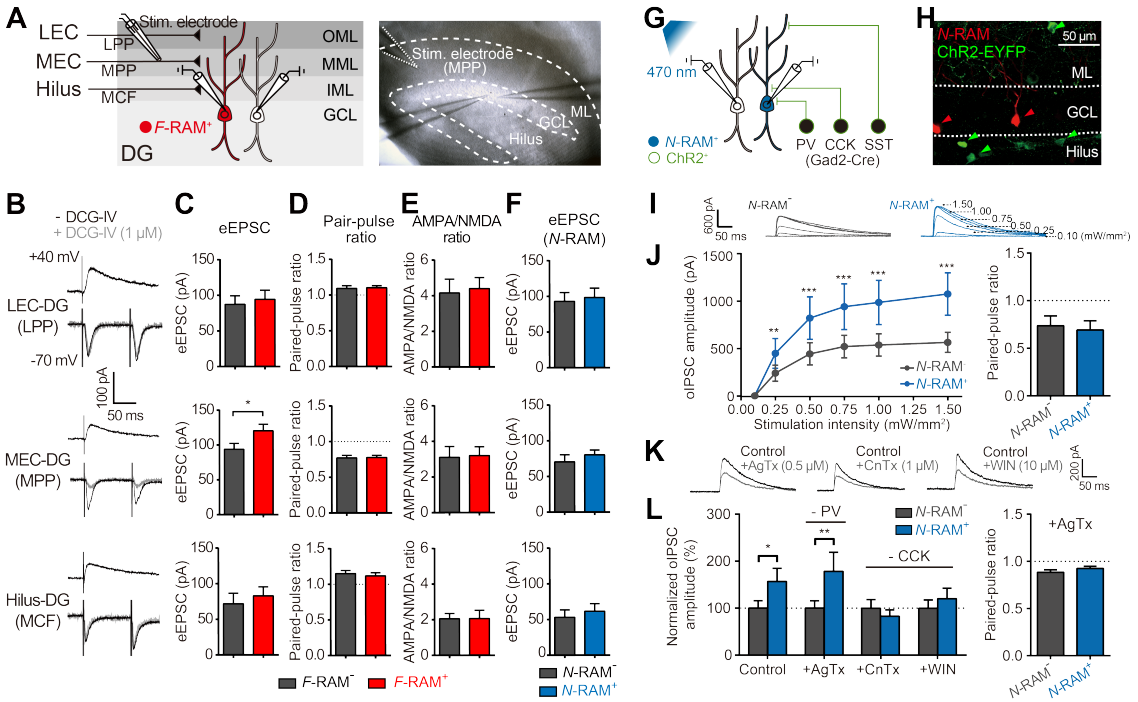

Figure 3.3. The *F*-RAM Ensemble Receives Increased Excitatory Inputs from the MEC and the *N*-RAM Ensemble Receives Enhanced Inhibitory Inputs from DG CCK$^+$ Interneurons

(A) Left, experimental scheme for simultaneous recording of eEPSCs, elicited by stimulating the LPP, MPP or MCF, on pairs of *F*-RAM$^+$ or *N*-RAM$^+$ neurons and nearby unlabeled neurons. Right, representative image of MPP stimulation.

(B) Representative traces of eEPSCs during LPP, MPP and MCF stimulation. Grey traces denote eEPSCs in the presence of DCG-IV.

(C-E) Bar graphs comparing eEPSC amplitudes (C, Wilcoxon signed-rank test, n = 15, 18, 21 pairs for LPP, MPP and MCF, respectively), paired-pulse ratios (D, n = 18, 20, 13) and AMPA/NMDA ratios (E, n = 15, 19, 13) between pairs of *F*-RAM$^+$ and *F*-RAM$^-$ neurons.

(F) Bar graph comparing eEPSC amplitudes between pairs of *N*-RAM$^+$ and *N*-RAM$^-$ neurons (n = 10, 13, 11).

(G) Experimental scheme for simultaneous recording of oIPSCs on pairs of *N*-RAM$^+$ or *F*-RAM$^+$ and nearby unlabeled neurons. oIPSCs were elicited by optogenetically stimulating ChR2-expressing GABAergic interneurons in Gad2-Cre mice.

(H) Representative image showing *N*-RAM and ChR2 expression.

(I) Representative traces showing oIPSCs recorded in pairs of nearby *N*-RAM$^+$ and *N*-RAM$^-$ neurons.

(J) Comparison of oIPSC amplitudes (left; two-way repeated measures ANOVA, Sidak's test, n = 10 pairs) and paired-pulse ratios (right; 200 ms interval, 0.50 mW/mm^2, Wilcoxon signed-rank test, n = 10) between *N*-RAM$^+$ and *N*-RAM$^-$ neurons.

(K) Representative traces showing that oIPSC amplitudes were reduced with bath application of AgTx, CnTx and WIN.

(L) Left, oIPSC amplitudes in *N*-RAM^{+} and *N*-RAM^{-} neurons with and without blockers (two-way mixed ANOVA, Sidak's test, n = 16, 10, 12, 13 pairs for control, AgTx, CnTx and WIN). Right, paired-pulse ratios in the presence of AgTx (n = 12).

Data are shown as mean ± SEM. *p < 0.05, **p < 0.01, ***p < 0.001.

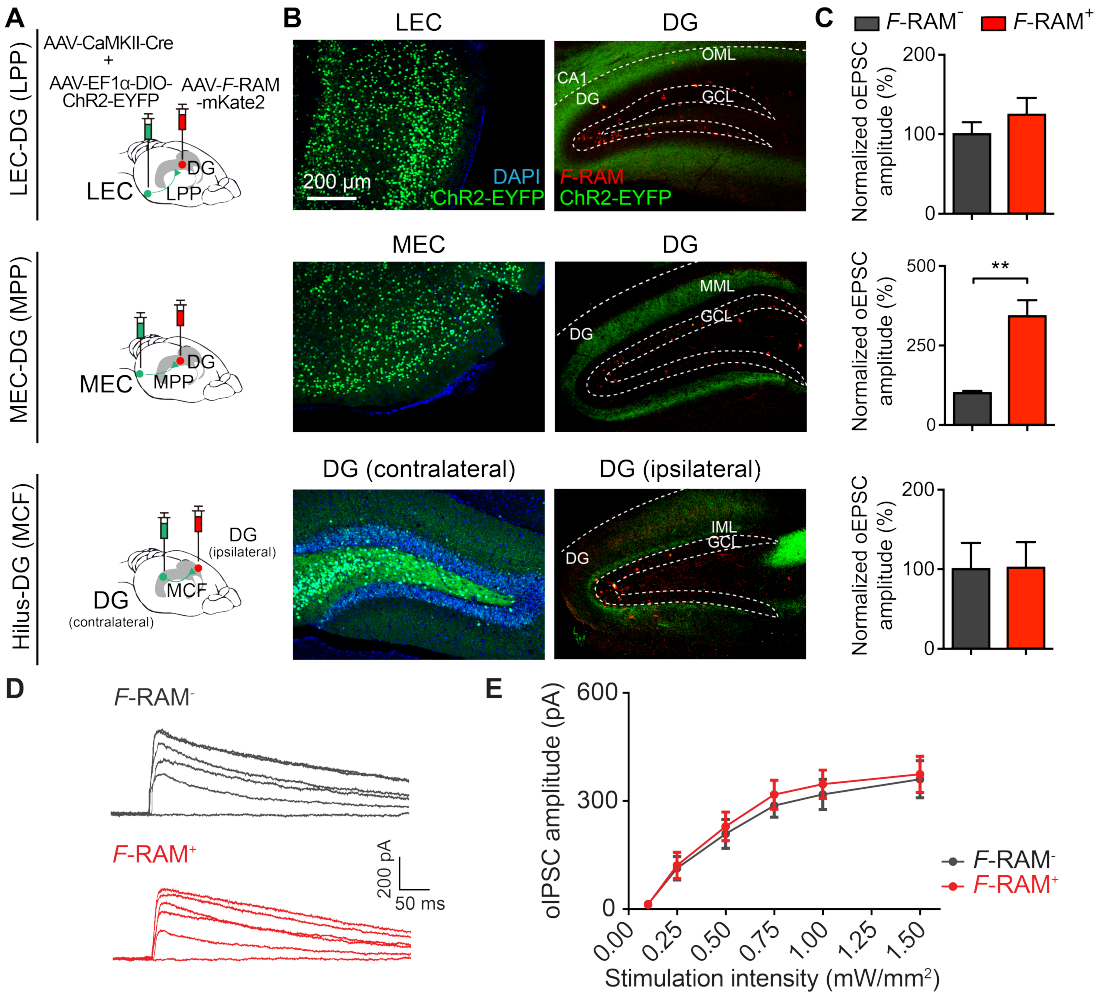

Figure 3.4. *F*-RAM$^+$ Neurons Showed Increased oEPSC Amplitudes upon Optogenetic Stimulation of the MPP, but Unchanged oIPSCs upon Optogenetic Stimulation of Local Interneurons.

(A) Experimental scheme. To target the LPP and MPP pathways, animals were co-injected with AAV-CaMKII-Cre and AAV- EF1α-DIO-ChR2-EYFP to express ChR2 in the LEC or MEC, and also injected with AAV-*F*-RAM-mKate2 in the DG. To target the MCF pathway, AAV-CaMKII-Cre and AAV- EF1α-DIO-ChR2-EYFP were co-injected unilaterally into the contralateral DG, which labeled the hilar mossy cells that send axonal projections to the ipsilateral DG through MCFs. AAV-*F*-RAM-mKate2 was injected unilaterally into the ipsilateral DG, where whole-cell patch-clamp recordings were carried out.

(B) Representative images showing ChR2 and *F*-RAM expression.

(C) *F*-RAM$^+$ neurons had increased optically evoked EPSC (oEPSC) amplitudes upon MPP but not LPP or MCF stimulation (Wilcoxon signed-rank test, n = 16, 11, 10 pairs for LPP, MPP and MCF). Tetrodotoxin (TTX, 0.5 μM) and 4-aminopyridine (4-AP, 100 μM) were added to isolate monosynaptic inputs. Picrotoxin (50 μM) was added to block $GABA_A$ receptors. Data are shown as mean ± SEM. **p < 0.01.

(D) Example traces showing oIPSCs recorded simultaneously in *F*-RAM$^+$ and *F*-RAM$^-$ neurons stimulated by 2 ms of 0.10, 0.25, 0.50, 0.75, 1.00, 1.50 mW/mm^2 470 nm LED light pulses.

oIPSCs were elicited by optogenetically stimulating ChR2-expressing GABAergic interneurons in Gad2-Cre mice.

(E) oIPSC amplitudes were similar in the two groups (two-way repeated measures ANOVA, Sidak's test, n = 12 pairs).

MCF, were strengthened (Figure 3.4A-C). These results indicate that the strengthened excitatory inputs to *F*-RAM$^+$ DGCs originate from the MEC and not the LEC or dentate hilus.

3.3.3. The *N*-RAM Ensemble Receives Enhanced Inhibitory Inputs from CCK$^+$ Interneurons

We next aimed to identify the source of the inhibitory inputs that were recruited onto *N*-RAM$^+$ DGCs (Figure 3.1C). We expressed light-activated channelrhodopsin, ChR2, in DG GABAergic neurons by delivering AAV-EF1α-DIO-ChR2-EYFP into Gad2-Cre mice (Figure 3.3G). Optically evoked inhibitory postsynaptic currents (oIPSCs) were then measured on *N*-RAM$^+$ or *F*-RAM$^+$ DGCs and their unlabeled neighbors in pairs (Figure 3.3I). Consistent with our previous finding that the *N*-RAM$^+$ neurons had higher mIPSC frequencies, robustly larger oIPSC amplitudes were observed on *N*-RAM$^+$ cells, with PPRs being similar in *N*-RAM$^+$ and *N*-RAM$^-$ cells (Figure 3.3J). In contrast, oIPSCs on *F*-RAM$^+$ neurons were similar to those of their unlabeled neighbors (Figure 3.4D-E).

The three major subtypes of GABAergic interneuron in DG are parvalbumin- (PV$^+$), somatostatin- (SST$^+$) and cholecystokinin-expressing (CCK$^+$) cells (Freund and Buzsaki, 1996; Pelkey et al., 2017). To determine whether inputs from some of these interneuron subtypes were selectively recruited to *N*-RAM$^+$ DGCs, oIPSCs were measured on pairs of *N*-RAM$^+$ and *N*-RAM$^-$ cells in the presence of the P/Q-type Ca^{2+} channel blocker ω-agatoxin IVa (AgTx), which selectively inhibits transmission from PV$^+$ interneurons, or the N-type Ca^{2+} channel antagonist ω-conotoxin GVIa (CnTx), which selectively inhibits transmission from CCK$^+$ interneurons (Hefft and Jonas, 2005) (Figure 3.3K). The difference in oIPSC amplitudes between *N*-RAM$^+$ and *N*-RAM$^-$ neurons was abolished in the presence of CnTx, but not AgTx (Figure 3.3L), suggesting that the increased inhibition on *N*-RAM$^+$ neurons comes mainly from CCK$^+$ interneurons. Consistently, the increase in oIPSC amplitudes on *N*-RAM$^+$ neurons was also abolished by the

CB_1R agonist WIN 55,212-2 (WIN), which selectively inhibits CCK^+ interneurons via the endocannabinoid pathway (Tsou et al., 1999). These results suggest that *N*-RAM^+ neurons recruit enhanced inhibitory drive selectively from CCK^+ interneurons.

3.3.4 The Distinct Synaptic Properties of Ensemble Neurons are Induced by Learning

Are the distinct synaptic properties of *F*-RAM^+ and *N*-RAM^+ neurons intrinsic features of the cells or acquired through learning? We hypothesized that these synaptic properties were triggered by contextual fear learning, through the activation of the *Fos*- and *Npas4*-dependent pathways. We first tested if these synaptic properties can be created merely by the expression of *Fos* or *Npas4*. We artificially induced *Fos* and *Npas4* expression (FOS_{ind} and $NPAS4_{ind}$) in sparse and randomly selected DGCs (Figure 3.5A-B), and subsequently compared mEPSCs and mIPSCs on those neurons to their un-manipulated neighbors. *Fos* expression led to an increase in mEPSC frequencies (Figure 3.5C), recapitulating this synaptic feature of *F*-RAM^+ neurons. *Npas4* expression resulted in elevated mIPSC frequencies (Figure 3.5D), mimicking the synaptic changes observed on *N*-RAM^+ cells. Neither mIPSCs of FOS_{ind} neurons nor mEPSCs of $NPAS4_{ind}$ neurons were altered (Figure 3.6A-B). These results suggest that activations of *Fos*- and *Npas4*-dependent pathways are sufficient to induce the synaptic properties observed in *F*-RAM^+ and *N*-RAM^+ neurons, respectively.

Since expression levels of *Fos* and *Npas4* are very low at baseline and highly activated by learning (Ramamoorthi et al., 2011), we predicted that the synaptic properties of the ensemble neurons are not pre-existing, but rather are induced by learning. Like all other activity reporters, *F*-RAM and *N*-RAM can only label ensembles after learning, and thus do not allow us to compare ensemble neurons before and after CFC. However, if the synaptic properties of interest are indeed induced by learning, we reasoned that a stronger learning experience that results in a

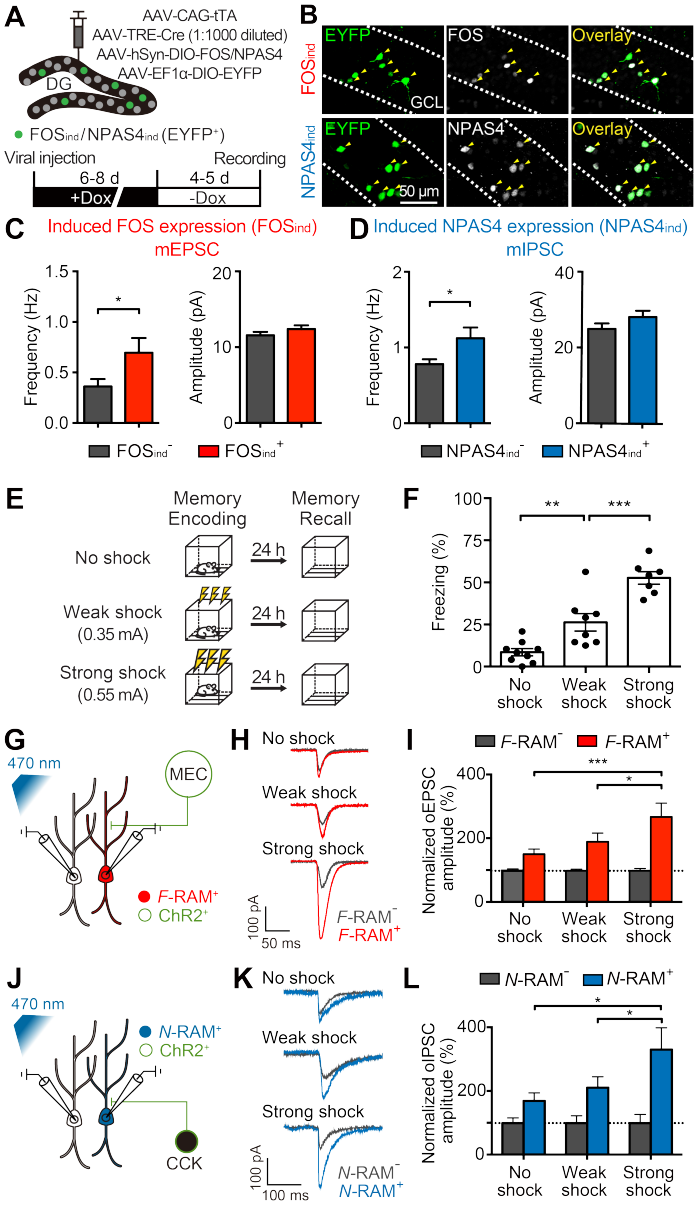

Figure 3.5. Synaptic Changes on Ensemble Neurons Are Correlated with the Strength of Learning.

(A) Experimental scheme for inducing FOS or NPAS4 expression in sparse and randomly selected DG neurons.

(B) Representative images showing induced FOS or NPAS4 expression (FOS_{ind} or $NPAS4_{ind}$) in randomly selected neurons ($EYFP^+$, white arrows).

(C) FOS_{ind} increased mEPSC frequency (Mann-Whitney test; $EYFP^-$, n = 19; $EYFP^+$, n = 20).

(D) $NPAS4_{ind}$ increased mIPSC frequency (n = 19, 20).

(E and F) Experimental scheme (E) showing that training of animals in context A with no shock, weak (0.35 mA) or strong shock (0.55 mA) resulted in different memory strengths, as indicated by levels of freezing (F; one-way ANOVA, Tukey's test, n = 7-9).

(G and H) Experimental scheme (G) and representative traces (H) showing simultaneous recording of oEPSCs on *F*-RAM$^+$ and *F*-RAM$^-$ cells with optogenetic stimulation of the MEC inputs.

(I) *F*-RAM$^+$ cells showed the largest oEPSC amplitudes in the strong shock group (two-way mixed ANOVA, Tukey's test, n = 24, 28, 21 pairs for no shock, weak shock and strong shock, respectively).

(J and K) Experimental scheme (J) and representative traces (K) showing simultaneous recording of oIPSCs on *N*-RAM$^+$ and *N*-RAM$^-$ cells with optogenetic stimulation of the CCK$^+$ interneurons.

(L) *N*-RAM$^+$ cells showed the largest oIPSC amplitudes in the strong shock group (n = 19, 15, 9).

Data are shown as mean ± SEM. *p < 0.05, **p < 0.01, ***p < 0.001.

stronger memory will induce stronger synaptic modifications on the ensemble neurons (Choi et al., 2018). We therefore trained mice in a novel context with no foot shocks, weak foot shocks (0.35 mA) or strong foot shocks (0.55 mA, the strength used in other experiments in this paper) (Figure 3.5E). These 3 treatments resulted in correspondingly different strengths of contextual fear memory, since the animals displayed freezing levels that were closely correlated with the intensity of shocks they received (Figure 3.5F). The numbers of labeled *F*-RAM$^+$ and *N*-RAM$^+$ neurons were comparable in the three groups (Figure 3.6C-D). Measuring oEPSCs from the MEC onto paired *F*-RAM$^+$ and *F*-RAM$^-$ DGCs and oIPSCs from CCK$^+$ interneurons onto paired *N*-RAM$^+$ and *N*-RAM$^-$ DGCs, we found that MEC input to *F*-RAM$^+$ and CCK inhibition on *N*-RAM$^+$ cells were strongest in mice that received strong foot shocks, followed by animals that received weak foot shocks and then those that received no foot shocks (Figure 3.5G-L; CCK$^+$ interneurons were labeled using a genetic intersection strategy described in Figure 3.7I).

Altogether, our data so far support a working model in which the distinct synaptic properties of the ensemble neurons arise from learning-induced synaptic modification as a result of activation of distinct activity-dependent pathways.

3.3.5. The MEC and Its Inputs to the DG Mediate Memory Generalization, whereas DG CCK$^+$ Interneurons Mediate Memory Discrimination

The learning-induced circuit modifications on the *F*-RAM and *N*-RAM ensembles suggest previously unknown roles for the MEC and DG CCK$^+$ interneurons in memory discrimination-generalization. We first directly examined whether the MEC, like the *F*-RAM ensemble, promotes memory generalization. MEC activity was inhibited during memory recall by virally delivering hM4Di to MEC projection neurons. MEC axonal projections to the MML were strongly labeled (Figure 3.7A), indicating precise viral targeting. CNO injection robustly suppressed, although did not completely abolish, the activity of MEC neurons (Figure 3.8A-C).

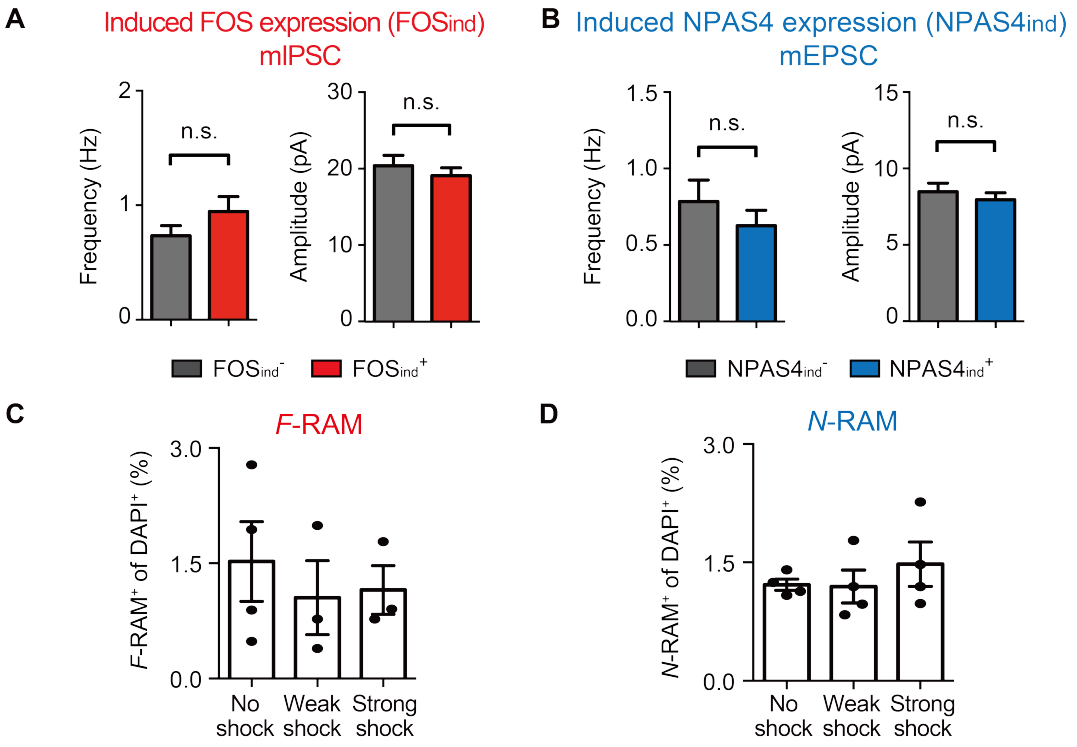

Figure 3.6. Induced FOS Expression Does Not Affect mIPSCs and Induced NPAS4 Expression Does Not Affect mEPSCs.

(A) mIPSC frequencies and amplitudes were similar in neurons with ($EYFP^+$) and without ($EYFP^-$) induced FOS expression (FOS_{ind}). Mann-Whitney test; $EYFP^-$, n = 18; $EYFP^+$, n = 16.

(B) mEPSC frequencies and amplitudes were similar in neurons with ($EYFP^+$) and without ($EYFP^-$) induced NPAS4 expression ($NPAS4_{ind}$, n = 17, 19).

(C) There is no significant difference in the number of *F*-RAM^+ cells under no shock, weak shock and strong shock conditions (one-way ANOVA, n = 3-4).

(D) There is no significant difference in the number of *N*-RAM^+ cells under no shock, weak shock and strong shock conditions (n = 4 per condition).

Data are shown as mean ± SEM.

Using the same memory discrimination-generalization assay described above (Figure 3.7B), we found that inhibiting the MEC suppressed memory generalization and enhanced discrimination between contexts A and B (Figure 3.7C), recapitulating the behavioral effect seen with inhibition of the *F*-RAM ensemble. As a control, viral delivery to the LEC labeled axonal projections to the OML (Figure 3.7A) and inhibiting the LEC in this manner did not affect memory generalization (Figure 3.7D).

To further demonstrate that the MEC-DG pathway promotes memory generalization, we sought to inhibit MEC terminals within the DG optogenetically (Figure 3.7E-F). Illumination of the DG with 561 nm light in animals expressing the inhibitory opsin eNpHR3.0 in the MEC significantly reduced the number of FOS^+ cells in DG, but not in the nearby CA1 that also receives MEC inputs, indicating selective inhibition of the MEC-DG pathway (Figure 3.8E). Inhibiting the MEC-DG projections in this way enhanced memory discrimination between contexts A and B (Figure 3.7G-H), similar to what was observed when the *F*-RAM ensemble was inhibited. In control experiments without light stimulation mice injected with NpHR were indistinguishable from those injected with EYFP (Figure 3.8G). These results reveal a critical role for the MEC-DG pathway in mediating memory generalization, likely involving the *F*-RAM^+ ensemble neurons.

Our finding that the *N*-RAM ensemble receives enhanced inputs from CCK^+ interneurons implies a role for these interneurons in mediating memory discrimination, which we next examined by chemogenetically inhibiting DG CCK^+ interneurons during memory recall. CCK is expressed in both GABAergic and some glutamatergic neurons (Dimidschstein et al., 2016; Taniguchi et al., 2011), so we adopted a genetic intersection strategy to label only the GABAergic CCK^+ cells: using AAV-Dlx5/6-DIO-hM4Di-mCherry to drive Cre-dependent expression of hM4Di from an interneuron-specific promoter, Dlx5/6 (Dimidschstein et al., 2016; Kohwi et al., 2007; Potter et al., 2009), in CCK-Cre mice (Figure 3.7I). The majority of labeled neurons were $GAD67^+$, indicating successful intersectional labeling (Figure 3.7J-K). Labeled neurons also

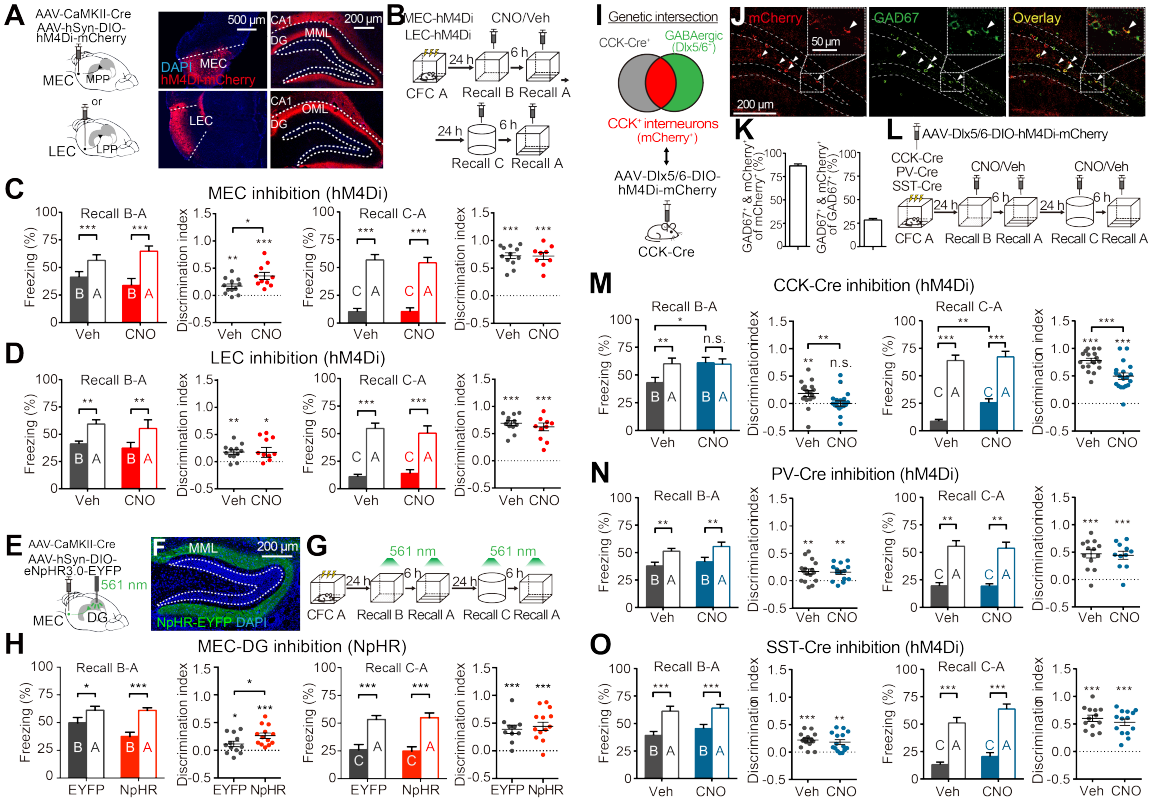

Figure 3.7. The MEC-DG Pathway Mediates Memory Generalization and DG CCK$^+$ Interneurons Mediate Memory Discrimination.

(A) Schematics and representative images showing selective expression of hM4Di in MEC and LEC projection neurons, which send their axonal terminals to the DG MML or OML, respectively.

(B) Experimental scheme for inhibition of MEC or LEC during memory discrimination-generalization.

(C) Inhibiting the MEC enhanced discrimination between contexts A and B (Veh, n = 12; CNO, n = 10), but not A and C (n = 12, 9).

(D) Inhibiting the LEC did not affect generalization between contexts A and B (n = 12, 11) or A and C (n = 12, 10).

(E and F) Schematic (E) and representative image (F) for selective expression of NpHR in MEC projection neurons, which project to the MML of the DG.

(G) Experimental scheme to optogenetically inhibit the MEC-DG pathway during memory recall with 561 nm constant light.

(H) Inhibition of the MEC-DG pathway enhanced discrimination between contexts A and B (EYFP, n = 12; NpHR, n = 13), but not between contexts A and C (n = 10, 13).

(I) Genetic intersection strategy to target CCK$^+$ GABAergic interneurons in DG.

(J) Representative images showing co-localization (white arrows) of labeled cells (mCherry$^+$) with GAD67.

(K) Quantifications showing that labeled neurons were mostly GABAergic (GAD67$^+$) and made up 28% of the GABAergic interneurons in the DG (n = 3).

(L) Experimental scheme to determine which interneuron subtypes are involved in memory discrimination-generalization.

(M) Inhibiting CCK^+ interneurons in the DG reduced discrimination between contexts A and B (Veh, n = 17; CNO, n = 20), and between A and C (n = 17, 19).
(N and O) Discrimination was not affected by inhibiting PV^+ interneurons (N, A and B: n = 16, 14; A and C: n = 13, 11) or SST^+ interneurons (O, A and B: n = 14, 15; A and C: n = 13, 14).
Two-way mixed ANOVA with Sidak's test was used for freezing levels, Mann-Whitney test for comparing discrimination indices, and one-sample t-test to compare discrimination indices with zero. Data are shown as mean ± SEM. *p < 0.05, **p < 0.01, ***p < 0.001.

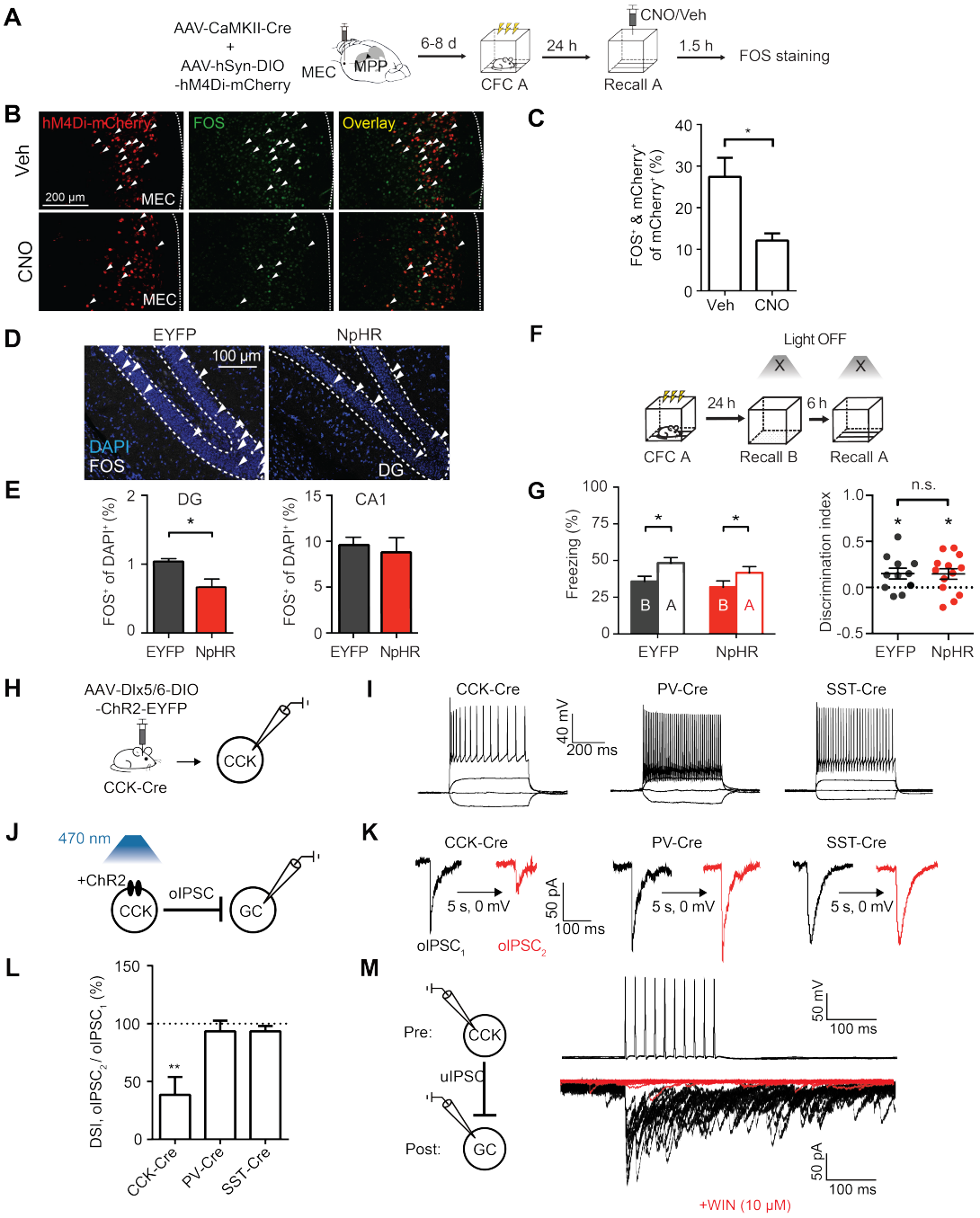

Figure 3.8. Validation Experiments for Manipulating the MEC and CCK$^+$ Interneurons.

(A) Experimental scheme. Mice were co-injected with AAV-CaMKII-Cre and AAV-hSyn-DIO-hM4Di-mCherry to express the inhibitory DREADD hM4Di in MEC excitatory neurons (CaMKII$^+$). Mice were fear conditioned in context A, memory was recalled 24 hours later and animals sacrificed 1.5 hours after recall. CNO (4 mg/kg) or vehicle (Veh) was injected i.p. 30 minutes before recall. Neuronal activity was examined by FOS staining.

(B) Representative images of the MEC (dashed lines) showing hM4Di and FOS expression. White arrows indicate double-positive cells.

(C) Chemogenetic inhibition robustly suppressed, but did not completely abolish, the activity of MEC projection neurons. Percentages of hM4Di-mCherry$^+$ cells that were also FOS$^+$ were quantified (Mann-Whitney test, n = 4 per group).

(D) Representative images showing FOS$^+$ cells (white arrows) in the DG GCL (dashed lines) after recall in context A.

(E) Optogenetic inhibition of the MEC-DG pathway reduced the number of FOS$^+$ cells in DG but not in CA1 after recall (Mann-Whitney test, n = 4 per group).

(F) Experimental scheme. Memory discrimination-generalization was examined in the absence of 561 nm laser stimulation (light OFF). Animals were injected with NpHR or EYFP in the MEC and implanted with optical fibers in the DG.

(G) In the absence of laser stimulation, NpHR and EYFP groups showed comparable discrimination between the similar contexts A and B (two-way mixed ANOVA with Sidak's test was used for freezing levels, Mann-Whitney test for comparing discrimination indices, and one-sample t-test to compare discrimination indices with zero; EYFP, n = 11; NpHR, n = 13).

(H) Experimental scheme. Putative CCK$^+$, PV$^+$ and SST$^+$ interneurons were identified by injecting a reporter virus (AAV-Dlx5/6-DIO-ChR2-EYFP) into CCK-Cre, PV-Cre and SST-Cre mice. Whole-cell patch-clamp recordings were carried out on labeled cells to examine their firing properties.

(I) CCK$^+$ interneurons (identified by EYFP expression) showed the strongest firing adaptation among the three interneuron subtypes. Example traces showing the membrane potentials of CCK$^+$, PV$^+$ and SST$^+$ interneurons in response to -50, 0, 50, and 500 pA current injections.

(J) Schematic for measurement of depolarization-induced suppression of inhibition (DSI). ChR2 (AAV-Dlx5/6-DIO-ChR2-EYFP) was expressed in CCK$^+$, PV$^+$ or SST$^+$ interneurons to induce optically evoked IPSCs (oIPSCs).

(K) DSI was observed in the CCK$^+$ interneuron (CCK) to granule cell (GC) synapses. oIPSCs were induced by 2 ms 470 nm LED light stimulation and recorded in GCs voltage clamped at -70 mV, with high-Cl$^-$ internal solution, in the presence of APV (50 μM) and DNQX (20 μM). DSI was induced by elevating the holding potential of GCs to 0 mV for 5 s. oIPSCs recorded before ($oIPSC_1$) and 200 ms after ($oIPSC_2$) depolarization, averaged from ten sweeps, were compared to calculate DSI.

(L) Quantification of DSI (one-way ANOVA, one-sample t-test for individual columns, n = 6 per group).

(M) Asynchronous releases were observed in the CCK to GC synapses, and were blocked by bath application of WIN 55,212-2 (WIN, 10 uM). Paired whole-cell patch-clamp recordings targeting presynaptic CCK$^+$ interneurons and postsynaptic GCs were carried out. Superimposed traces (black) from 15 sweeps are shown. Trains of ten action potentials (50 Hz) were evoked in the presynaptic CCK$^+$ interneurons, and unitary IPSCs (uIPSCs) were recorded in the postsynaptic GCs voltage clamped at -70 mV. uIPSCs were recorded with high-Cl$^-$ internal solution in the presence of APV (50 μM) and DNQX (20 μM). Red traces show superimposed traces of 15 sweeps after bath application of WIN.

Data are shown as mean ± SEM. *$p < 0.05$, **$p < 0.01$.

displayed the electrophysiological properties reported for CCK^+ interneurons, including adaptive firing, depolarization-induced suppression of inhibition (DSI), and asynchronous synaptic transmission (Bartos and Elgueta, 2012) (Figures 3.8H-M). Using the same behavioral assay (Figure 3.7L), we then found that inhibiting DG CCK^+ interneurons abolished memory discrimination between contexts A and B, and also significantly reduced discrimination between A and C (Figure 3.7M). In contrast, inhibiting PV^+ or SST^+ interneurons in the DG did not affect memory discrimination (Figures 3.7N-O). These results suggest that DG CCK^+ interneurons are involved in memory discrimination.

3.4. Discussion

In this study, we describe synaptic mechanisms underlying the functional heterogeneity of memory engrams. The *F*-RAM and *N*-RAM ensembles show "heterogeneous plasticity" (Grewe et al., 2017) after learning: they selectively recruit excitatory and inhibitory inputs, respectively, from different upstream circuits. Besides, we uncover circuit components that are selectively associated with each ensemble and regulate the discrimination-generalization balance: the MEC is required for memory generalization and DG CCK^+ interneurons for memory discrimination.

The synaptic properties observed in *F*-RAM^+ and *N*-RAM^+ neurons (Figure 3.1A-C) are most likely the results of neuronal activity triggered during contextual fear learning, because these synaptic properties correlate with memory strength and can be induced by the expression of FOS and NPAS4, respectively (Fleischmann et al., 2003; Lin et al., 2008; Sun and Lin, 2016). It's consistent with previous findings that synaptic changes onto *Fos*-expressing cells were blocked by protein-synthesis inhibitor administrated immediately after training (Ryan et al., 2015). However, since the ensembles can only be labeled after they have been activated, we cannot exclude the possibility that subtle differences between these two neuronal ensembles already pre-exist before the experience.

In addition to the potentiation of excitatory inputs, which have been the primary focus of mechanisms for memory encoding, our data support the emerging view that the plasticity of inhibitory inputs is also heavily involved in the process (Litwin-Kumar and Doiron, 2014; Vogels et al., 2011; Xue et al., 2014b). Furthermore, the strengthening of excitatory and inhibitory inputs occurs on two different neuronal ensembles within the memory engram. This could provide a mechanism for a neural system to balance the behavioral output (discrimination vs. generalization) through the "push and pull" of different neuronal ensembles. It remains to be seen whether the *F*-RAM and *N*-RAM ensembles interact with each other.

Our data strongly support a role for the MEC-DG pathway in memory generalization, in line with observations that grid cells in the MEC maintain relatively stable spatial firing patterns across similar contexts (Fyhn et al., 2007; Leutgeb et al., 2007). In our study, memory retrieval (in context A) was not impaired by suppressing MEC activity (Figure 3.7C). This observation, though consistent with a number of published studies (Hales et al., 2014; Kanter et al., 2017), is contradictory to some others (Kitamura et al., 2015; Miao et al., 2015; Zhao et al., 2016). The discrepancy may be explained by the different MEC cell populations being targeted and the different manners they are being inhibited (e.g. via lesion, optogenetics or chemogenetics). Future work is needed to pinpoint which MEC subpopulations (Diehl et al., 2017) relay the generalization signals to the DG.

Of the three major subtypes of interneurons providing inhibitory inputs to DG granule cells, CCK^+ and not PV^+ or SST^+ interneurons are important for memory discrimination. The reason behind this specific requirement for CCK^+ neurons is unknown at the moment. In fact, the roles of CCK^+ interneurons in learning and memory haven't been extensively studied. CCK^+ interneurons are known to have unique synaptic outputs, such as endocannabinoid-dependent short-term and long-term synaptic plasticity (Castillo et al., 2012; Hartzell et al., 2018) and asynchronous synaptic release (Hefft and Jonas, 2005), which may be related to their unique role

in memory discrimination. Our findings open exciting opportunities for future work to identify specific synaptic mechanisms provided by CCK^+ interneurons to regulate memory discrimination.

3.5. Methods

Mice

C57BL/6 male and female mice 7-11 weeks old were used for all experiments. Wildtype mice were purchased from the Charles River Laboratory. *Npas4*$^{flx/flx}$ (*Npas4* conditional knockout) mice were generated previously (Lin et al., 2008) and *Fos*$^{flx/flx}$ (*Fos* conditional knockout) mice were generously provided by Dr. Ming Xu at the University of Chicago. Gad2-Cre (*Gad2*$^{tm2(cre)Zjh}$/J), CCK-Cre (*Cck*$^{tm1.1(cre)Zjh}$/J), PV-Cre (*Pvalb*$^{tm1(cre)Arbr}$/J), SST-Cre (*Sst*$^{tm2.1(cre)Zjh}$/J) and Fos-Cre^{ER} (*Fos*$^{tm1.1(cre/ERT2)Luo}$/J) mice were purchased from the Jackson Laboratory. To produce Cre-expressing animals, heterozygous or homozygous mice carrying the Cre allele were bred with wildtype animals from the Charles River Laboratory. All mice were housed with a 12 hour light-dark cycle. Animal protocols were performed in accordance with NIH guidelines and approved by the Massachusetts Institute of Technology Committees on Animal Care and the Institutional Animal Care and Use Committee at SUNY Upstate Medical University.

Viral vectors

AAV1-hSyn-GFP, AAV1-hSyn-GFP-Cre, AAV1-EF1α-DIO-ChR2-EYFP were obtained from the University of Pennsylvania Vector Core via Addgene. All other AAVs were produced in house. AAVs were generated in HEK293T cells and purified using an adapted h gradient purification protocol as previously described (Sørensen et al., 2016). Viral dilutions were determined for individual experiments through pilot injections.

In experiments to label the *F*-RAM and *N*-RAM ensembles *in vitro* and *in vivo*, AAV2/AAV8-*F*-RAM-d2tTA-TRE-mKate2 or AAV2/AAV8-*N*-RAM-d2tTA-TRE-mKate2

virus was used. AAV2/AAV8s were mixtures of AAV2/2 (rep/cap) and AAV2/8 serotypes at a 1:1 ratio (Sørensen et al., 2016). In most experiments a control virus (AAV2/AAV8-EF1α-EGFP) was co-injected to determine the injection accuracy and infection efficiency.

To examine optically evoked IPSCs (oIPSCs) from DG interneurons, AAV2/AAV8-*F*-RAM-d2tTA-TRE-mKate2 or AAV2/AAV8-*N*-RAM-d2tTA-TRE-mKate2 virus was co-injected with AAV2/AAV8-EF1α-DIO-ChR2-EYFP virus into Gad2-Cre mice. To examine oIPSCs from DG CCK^+ interneurons, AAV9-*F*-RAM-d2tTA-TRE-mKate2 or AAV9-*N*-RAM-d2tTA-TRE-mKate2 virus was co-injected with AAV9-Dlx5/6-DIO-ChR2-EYFP virus into CCK-Cre mice. To examine optically evoked EPSCs (oEPSCs) that originate from the medial entorhinal cortex (MEC) and the lateral entorhinal cortex (LEC), AAV9-EF1α-DIO-ChR2-EYFP and AAV1-CaMKII-Cre-GFP were co-injected into these regions, and AAV9-*F*-RAM-d2tTA-TRE-mKate2 was injected into the DG. To examine oEPSCs that originate from the dentate hilus, AAV9-EF1α-DIO-ChR2-EYFP and AAV1-CaMKII-Cre-GFP were co-injected into the contralateral DG, and AAV9-*F*-RAM-d2tTA-TRE-mKate2 was injected into the ipsilateral DG, where whole-cell patch-clamp recordings were carried out.

To over-express FOS or NPAS4 in sparse populations of DG neurons, animals were injected with the following viral cocktail: AAV9-CAG-tTA, AAV1-TRE-Cre (1:1,000 dilution), AAV9-hSyn-DIO-FOS/NPAS4, and AAV1-EF1α-DIO-EYFP.

In experiments to suppress the activity of MEC or LEC projection neurons, AAV1-CaMKII-Cre-GFP and AAV9-hSyn-DIO-hM4Di-mCherry were co-injected into the MEC or LEC. In experiments to optogenetically inhibit the MEC-DG pathway, AAV9-EF1α-DIO-eNpHR3.0-EYFP or AAV9-EF1α-DIO-EYFP was co-injected with AAV1-CaMKII-Cre-GFP into the MEC. To manipulate the activity of DG interneurons with DREADD, AAV9-Dlx5/6-DIO-hM4Di-mCherry was injected into CCK-Cre, PV-Cre or SST-Cre mice.

Electrophysiology

Mice were subjected to electrophysiology 24-48 hours after CFC. Mice were anesthetized and perfused with carbogenated (95% O_2, 5% CO_2) ice-cold cutting solution containing (in mM): 210 sucrose, 2.5 KCl, 1.24 NaH_2PO_4, 8 $MgCl_2$, 1 $CaCl_2$, 26 $NaHCO_3$, 20 Glucose and 1.3 sodium-L-ascorbate, ~340 mOsm osmolarity, pH 7.3. Brains were then immediately dissected out. 300 μm transverse slices were cut using a vibratome (VT1200, Leica). Slices were transferred to warm (32 ˚C) carbogenated recovery solution, containing 50% cutting solution and 50% ACSF. ACSF contains (in mM): 119 NaCl, 2.5 KCl, 1.24 NaH_2PO_4, 1.3 $MgCl_2$, 2.5 $CaCl_2$, 26 $NaHCO_3$, and 10 glucose, 305 mOsm osmolarity, pH 7.3. Sliced were recovered at 32 ˚C for 15 minutes, then transferred to another chamber filled with room temperature (~23 ˚C) ACSF. Slices were kept in ACSF for at least 30 minutes before recording.

All experiments were performed in a recording chamber perfused with carbogenated ACSF maintained at room temperature at a flow rate of 2 mL/min. Whole-cell patch-clamp recordings were performed using borosilicate glass pipettes (3-6 MΩ tip resistance). mEPSCs were pharmacologically isolated with 0.5 μM tetrodotoxin (TTX, Tocris) and 50 μM picrotoxin (Tocris), and recorded from cells voltage clamped at -70 mV using Cs-based internal solution containing (in mM): 130 $CsMeSO_3$, 10 phosphocreatine, 1 $MgCl_2$, 10 HEPES, 0.2 EGTA, 4 Mg-ATP, 0.5 Na-GFP, pH adjusted to 7.25 with CsOH, 295 mOsm osmolarity. mIPSCs were isolated with 0.5 μM TTX, 50 μM APV (Tocris) and 20 μM DNQX (Tocris), and recorded from cells voltage clamped at -70 mV using high-Cl internal solution containing (in mM): 103 CsCl, 12 $CsMeSO_3$, 5 TEA-Cl, 10 HEPES, 4 Mg-ATP, 0.5 Na-GTP, 0.5 EGTA, 1 MgCl2, pH adjusted to 7.25 with CsOH, 295 mOsm osmolarity. Intrinsic excitability and passive membrane properties were recorded in the current clamp mode with the following internal solution (in mM): 130 K^+-D-gluconate, 10 KCl, 10 HEPES, 4 Mg-ATP, 0.5 Na-GTP, 0.2 EGTA, 1 MgCl2, pH adjusted to 7.25 with CsOH, 295 mOsm osmolarity. To determine the excitability of cells, membrane

potentials were measured in response to intracellular injection of step currents (500 ms duration, magnitudes ranging from -20 to 200 pA in steps of 20 pA). Data were collected using a Multiclamp 700B (Molecular Devices), filtered at 3 kHz and digitized at 10 kHz using a Digidata 1440A and Clampex 10.2 software (Molecular Devices). Recordings with access resistance greater than 30 MΩ or changes exceeding 15% were discarded.

To record evoked EPSCs (eEPSCs) from different excitatory pathways to the DG, stimulating theta glass pipettes (World Precision Instruments) with broken tips (~10-20 μm) were filled with ACSF and placed in the inner molecular layer (IML, <40um from the border of the granule cell layer), middle molecular layer (MML, middle third of the molecular layer) or outer molecular layer (OML, outer third of the molecular layer) to stimulate different excitatory inputs onto DG granule cells (GCs). Bipolar square-wave voltage pulses (100-200 μs, 5-25 V) were delivered through a stimulus isolator (ISO-Flex, AMPI). Stimulation intensity was adjusted to obtain comparable amplitudes of AMPA eEPSCs (50-150 pA) across conditions. Paired whole-cell recordings were carried out on labeled (*F*-RAM$^+$ or *N*-RAM$^+$) and unlabeled neighboring neurons. Cells were first voltage clamped at -70 mV to record AMPA currents, and paired pulses with a 100 ms interval were stimulated. The peak amplitude of the first pulse was used to calculate the eEPSC amplitudes. The cells were subsequently voltage clamped at +40 mV and a single pulse was stimulated. NMDA currents were measured at 100 ms after the onset of the stimulation. Values were averaged from 10 sweeps that were repeated every 20-30 seconds. Picrotoxin (50 μM) was added throughout the recording to block $GABA_A$ receptors. To confirm the specificity of stimulations, the mGluR2/3 agonist DCG-IV (1 μM) was routinely bath applied at the end of experiments, which reduced the amplitudes of eEPSCs selectively evoked by stimulating the MEC-DG pathway (medial perforant path, MPP).

To record optically evoked IPSCs (oIPSCs) or optically evoked EPSCs (oEPSCs) in the DG, 2 ms 470 nm LED stimulations at 0.1, 0.25, 0.50, 0.75, 1.00, 1.50 mW/mm^2, generated from

a mounted LED (Thorlabs), were controlled by TTL input and delivered through the 40× objective. Paired whole-cell recordings were carried out on labeled (*F*-RAM$^+$ or *N*-RAM$^+$) and unlabeled neighboring neurons. oIPSCs were recorded, in the presence of DNQX (20 μM) and APV (50 μM), from cells voltage clamped at 0 mV with Cs-based internal solution. In the experiments where CCK$^+$ interneurons were specifically stimulated, oIPSCs were recorded from cells voltage clamped at -70 mV with high-Cl internal solutions to minimize the effects of depolarization-induced suppression of inhibition (DSI) from CCK$^+$ interneurons. Average peak responses were calculated from 10 sweeps, stimulated every 10-15 seconds. Paired light pulses with an interval of 200 ms were given at 0.50 mW/mm^2 to measure paired-pulse ratios. To block transmission from individual interneuron subtypes, ω-agatoxin IVa (AgTx, 0.5 μM, Bachem), ω-conotoxin GVIa (CnTx, 1 μM, Bachem) and WIN 55,212-2 (WIN, 10 μM, Tocris) were bath applied in the ACSF during oIPSC recordings. oEPSCs were recorded in the presence of picrotoxin (50 μM), TTX (0.5 μM) and 4-aminopyridine (100 μM) from cells voltage clamped at -70 mV with Cs-based internal solution.

To characterize the CCK$^+$ interneurons, depolarization-induced suppression of inhibition (DSI) was induced by elevating the holding potential of the postsynaptic GCs from -70 mV to 0 mV for 5 seconds. oIPSCs were measured in GCs voltage clamped at -70 mV and recorded with high-Cl$^-$ internal solution in the presence of APV (50 μM) and DNQX (20 μM). oIPSCs recorded before and 200 ms after the depolarization, averaged from 10 sweeps, were compared to calculate the DSI. To examine asynchronous release from CCK$^+$ interneurons, trains of ten action potentials (50 Hz) were evoked in the presynaptic CCK$^+$ interneurons, and unitary IPSCs (uIPSCs) recorded in the postsynaptic GCs voltage clamped at -70 mV. uIPSCs were also measured in the presence of WIN (10 μM) in the ACSF.

Data were analyzed using MiniAnalysis (Synaptosoft) and Clampfit 10.2 (Molecular Devices) by investigators that were blind to the experimental conditions.

Optogenetics

To optogenetically inhibit the MEC-DG pathway, animals were bilaterally implanted with optical fibers (Thorlabs) in the DG after viral injection into the MEC. After CFC, animals were recalled in different contexts with optogenetic inhibition. Laser stimulation (561 nm, constant, 10 mW) was generated using a 561 nm DPSS laser (Opto Engine LLC) and delivered bilaterally to the DG through 200 μm 0.22 NA optical fibers (Thorlabs). A rotatory joint (Thorlabs) was used to allow animals to move freely. The laser was constantly on during the entire 4-minute recall session.

Chapter 4

The Roles of Activity-dependent Pathways in Engrams

Chapter 4 – The Roles of Activity-dependent Pathways in Engrams

4.1. Abstract

Activity-dependent pathways are wildly used to define neuronal ensembles within the memory engram. However, it remains unclear how these activity-dependent pathways contribute to the formation of memory engrams. Our previous works demonstrated that the *N*pas4-dependent ensembles received enhanced inhibitory synaptic inputs. Here we test if *Npas4*-dependent pathway is directly involved in the regulation of inhibition. We found that deletion of *Npas4* in the hippocampal dentate gyrus (DG) reduced inhibitory synaptic inputs and abolished contextual fear memory discrimination, recapitulating the functions of the *N*pas4-dependent ensemble. Consistently, deletion of *Npas4* in the primary visual cortex (V1) also selectively decreased inhibitory drive. Moreover, the loss of *Npas4* in V1 led to impaired orientation-selective habituation (OSH), a form of visual recognition memory. These results together suggest that *Npas4* regulates an activity-dependent pathway that controls inhibitory synapses and are indispensable for multiple forms of memories.

4.2. Introduction

Neuronal ensembles defined by the induction of activity-dependent pathways undergo experience-dependent plasticity and drive memory-guided behavioral outputs (Chapter 2&3). However, it remains unknown whether activity-dependent pathways merely serve as the markers for the ensembles, or they play causal roles in determining the plasticity and functionality of the memory engram. Activity-dependent pathways are known to mediate long-lasting synaptic changes and memory formation (Flavell and Greenberg, 2008; Fleischmann et al., 2003; Korte et al., 1995; Sun and Lin, 2016). Disruption of learning-related gene transcription or translation prevented synaptic plasticity and the formation of long-term memory (Meiri and Rosenblum, 1998; Schafe and LeDoux, 2000). Furthermore, synaptic modifications onto the *Fos*-expressing engram neurons were abolished by blocking *de novo* protein synthesis triggered by learning (Ryan et al., 2015). These results together suggest a key role of activity-dependent pathways in the formation of memory engram. However, further investigations are needed to pinpoint the specific contribution of each activity-dependent pathway. Such investigations have profound translational implications, as they may reveal new therapeutic targets for memory-related disorders such as amnesia and Alzheimer's disease (Burns and Iliffe, 2009; Morris and Kopelman, 1986).

Among the genes that are required for learning and memory, we have focused on *Npas4*, an immediate early gene (IEG) that is unique in the following aspect: 1) unlike most activity-dependent genes, *Npas4* is only expressed in neurons; 2) *Npas4* is unique in that it is activated selectively by neuronal activity, and not by extracellular stimuli such as growth factors and neurotrophins; 3) *Npas4* protein appears to directly control the expression of a very large number of important activity-dependent genes, including *BDNF*, *Nptx2*, and *Plk2*; 4) *Npas4* preferentially regulate inhibitory circuits (Bloodgood et al., 2013; Lin et al., 2008; Ramamoorthi et al., 2011; Spiegel et al., 2014; Sun and Lin, 2016; Weng et al., 2018). Studying the functions of *Npas4*

therefore provides a unique opportunity to understand the related molecular and synaptic processes mediate by *Npas4* during memory formation.

Our previous works demonstrated that the *Npas4*-dependent ensembles in the DG received enhanced inhibitory inputs (Figure 2.7). However, it remains unclear if *Npas4* is directly involved in the regulation of inhibition in the DG. Initial studies on *Npas4* demonstrated that it selectively up-regulated inhibitory synapses in the hippocampal CA1 region (Bloodgood et al., 2013; Lin et al., 2008). However, a recent study revealed that *Npas4* did not regulate inhibitory synapses in the hippocampal CA3, but selectively down-regulated excitatory inputs from the mossy fiber pathway (Weng et al., 2018). Besides, *Npas4* in the primary visual cortex (V1) selectively recruited excitatory inputs onto SST-expressing interneuron (Spiegel et al., 2014). These date together suggest that *Npas4* seems to either increase the inhibitory tone or reduce the excitatory tone in the network, reducing the excitatory-inhibitory (E-I) ratio (Sun and Lin, 2016; Vogels et al., 2011; Xue et al., 2014b). However, the region-specific synaptic functions of *Npas4* remain to be further explored. Therefore, we study the synaptic functions of *Npas4* in two brain regions, the DG and V1. To also understand how the *Npas4*-dependent pathway contributes to memory formation, we examine the necessity of *Npas4* in the DG for contextual fear memory (Ramamoorthi et al., 2011; Rudy et al., 2004), and in V1 for visual recognition memory (Cooke et al., 2015; Fong et al., 2019; Kim et al., 2020).

4.3. Results

4.3.1. *Npas4* in the DG Regulates Inhibitory Synapses and Memory Discrimination

The *Npas4*-dependent ensemble in the DG received enhanced inhibitory inputs (Figure 3.1), but it's unclear if this synaptic phenotype was mediated by *Npas4 per se*. To study the role of *Npas4* in regulating inhibitory synapses, we examined the synaptic properties of dentate granule cells

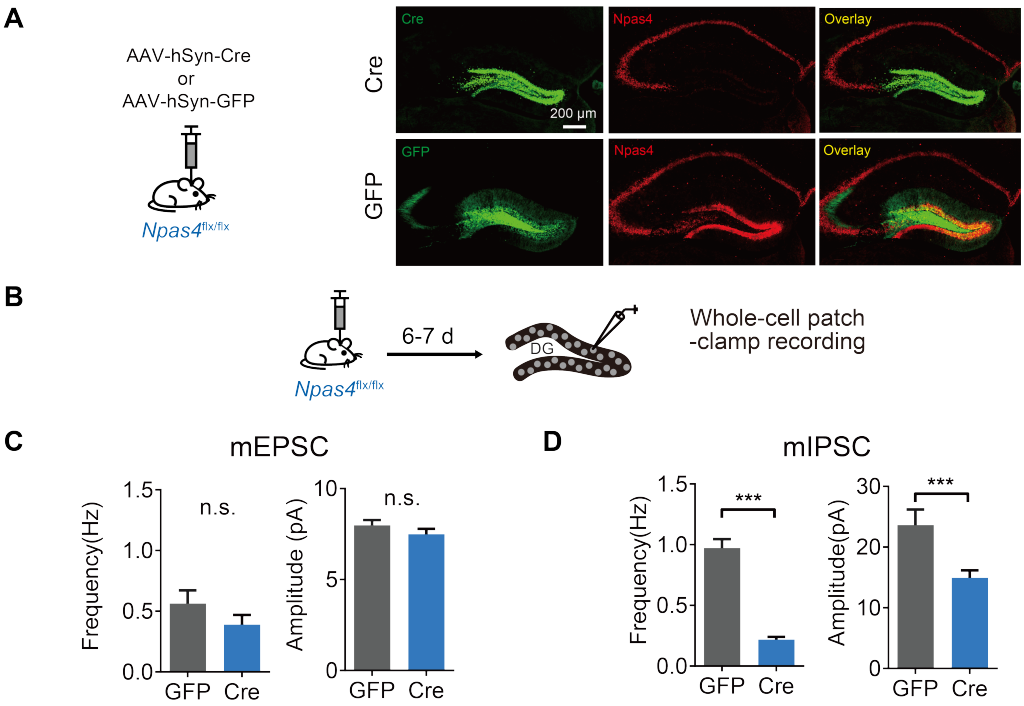

Figure 4.1. Acute Deletion of *Npas4* in the DG Reduced Inhibitory Synaptic Transmission.

(A) Schematics and representative imaging showing acute deletion of *Npas4* by injecting Cre-expressing viruses into *Npas4* conditional knockout mice (*Npas4*$^{flx/flx}$). *Npas4* expression was induced by KA-induced seizure (20 mg/kg).

(B) Experimental scheme to measure mEPSCs and mIPSCs with acute deletion of *Npas4* in the DG.

(C) Animals with acute deletion of *Npas4* showed normal mEPSCs (GFP, n = 13; Cre, n = 17). Mann-Whitney test.

(D) Animals with acute deletion of *Npas4* showed reduced mIPSC frequency and amplitude (n = 16, 20). Mann-Whitney test, ***p < 0.001.

(DGCs) after *Npas4* acute deletion. We delivered Cre-expressing viruses (AAV-hSyn-Cre) in the DG of adult *Npas4* conditional knockout animals (*Npas4*$^{flx/flx}$) to acutely deleted *Npas4*. Cre expression was selectively detected in the DG, but not CA3 or CA1 of the hippocampus, which blocked the seizure-induced *Npas4* expression in the DG (Figure 4.1A). Whole-cell patch-clamp recordings were then carried out to compare mEPSC and mIPSC between *Npas4* knockout animals with control animals (Figure 4.1B). *Npas4* acute deletion did not affect mEPSCs (Figure 4.1C). However, mIPSC frequencies and amplitudes were substantially reduced in the *Npas4* knockout animals (Figure 4.1D). These results suggest that *Npas4* up-regulates inhibitory synapses in the DG, recapitulating our previous finding that the *Npas4*-dependent ensembles receive enhanced inhibitory inputs (Figure 3.1). The observed role of *Npas4* in regulating inhibitory synapses is also consistent with previous studies on the synaptic function of *Npas4* in CA1 (Bloodgood et al., 2013; Hartzell et al., 2018).

The *Npas4*-dependent ensemble in the DG mediates contextual fear memory discrimination (Figure 2.7). However, the causal role of *Npas4* in memory discrimination remains unclear. Therefore, animals with *Npas4* deletion in the DG were tested in the contextual fear memory discrimination-generalization assay as described before (Figure 4.2A). We found that acute deletion of *Npas4* abolished the discrimination between similar contexts A and B (Figure 4.2B). Freezing levels in context A were not significantly changed, suggesting that memory expression towards the original stimuli was normal. In addition, discrimination between distinct contexts A and C was not affected, suggesting that *Npas4* deletion did not cause general motor or anxiety deficit. Together, these results suggest that *Npas4* in the DG, similar to the *Npas4*-dependent ensemble, mediates memory discrimination.

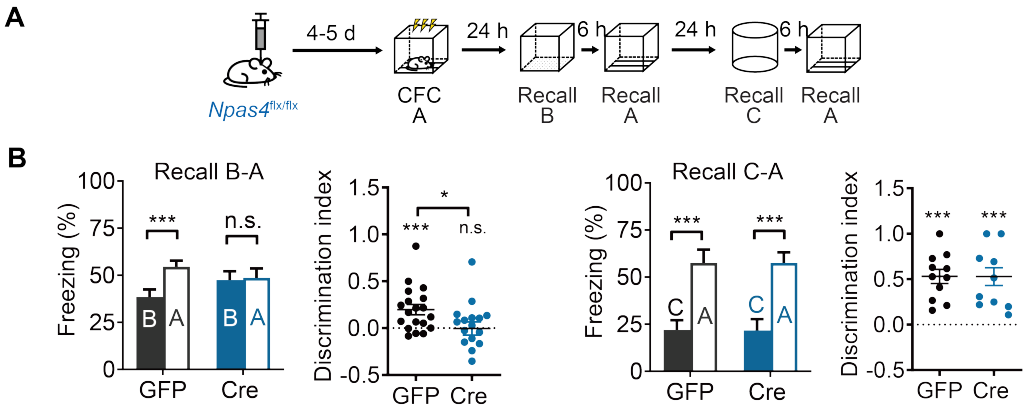

Figure 4.2. Acute Deletion of *Npas4* in the DG Impaired Memory Discrimination.

(A) Experimental scheme to examine the causal roles of *Npas4* in contextual fear memory discrimination-generalization.

(B) Animals wih acute deletion of *Npas4* showed impaired discrimination between contexts A and B (GFP, n = 19; Cre, n = 17), but not A and C (n = 11, 10). Two-way mixed ANOVA with Sidak's test was used for freezing levels, Mann-Whitney test for comparing discrimination indices, and one-sample t-test to compare discrimination indices with zero. Data are shown as mean ± SEM. *p < 0.05, ***p < 0.001.

4.3.2. Deleting *Npas4* in the V1 Selectively Reduces Inhibitory Inputs from PV^+ Interneurons

How general is the role of *Npas4* in regulating inhibitory synapses? Which subtypes of inhibitory synapses does it control? We further study how *Npas4* deletion affects the inhibitory microcircuit in another brain region, the V1. We decided to focus on the V1 because it has been shown that *Npas4* is robustly induced in the V1 in response to visual stimulation (Lin et al., 2008; Mardinly et al., 2016; Spiegel et al., 2014). We acutely deleted *Npas4* from the V1 by delivering Cre-expressing viruses (AAV-hSyn-Cre) in adult *Npas4* conditional knockout animals ($Npas4^{flx/flx}$) (Figure 4.3A). Seizure-induced expression of *Npas4* in the V1 was largely abolished in animals injected with Cre-expressing viruses, suggesting effective gene knockout (Figure 4.3B). Whole-cell patch-clamp recordings were carried out to measure mEPSC and mIPSC from randomly selected layer 4 neurons in the V1 binocular region (Figure 4.3C). We found that *Npas4* deletion substantially reduced the inhibitory synaptic drive onto layer 4 neurons (Figure 4.3E), but leave the excitatory transmission unaffected (Figure 4.3D). We also confirmed these findings by measure sEPSC and sIPSC. *Npas4* deletion substantially reduced the sIPSC frequency, but did not affect sEPSCs (Figure 4.53-G).

Neurons in the cortex receive inhibitory synaptic inputs mainly from PV^+ and SST^+ interneurons (Isaacson and Scanziani, 2011; Jiang et al., 2015; Kullmann et al., 2012). To pinpoint which subtypes of interneurons were affected by *Npas4* deletion, we measured inhibitory inputs onto V1 layer 4 neurons from either PV^+ or SST^+ interneurons. Dual patch-clamp recordings were carried out on parried presynaptic PV^+ or SST^+ neurons and postsynaptic pyramidal cells (PCs). PV^+ and SST^+ interneurons were identified and distinguished by their characteristic firing patterns (non-adaptive vs. adaptive) and short-term plasticity (depression vs. non-depression) (Isaacson and Scanziani, 2011; Jiang et al., 2015; Miao et al., 2016). Unitary

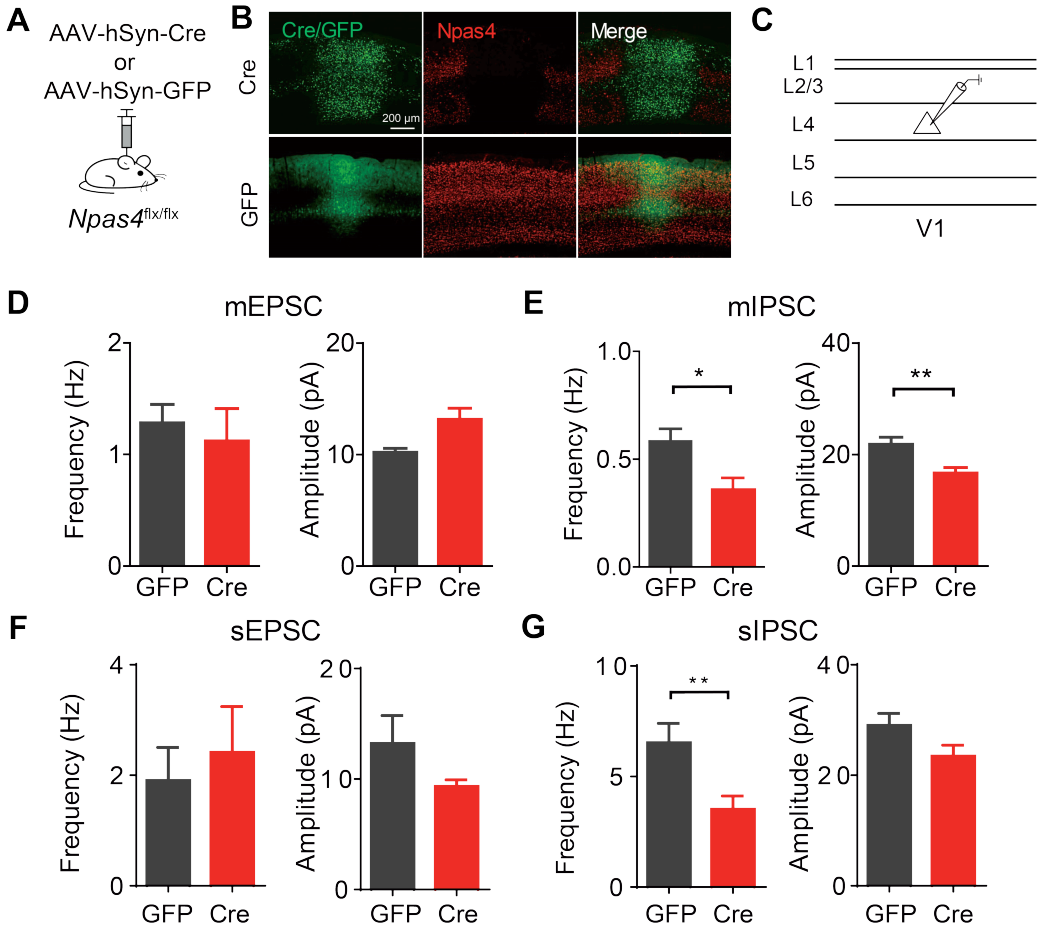

Figure 4.3. Acute Deletion of *Npas4* in the V1 Reduced Inhibitory Synaptic Inputs onto Layer 4 Pyramidal Cells.

(A and B) Schematics (A) and representative imaging (B) showing acute deletion of *Npas4* by injecting Cre-expressing viruses into *Npas4* conditional knockout mice (*Npas4*$^{flx/flx}$). *Npas4* expression was induced by PTZ-induced seizure (50 mg/kg).

(C) Experimental scheme to measure mEPSCs and mIPSCs in V1 layer neurons with acute deletion of *Npas4*.

(D) Animals with acute deletion of *Npas4* showed normal mEPSCs (GFP, n = 18; Cre, n = 14). Mann-Whitney test.

(E) Animals with acute deletion of *Npas4* showed reduced mIPSC frequency and amplitude (n = 30, 22). Mann-Whitney test, *p < 0.05, **p < 0.01.
(F) Animals with acute deletion of *Npas4* showed normal sEPSCs (GFP, n = 14; Cre, n = 15). Mann-Whitney test.

(G) Animals with acute deletion of *Npas4* showed reduced sIPSC frequency (n = 17, 17). Mann-Whitney test, **p < 0.01.

IPSCs (uIPSCs) were measured on postsynaptic PCs during the simulations of presynaptic PV^+ or SST^+ neurons (Figure 4.4A and Figure 4.4D). We found that amplitudes of uIPSC from PV-PC synapses were significantly reduced in *Npas4* deleted animals, suggesting the *Npas4* in the V1 regulates inhibitory inputs from PV+ interneurons (Figure 4.4B). Consistently, the probability that the recorded pairs of presynaptic PV^+ cells and postsynaptic PC were connected was also lower in the knockout group. Short-term plasticity was not affected, suggesting that presynaptic release properties were unchanged (Figure 4.4C). On the contrary, SST-PC synapses were not affected by *Npas4* deletion (Figure 4.4D-E). Taken together, these findings suggest that *Npas4* in the V1 selectively regulates the inhibitory inputs from PV^+ interneurons.

4.3.3. *Npas4* in the V1 Is Required for Visual Recognition Memory

How does the loss of *Npas4* in the V1 affect learning and memory? To this end, we have examined the role of *Npas4* in a form of V1-dependent visual recognition memory. Familiarization of phase-reversing grating stimuli leads to the formation of long-term visual recognition memory in mice, manifested as orientation-selective habituation (OSH) (Cooke et al., 2015). As a result, animals showed reduced visually-induced fidget (Vidget) behaviors to the familiar, but not a novel, stimulus (Figure 4.5A). In addition, the grating stimuli that elicit OSH also induces stimulus-selective response potentiation (SRP) of visually evoked potentials (VEPs) recorded in the layer 4 of the V1 (Cooke and Bear, 2010; Cooke et al., 2015; Frenkel et al., 2006). Importantly, inhibitory circuits are believed to be essential for the normal expression of SRP and OSH (Kaplan et al., 2016; Kim et al., 2020). This implies that the *Npas4*-dependent pathway, which regulates inhibitory synapses, may be involved in SRP and OSH.

Here, we directly examine how the disruption of the *Npas4*-dependent pathway affects SRP and OSH. We first examined SRP and OSH in *Npas4* total knockout mice ($Npas4^{-/-}$). During training, animals were exposed daily to oriented grating stimuli (45 degrees) for 6 days, and were

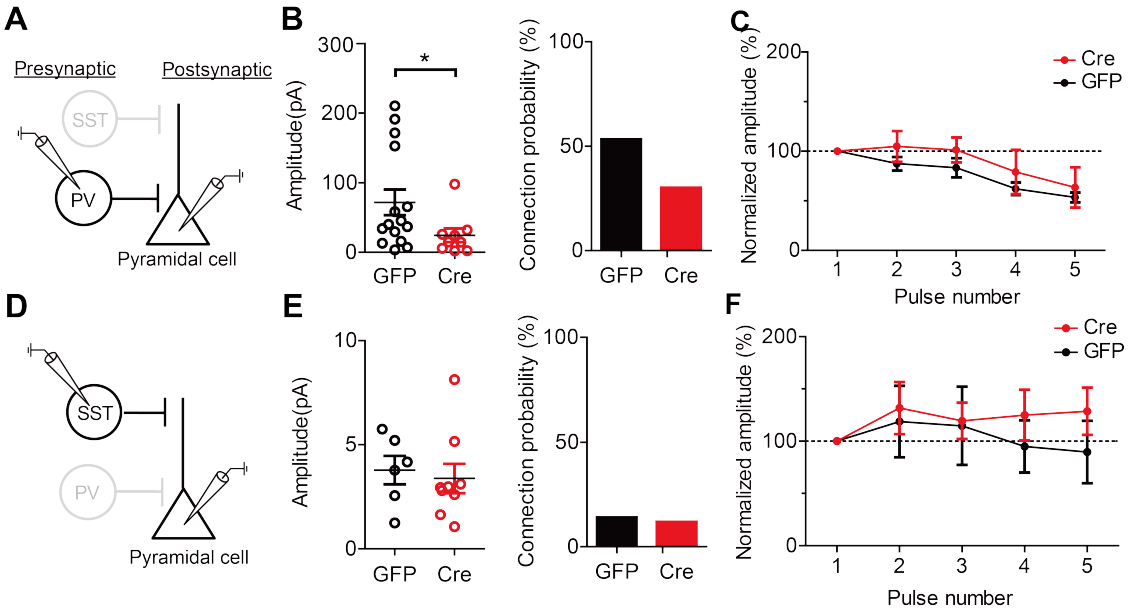

Figure 4.4. Acute Deletion of *Npas4* Reduced Inhibitory Synaptic Transmission from PV$^+$, but not SST$^+$, Interneurons.

(A) Experimental scheme to measure uIPSCs from PV$^+$ interneurons. Paired whole-cell patch-clamp recordings targeting presynaptic PV$^+$ interneurons and postsynaptic pyramidal cells (PC) were carried out. Trains of five action potentials (100 Hz) were evoked in the presynaptic PV$^+$ interneurons, and unitary IPSCs (uIPSCs) were recorded in the postsynaptic cells voltage clamped at -70 mV. uIPSCs were recorded with high-Cl$^-$ internal solution.

(B) Animals with acute deletion of *Npas4* showed reduced uIPSC amplitudes and connection probability at the PV-PC synapses (GFP, n = 15; Cre, n = 9). Mann-Whitney test, *p < 0.05.

(C) Short-term plasticity at the PV-PC synapses was normal with *Npas4* deletion (GFP, n = 15; Cre, n = 9).

(D) Experimental scheme to measure uIPSCs from SST$^+$ interneurons. Paired whole-cell patch-clamp recordings targeting presynaptic SST$^+$ interneurons and postsynaptic pyramidal cells were carried out. Trains of five action potentials (100 Hz) were evoked in the presynaptic SST$^+$ interneurons, and unitary IPSCs (uIPSCs) were recorded in the postsynaptic cells.

(E) Animals with acute deletion of *Npas4* showed normal uIPSC amplitudes and connection probability at the SST-PC synapses (GFP, n = 5; Cre, n = 9).

(F) Short-term plasticity at the SST-PC synapses was normal with *Npas4* deletion (GFP, n = 5; Cre, n = 9).

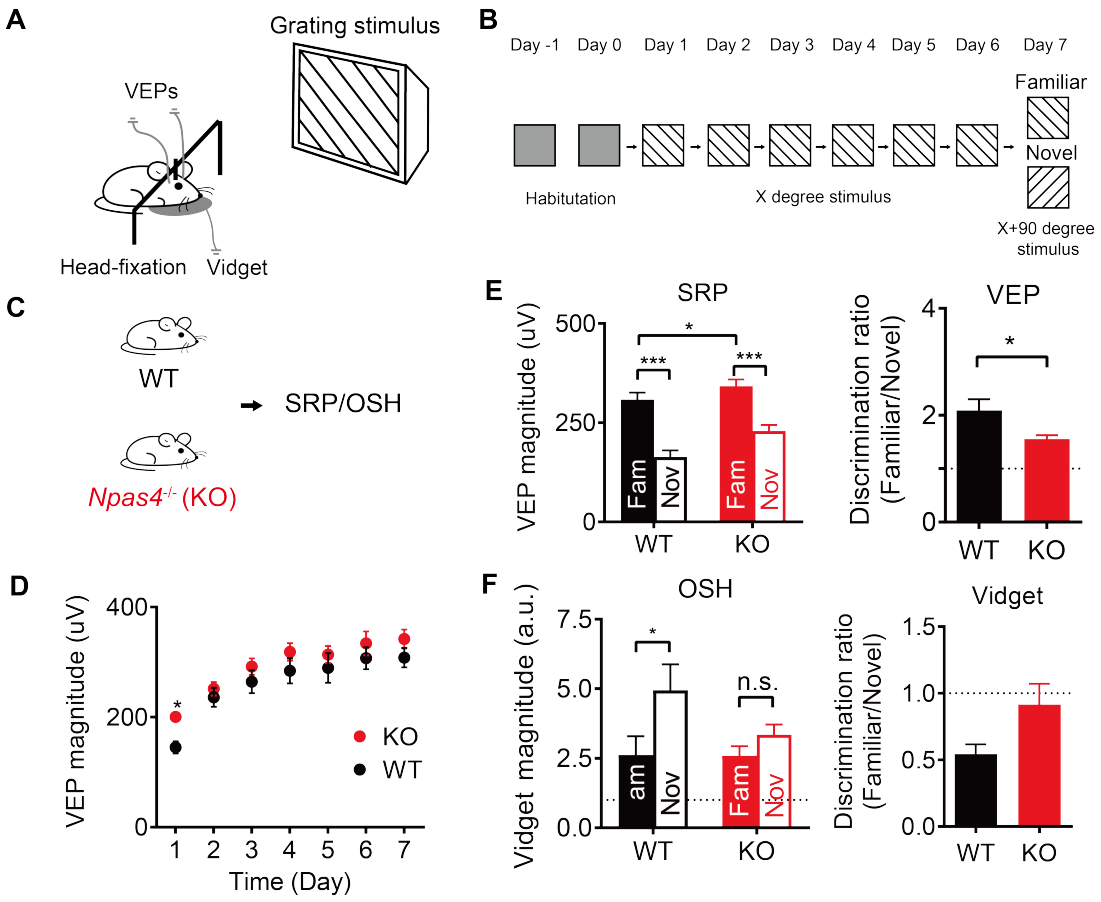

Figure 4.5. *Npas4-/-* Animals Showed Defective SRP and OSH.

(A) Animals were exposed to phase-reversing grating stimulus, while their visually induced fidget (Vidget) and visually evoked potentials (VEPs) in the V1 layer 4 were recorded.

(B) Aniamls were habituated to the setup and grey screen for two days. During the training, animals were daily exposed to oriented grating stimulus (X, 45 degree) for 6 days, and were tested for on the 7 days with both a familiar (X, 45 degree) and a novel stimulus (X+90, 135 degree).

(C) *Npas4-/-* animals and their wild-type littermates were tested for SRP and OSH.

(D) VEPs during daily exposure to the familiar stimulus (WT, n = 17; KO, n = 13). Two-way mixed ANOVA with Sidak's test.

(E) *Npas4-/-* animals showed reduced SRP comparing with their wild-type littermates (WT, n = 17; KO, n = 13). Two-way mixed ANOVA with Sidak's test was used for compare VEP magnitudes, Mann-Whitney test for comparing discrimination ratio. Data are shown as mean ± SEM. *p < 0.05, ***p < 0.001.

(F) *Npas4-/-* animals showed impaired OSH comparing with their wild-type littermates (WT, n = 17; KO, n = 13). Two-way mixed ANOVA with Sidak's test was used for compare vidget magnitudes, Mann-Whitney test for comparing discrimination ratio. Data are shown as mean ± SEM. *p < 0.05.

tested for on the 7 days with both a familiar (45 degrees) and a novel stimulus (135 degrees) (Figure 4.5A). Comparing to their wild-type littermates, *Npas4*$^{-/-}$ animals showed a higher baseline of VEPs (Figure 4.5C-D). As a result, the animals exhibited reduced SRP and less discriminative VEPs towards the familiar versus the novel stimuli (Figure 4.5E). At the behavioral level, OSH was significantly disrupted in *Npas4*$^{-/-}$ animals (Figure 4.5F). *Npas4*$^{-/-}$ animals showed similar vidget magnitudes towards the familiar versus novel stimuli. Taken together, these results suggest that *Npas4* is required for both SRP and OSH.

The V1 is required for visual recognition memory, as blocking synaptic plasticity in the V1 prevented the formation of OSH (Cooke et al., 2015; Fong et al., 2019; Kaplan et al., 2016). To test if OSH requires *Npas4* specifically in the V1, we acutely deleted *Npas4* in the V1 in adult *Npas4*$^{flx/flx}$ animals (Figure 4.6A). Comparing with the control group, animals with *Npas4* deletion showed reduced potentiation of VEPs during training (Figure 4.6B), and did not show differential responses to the familiar and novel stimuli (Figure 4.6C). At the behavioral level, animals with *Npas4* acute deletion showed substantially impaired OSH, and they could not distinguish the familiar versus novel stimuli (Figure 4.6D). Importantly, these effects were not due to visual perceptual deficits, as animals with deleted *Npas4* showed normal contrast sensitivity and spatial acuity (Figure 4.6E-F). Together, these results suggest that SRP and OSH require *Npas4* specifically in the V1.

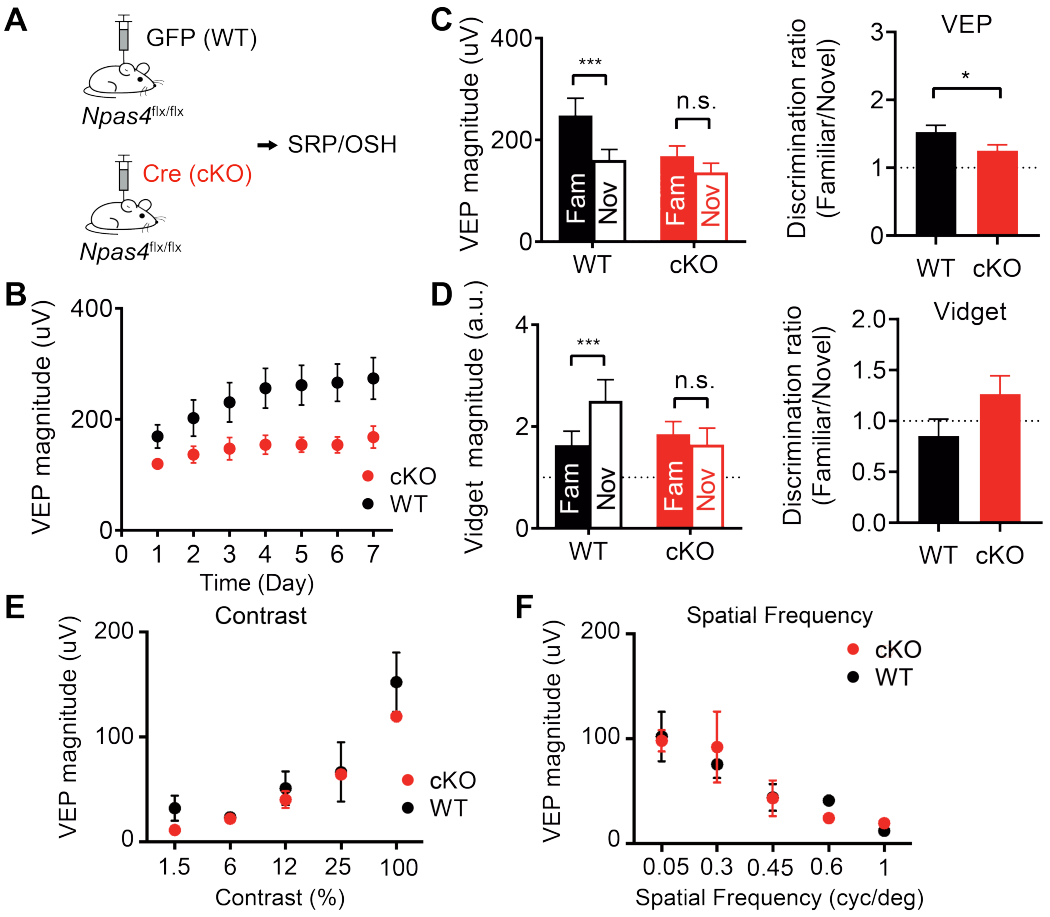

Figure 4.6. Acute Deletion of *Npas4* in the V1 Impaired SRP and OSH.

(A) *Npas4*$^{flx/flx}$ animals injected with Cre-expressing (conditional knockout, cKO) of GFP-expressing control viruses (wild-type, WT) were tested for SRP and OSH.

(B) VEPs during daily exposure to the familiar stimulus WT, n = 13; cKO, n = 10). Two-way mixed ANOVA with Sidak's test.

(C) Acute deletion of *Npas4* reduced SRP (WT, n = 13; cKO, n = 10). Two-way mixed ANOVA with Sidak's test was used for compare VEP magnitudes, Mann-Whitney test for comparing discrimination ratio. Data are shown as mean ± SEM. *p < 0.05, ***p < 0.001.

(D) Acute deletion of *Npas4* impaired OSH (WT, n = 15; cKO, n = 10). Two-way mixed ANOVA with Sidak's test was used for compare vidget magnitudes, Mann-Whitney test for comparing discrimination ratio. Data are shown as mean ± SEM. ***p < 0.001.

(E and F) Animals with *Npas4* deletion showed normal contrast sensitivity (E) and spatial acuity (F) (WT, n = 3; cKO, n = 3).

4.4. Discussion

In the DG, the synaptic and memory functions of *Npas4* are consistent with the ones of the *Npas4*-dependent ensemble. At the behavioral level, both the *Npas4*-dependent ensemble and *Npas4* are required for memory discrimination. At the synaptic level, the finding that *Npas4* regulates inhibitory synapses is consistent with the result that the *Npas4*-dependent ensemble receives enhanced inhibitory synaptic inputs. Furthermore, a recent study found that *Npas4* in the hippocampus selectively regulates inhibitory drive from CCK^+, but not PV^+, interneurons (Hartzell et al., 2018), which is consistent with our observation that *Npas4*-dependent ensemble selectively recruits inputs CCK^+ interneurons. These results strongly imply that, at least in the DG, the activation of *Npas4*-dependent pathway is likely to account for the synaptic property and functionality of the *Npas4*-dependent ensemble. As *Npas4* functions as a transcription factor and regulates large-scale gene programs (Kim et al., 2010; Lin et al., 2008; Spiegel et al., 2014), future studies are needed to further pinpoint the genes downstream of *Npas4* that are critical for the functions of the *Npas4*-dependent ensemble.

In the V1, how does *Npas4* support visual cognition memory? We found that *Npas4* in the V1 preferentially regulates inhibitory synapses, suggesting that the loss of inhibition in the network may contribute to the impairment of visual recognition memories (Kaplan et al., 2016; Kim et al., 2020). Reducing inhibition in the network would disrupt the excitatory-inhibitory balance and impaired circuit functions (Froemke, 2015; Lim and Goldman, 2013; Xue et al., 2014b). Alternatively, the disruption of the *Npas4*-dependent pathway may disrupt inhibitory synaptic plasticity, which has been postulated to play essential roles in recognition memory (Barron et al., 2017; Hamm and Yuste, 2016; Ramaswami, 2014; Sadanandappa et al., 2013). It's currently unknown how other cellular and circuit processes are disrupted in the absence of *Npas4*. Notably, both $Npas4^{-/-}$ and *Npas4* conditional knockout mice showed reduced vidget magnitude to the novel stimuli, similar to a level when control animals respond to the familiar stimulus

(Figure 4.5 & Figure 4.6). This implies that neural processes related to novelty detection and motivation may be affected by *Npas4* deletion (Olarte Sánchez et al., 2015; Warburton and Brown, 2015). In addition, *Npas4* may also regulate other cellular processes such as intrinsic excitability, firing patterns, and neural oscillation (Meeter et al., 2004; Spiegel et al., 2014).

We found that *Npas4* regulates inhibitory circuits in a cell-type-specific manner. *Npas4* in the V1 selectively regulates inhibitory synapses from PV^+, but not SST^+, interneurons. It's consistent with other works suggesting that PV^+ interneurons are required for visual learning (Kaplan et al., 2016; Lee et al., 2012; Pfeffer et al., 2013). However, this is different from what was reported in the CA1, where *Npas4* regulates inhibitory synapses from CCK^+, but not PV^+, interneurons (Hartzell et al., 2018). The difference may be potentially explained by that *Npas4* is known to be able to initiate distinct downstream gene programs by interacting with different co-activators (Brigidi et al., 2019). Future studies are needed to study how *Npas4* regulates subtypes of interneurons in different brain regions.

Using *Npas4* as an example, we showed that activity-dependent genes participate in a various types of learning. Contextual fear conditioning is a form of associative learning (Curzon et al., 2009; Rudy et al., 2004), and acute deletion of *Npas4* in the DG impaired contextual fear memory discrimination. *Npas4* in the V1, on the other hand, supports visual recognition memory, a type of non-associative learning (Barron et al., 2017; Cooke et al., 2015; Eichenbaum et al., 2007). The two types of memories likely involve different circuit and synaptic mechanisms (Barco et al., 2006; Gluck et al., 2016; Wilson et al., 2013). However, the requirement of *Npas4* in both forms of memories suggests that activity-dependent genes like *Npas4* likely mediate fundamental activity-dependent cellular and synaptic processes that are essential for multiple types of experience-dependent learning.

4.5. Methods

Mice

C57BL/6 male and female mice 7-11 weeks old were used for all experiments. Wildtype mice were purchased from the Charles River Laboratory. *Npas4*$^{flx/flx}$ (*Npas4* conditional knockout) mice were generated previously (Lin et al., 2008). All mice were housed with a 12 hour light-dark cycle. Animal protocols were performed in accordance with NIH guidelines and approved by the Massachusetts Institute of Technology Committees on Animal Care and the Institutional Animal Care and Use Committee at SUNY Upstate Medical University.

Viral vectors

AAV1-hSyn-GFP, AAV1-hSyn-GFP-Cre, AAV1-EF1α-DIO-ChR2-EYFP were obtained from the University of Pennsylvania Vector Core via Addgene. All other AAVs were produced in house. AAVs were generated in HEK293T cells and purified using an adapted h gradient purification protocol as previously described (Sørensen et al., 2016). Viral dilutions were determined for individual experiments through pilot injections.

Stereotaxic viral injection and electrode implantation

C57BL/6 mice 7-11 weeks old were anesthetized with 1.5-2% isoflurane in O_2. To target the DG, stereotaxic injections were performed bilaterally into the dorsal hippocampal dentate gyrus with the following coordinates (relative to bregma) and volumes: DG (AP -1.90 mm, ML ±1.30 mm, DV -2.00 mm, 150-200 nL per hemisphere). Viruses were infused at a rate of 100 nL per minute, and needles were kept at the injection site for 5 minutes.

To target the V1, stereotaxic injections were performed bilaterally into V1 binocular areas with the following coordinates (relative to dura) and volumes: V1 (AP: same as lambda,

ML ±3.00 mm, DV -0.60/-0.45/-0.30/-0.15 mm, 100 nL per injection sites). Viruses were infused at a rate of 50 nL per minutes, and needles were kept at the injection site for 5 minutes.

Following viral injection in the V1, a steel headpost was affixed to the skull anterior to bregma using cyanoacrylate glue. Tungsten electrodes (FHC) 75 µm in diameter at the widest point were implanted in each hemisphere, 450 µm below the cortical surface. Silver wire (A-M Systems) reference electrodes were placed over the right prefrontal cortex. All implants were secured in place using cyanoacrylate glue. Finally, dental cement was applied to form a stable, protective head cap.

Contextual fear conditioning (CFC)

Prior to CFC, mice were handled daily in a holding room for 3 days. The behavioral training was typically carried out 48 hours after the last handling session.

On the training day, mice were first transported into the holding room and allowed to acclimatize for at least 30 minutes. Mice were then transported into the behavioral room and placed in context A: 24 cm (L) × 19 cm (W) × 17.5 cm (H), with steel grid floors and 1% acetic acid (Sigma). Mice were conditioned with the following protocol: animals were allowed to explore the conditioned chamber freely for 4 minutes and received 2 second 0.55 mA foot shock at 1 minute intervals 3 times, starting at the 58th second. After each experiment, the chamber was cleaned with 70% ethanol and then with water. In experiments to examine whether synaptic features of ensemble neurons depend on memory strength, no foot shock, weak foot shocks (0.35 mA), or strong foot shocks (0.55 mA, the same as other CFC experiments) were delivered. For experiments with Dox-dependent ensemble labeling, animals were switched back to Dox diet 24 hours after CFC if subsequent behavioral experiments were needed.

To test contextual fear memory discrimination-generalization, 24-48 hours after CFC fear conditioned mice were brought back to the same behavioral room and placed in the conditioned

context (A), a similar context (B) or a distinct context (C) for memory recall for 4 minutes. Context B shares all features with context A except that a soft pad insert is used as the floor. Context C uses a different chamber that has white opaque walls, 32 cm (L) × 25 cm (W) × 32 cm (H), a soft padded floor, and is scented with 0.25% benzaldehyde (Sigma). In some of the experiments, animals were tested for memory recall in only one context, either A, B or C, and sacrificed 1.5 hours later for immunohistochemistry. In chemogenetics and fiber photometry experiments, the same animals were tested in multiple contexts in order to examine their discrimination between contexts. In those cases, fear conditioned animals were tested in contexts B and A on the first day (with at least 6 hours in between), and contexts C and A on the following day.

Contextual fear memory expression was measured by manually scoring freezing behavior over the 4 minute recall period, sampling every 5 seconds, with freezing defined as absence of movement for at least 1 second. Discrimination indices (DIs) are calculated as $\text{Freezing}_{[(A-B)/(A+B)]}$ when comparing freezing levels in contexts A and B, or $\text{Freezing}_{[(A-C)/(A+C)]}$ when comparing freezing levels in contexts A and C. Scorers were blind to the experimental conditions.

Stimulus presentation

Visual stimuli were generated using custom software written in Matlab (MathWorks) using the PsychToolbox extension (http:// psychtoolbox.org). To present the stimuli, a screen was positioned 20 cm in front of the mouse, thereby occupying 92° × 66° of the visual field. Visual stimuli consisted of full-field sinusoidal grating stimuli phase reversing at a frequency of 2 Hz. Grating stimuli spanned the full range of monitor display values between black and white, with gamma correction to ensure constant total luminance in both gray-screen and patterned stimulus conditions. Each stimulus block consisted of 200 phase reversals with 30-s intervals between each stimulus presentation, during which the screen was gray but of equivalent luminance. If more

than one orientation was shown within a session (e.g., familiar vs. novel), stimuli were pseudo-randomly interleaved such that three consecutive presentations of the same stimulus never occurred. To test spatial acuity, stimuli ranged across 0.05, 0.15, 0.3, 0.45, 0.6 and 1 cycle per degree (stimulus contrast was fixed at 100%). To test contrast sensitivity, stimuli ranged across 1.5%, 3.125%, 6.25%, 12.5%, 25%, 50% and 100% contrast (spatial frequency was fixed at 0.05 cycle per degree).

Head-fixed behavior

All behavioral experiments were performed during the mouse subject's light cycle. A piezo-electrical recording device (C.B. Gitty) was placed under the forepaws of head-restrained mice during all sessions. Mice were habituated to the apparatus by sitting in front of a gray screen for 2 days. Mice underwent 5 min of gray-screen presentation before stimulus presentation. During the test, a continuous voltage signal was recorded from the piezo for the entire session. Movements were detected as a shift in the voltage signal. During the test sessions, white noise was played at 67 dB in order to mask outside noise.

To analyze the vidget, the continuous voltage signal was down-sampled to 100 Hz. The period of interest in the experiments described here lasted from 2 s before stimulus onset until 5 s after stimulus onset (which was the first ten phase reversals in a block). Quantification of movement driven by the onset of the stimulus (the vidget) was calculated by taking the root mean square (SQRT (X2)) of the voltage signal. The post-stimulus signal was then normalized to the average magnitude during the 2-s period before stimulus onset. The average normalized magnitude across the 5-s period subsequent to stimulus presentation was then used to quantify the degree of stimulus-driven movement, and this is presented throughout in arbitrary units (a.u.).

Eelectrophysiological data acquisition

All data were amplified and digitized using the Recorder-64 system (Plexon Inc.). Two recording channels were dedicated to recording EEG and VEPs from V1 in each implanted hemisphere and a third recording channel was reserved for the Piezo-electrical input carrying the behavioral information for the majority of experiments. Fields were recorded with 1-kHz sampling and a 500-Hz low-pass filter. All data were extracted from the binary storage files and analyzed using custom software written in Matlab. VEPs were averaged across all phase reversals within a block and trough-peak difference measured during a 200-ms period from phase reversal.

Chapter 5

Discussion: A Working Model on the Emergence of Functionally Distinct Neuronal Ensembles

Chapter 5 - Discussion: A Working Model on the Emergence of Functionally Distinct Neuronal Ensembles

5.1. Introduction

Recent studies on memory engram support the view that memories are stored by sparse ensembles of neurons within engrams (Barth, 2007; Deng et al., 2013; Denny et al., 2017; Han et al., 2009; Josselyn and Tonegawa, 2020; Kawashima et al., 2014; Liu et al., 2014; Reijmers et al., 2007; Yokose et al., 2017). Our findings provide additional evidence for this idea, and further reveal the functional heterogeneity within individual engrams (Sun et al., 2020). The existence of functionally distinct neuronal ensembles is consistent with theoretical studies suggesting that heterogeneous neural populations favor flexible memory expression in an ever-changing environment (Eichenbaum, 2004; Thompson, 2005). Our findings provide causal evidence for this idea by identifying two functionally distinct neuronal ensembles within the memory engram that oppositely regulate the experience-dependent behavioral output. Furthermore, we reveal synaptic and circuit mechanisms that are associated with each ensemble to support their distinct roles in regulating the discrimination-generalization balance.

However, substantial works are needed in the future to fully understand the heterogeneity within engrams. Our study focused on the fear memory engram in the DG, but it remains to be studied if such functional heterogeneity is a general phenomenon across brain regions (Hardcastle et al., 2017; Osborne et al., 2008; Tanaka and McHugh, 2018b). Besides, the computational meaning of such heterogeneity needs further investigation. Therefore, in this chapter, we aim to propose a hypothetical model of how functionally distinct neuronal ensembles emerge during learning. This model provides potential explanations to our key experimental observations and brings up important questions that need to be addressed moving forward.

We hypothesize that there are three critical steps in how heterogeneity within memory engrams arises:

1) **Activity-dependent recruitment of neuronal ensembles**: during learning, activity-dependent pathways are induced in sparse populations of neurons; these neurons are subsequently recruited into different neuronal subpopulations based on their activity-dependent gene expression patterns.
2) **Initiation of different learning-induced plasticity**: activity-dependent pathways triggered in each ensemble initiate different molecular, cellular, synaptic, and circuit modifications.
3) **Formation of functionally distinct ensembles**: different learning-induced modifications onto neuronal ensembles give rise to their distinct functionalities, and these ensembles collectively fine-tune the memory output and support adaptive behaviors.

This model though does not address how distinct neuronal ensembles interact with downstream circuits to drive differential behavioral outputs. Each step of the model is discussed further in detail in the following sections.

5.2. Step 1: Activity-dependent Recruitment of Neural Ensembles

As the first step, transient learning experience activates sparse populations of neurons in the memory circuits (e.g., hippocampus, amygdala, entorhinal cortex) (Barth, 2007; de Sousa et al., 2019; Kawashima et al., 2013; Reijmers et al., 2007; Zhou et al., 2019). As sensory stimuli trigger complex neural responses *in vivo*, neurons within the engram are not activated in identical

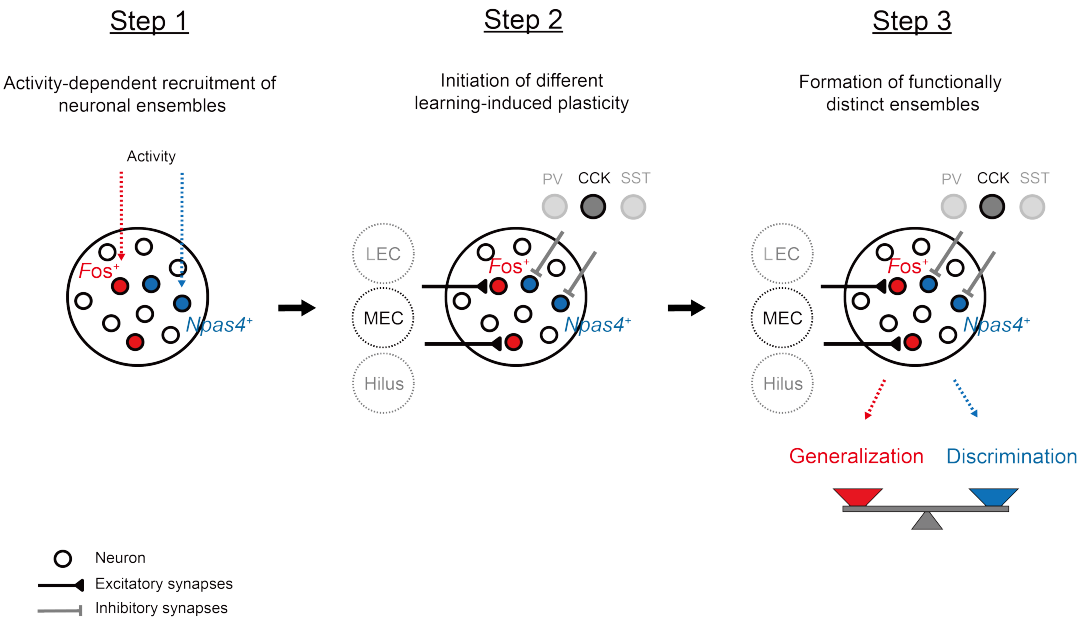

Figure 5.1. A Working Model on the Emergence of Functionally Distinct Neuronal Ensembles. First, different activity patterns induce activity-dependent pathways in different neuronal ensembles. Second, activity-dependent pathways within individual ensembles initiate different learning-induced molecular, cellular, synaptic, and circuit changes. Third, the learning-induced modifications onto neuronal ensembles give rise to their distinct functionalities.

ways (Grewe et al., 2017; Hardcastle et al., 2017; Mallory and Giocomo, 2018). As a result, different activity-dependent pathways are triggered in relatively discrete ensembles of neurons (Renier et al., 2016; Sun and Lin, 2016).

It's currently unknown how neurons are recruited into the memory engram. Early studies suggest that neurons with higher intrinsic excitability are more likely to participate in memory encoding (Han et al., 2007; Han et al., 2009). Artificially increasing the excitability of randomly selected neurons increase the chance that these neurons are recruited into the memory trace (Yiu et al., 2014; Zhou et al., 2009). Later studies suggest that the neurons may be selected to the engram based on their connectivity (Ryan et al., 2015; Tonegawa et al., 2015b). Engram neurons from upstream and downstream regions are preferentially connected even in the absence of learning-induced plasticity (Choi et al., 2018; Ryan et al., 2015). Furthermore, neurons that participate in stable memory representations tend to form interconnected local sub-network (Gonzalez et al., 2019). Lastly, one recent study suggests that engram neurons may be selected due to their unique temporal firing patterns (Tanaka et al., 2018). *Fos*-expressing neurons were significantly more theta modulated than the neighboring neurons and they showed more theta-burst events during learning. We speculate that all the above factors affect the formation of new engrams. It will be interesting for future studies to investigate how these factors interact to determine the recruitment of neurons into the memory engram.

How are neurons then "sorted" into the kinds of distinct neuronal ensembles we describe? The neurons may be recruited into different subpopulations based on their unique activity patterns. It has been shown that the activation of activity-dependent genes depends on the temporal patterns of action potentials (Fields et al., 1997; Tyssowski et al., 2018). For example, acute and prolonged stimulation triggered distinct activity-dependent gene programs (Tyssowski et al., 2018). Future works are needed to quantitatively correlate diverse neuronal firing patterns with the inductions of individual activity-dependent pathways.

Besides, neuromodulators may also contribute to the recruitment of distinct neuronal ensembles (Flavell and Greenberg, 2008; Guo et al., 2012; Radulovic et al., 2000; Sun and Lin, 2016). For example, activation of dopamine signaling through the dopamine D_1 receptors robustly induced *Fos* expression (Radulovic et al., 2000). In contrast, repeated, but not acute, administration of the psychostimulant amphetamine (AMPH) activated *Npas4* in the nucleus accumbens (Guo et al., 2012). Neurotrophic factors, such as BDNF, NT3, and NT4, activated *Fos* but not *Npas4* (Lin et al., 2008; Ramamoorthi et al., 2011). Besides, *Npas4* expression was down-regulated by stress-induced glucocorticoid signaling (Yun et al., 2010). It's conceivable that multiple signaling pathways would interact during learning, and they collectively determine the activation of activity-dependent pathways. It's therefore interesting to examine if the interaction between multiple pathways has synergistic or antagonistic effects (Nadim and Bucher, 2014).

5.3. Step 2: Initiation of Different Learning-induced Plasticity

Once the neural ensembles express activity-dependent genes, these genes trigger learning-induced plasticity through various types of activity-dependent cellular and synaptic mechanisms (Jones et al., 2001; Shepherd and Bear, 2011; Sun and Lin, 2016). Activity-dependent transcription factors such as *Fos*, *Npas4,* and *Egr1* activate downstream gene cascades (Flavell and Greenberg, 2008; Kim et al., 2010; Malik et al., 2014), whereas synaptic proteins like *Arc* and *Nptx2* could directly modulate the strength of synapses (Chang et al., 2010; Gu et al., 2013; Park et al., 2008; Waung et al., 2008). Most importantly, these genes trigger various forms of activity-dependent synaptic plasticity, such as LTP (Fleischmann et al., 2003; Korte et al., 1995; Okuno and Miyashita, 1996), LTD (Park et al., 2008), homeostatic plasticity (Gu et al., 2013; Shepherd et al., 2006), and modifications of inhibitory synapses (Lin et al., 2008). These activity-dependent modifications within engram neurons are likely the key processes underlying memory formation.

What types of synaptic plasticity occur on individual neuronal ensembles? Recent studies and our results together support the idea that neurons undergo heterogeneous plasticity during learning (Grewe et al., 2017; Sun et al., 2020). The *F*-RAM ensemble received enhanced excitation, whereas the *N*-RAM ensemble received enhanced inhibition (Figure 3.1). This observation is consistent with computational studies arguing that efficient learning requires the interaction between multiple forms of plasticity, such as Hebbian plasticity, homeostatic plasticity, spike-timing-dependent plasticity (Litwin-Kumar and Doiron, 2014; Vogels et al., 2011). The ability to genetically tag individual neural ensembles allows detailed characterization of various types of synaptic changes in the circuit. An exciting future direction is to systematically examine the synaptic changes on neuronal ensembles defined by other activity-dependent genes, such as *Arc* and *Egr1* (Denny et al., 2014; Xie et al., 2014).

Although the current study focused on synaptic plasticity, other forms of activity-dependent changes may also be important for the formation of memory engrams. Intrinsic plasticity, the modification of a neuron's intrinsic electrical properties, has been proposed to play critical roles in learning and memory (Debanne et al., 2019; Sehgal et al., 2013). For example, it has been shown that engram neurons change their intrinsic excitability during learning (Cai et al., 2016; Pignatelli et al., 2018). Similarly, we found that *N*-RAM$^+$ neurons show reduced intrinsic excitability, though it's unclear whether such property is learning-induced or pre-existing. Besides, structural plasticity may also contribute to the formation of neural ensembles. *Fos*-dependent ensembles in the DG and nucleus accumbens show increased spine density (Roy et al., 2016; Ryan et al., 2015; Zhou et al., 2019). Future investigations are needed to link these forms of learning-induced plasticity with specific activity-dependent pathways and the ensembles they define.

5.4. Step 3: Formation of Functionally Distinct Ensembles

As the last step, the activity-dependent plasticity within individual ensembles eventually gives rise to their functionality. *F*-RAM and *N*-RAM ensembles respectively promote memory generalization and discrimination, and these behavioral functions are likely associated with the specific activity-dependent plasticity that occurred on each ensemble. In support of this idea, we have shown that the *Npas4*-dependent pathway is required for regulating inhibitory synapse and memory discrimination (Chapter 4), consistent with the role of the *Npas4*-dependent ensemble. However, these results did not demonstrate the causal roles of inhibitory synaptic plasticity in memory discrimination. Future works need to develop perturbation tools that specifically disrupt the synaptic changes within the ensembles neurons (Nabavi et al., 2014; Roy et al., 2016; Zhou et al., 2019).

From an adaptive behavior point of view, a major advantage of having heterogeneous neuronal ensembles in the engram is that these subpopulations can be individually modulated to optimize situation-dependent behavioral output (Eichenbaum, 2004). It's conceivable that, under conditions where generalization is critically needed, the *F*-RAM ensemble that regulates generalization may play a dominant role over the *N*-RAM ensemble. Conversely, the *N*-RAM ensemble may be critically needed when the animals have to carefully differentiate the stimuli. These ideas can be experimentally tested by comparing the involvements of *F*-RAM and *N*-RAM ensembles under: 1) normal physiological conditions; 2) stressed conditions where animals typically show overgeneralization (Dymond et al., 2015; Ghirlanda and Enquist, 2003); 3) conditions where animals show enhanced discrimination, for example, in some models of autism spectrum disorder (ASD) (Brown and Bebko, 2012).

How do the neuronal ensembles differentially drive behavioral outputs? Neurons in the DG send inputs mainly to the downstream CA3 neurons (Amaral and Witter, 1989). Functionally distinct ensembles, such as *F*-RAM and *N*-RAM ensembles, may be either 1) connected with

different CA3 neurons, or 2) connected to the same CA3 neurons but with different strengths or input patterns. To directly tease these possibilities apart, novel activity-dependent labeling systems are needed in order to simultaneously tag multiple ensembles and their downstream targets in the same animals. Besides, it remains unclear how the ensembles interact or compete with each other within the local circuits. Lateral inhibition in the DG mediated by the SST^+ interneurons provides a potential mechanism for ensemble competition (Stefanelli et al., 2016).

5.5. Future Directions and Outstanding Questions

In summary, the model we proposed here summarizes the three key steps of how functionally distinct neuronal ensembles may arise. The hypotheses mentioned above need to be experimentally tested in the future. There are also major limitations about the model: 1) it does not illustrate how distinct neurons ensembles differentially trigger behavior outputs; 2) the molecular mechanisms that convert neuronal activation to the induction of distinct activity-dependent pathways remain unclear. Futures studies are urgently needed to revise and extend the current working model.

Lastly, we list a few outstanding questions that need to be addressed moving forward. The questions are grouped according to Marr's three levels of analysis.

At the *computational* level:

1) Is functional heterogeneity a general phenomenon for memory representations? What's the computational benefit of it?
2) What information do individual ensembles code? Can system-level approaches like large-scale recording or calcium imaging be used to decode the information from each ensemble?

3) Do these hippocampal ensembles mediate the discrimination-generalization balance of remote memories, which are believed to become hippocampus-independent after system consolidation?

At the *representation/algorithm* level:

1) How many ensembles are there in the memory engram? Could single-cell sequencing be used to systematically study all neuronal ensembles together?
2) What's the overall learning rule that determines the synaptic plasticity onto individual neuronal ensembles? Is the observed "heterogeneous plasticity" a general phenomenon?
3) How are memory engrams disrupted in diseased conditions such as PTSD?

At the *hardware implementation* level:

1) What intrinsic and extrinsic factors determine which neurons are recruited to the memory engram?
2) What's the role of inhibitory synaptic plasticity in learning? Why CCK^+ interneurons are selectively required for memory discrimination?
3) What are the molecular players downstream of *Fos* and *Npas4* that determine the functionality of distinct neuronal ensembles?

With the development of advanced conceptual frameworks and novel technologies, we hope that future studies will be able to address these questions and eventually provide a more complete picture of the memory engram.

References

Alberini, C.M., and Kandel, E.R. (2015). The regulation of transcription in memory consolidation. Cold Spring Harbor perspectives in biology *7*, a021741.

Amaral, D.G., and Witter, M.P. (1989). The three-dimensional organization of the hippocampal formation: A review of anatomical data. Neuroscience *31*, 571-591.

Andersen, N., Krauth, N., and Nabavi, S. (2017). Hebbian plasticity in vivo: relevance and induction. Current opinion in neurobiology *45*, 188-192.

Ball, J.M., Hummos, A.M., and Nair, S.S. (2012). Role of sensory input distribution and intrinsic connectivity in lateral amygdala during auditory fear conditioning: a computational study. Neuroscience *224*, 249-267.

Bambah-Mukku, D., Travaglia, A., Chen, D.Y., Pollonini, G., and Alberini, C.M. (2014). A positive autoregulatory BDNF feedback loop via C/EBPβ mediates hippocampal memory consolidation. The Journal of neuroscience : the official journal of the Society for Neuroscience *34*, 12547-12559.

Barco, A., Bailey, C.H., and Kandel, E.R. (2006). Common molecular mechanisms in explicit and implicit memory. Journal of neurochemistry *97*, 1520-1533.

Barron, H.C., Vogels, T.P., Behrens, T.E., and Ramaswami, M. (2017). Inhibitory engrams in perception and memory. Proceedings of the National Academy of Sciences of the United States of America *114*, 6666-6674.

Barth, A.L. (2007). Visualizing circuits and systems using transgenic reporters of neural activity. Current opinion in neurobiology *17*, 567-571.

Barth, A.L., Gerkin, R.C., and Dean, K.L. (2004). Alteration of neuronal firing properties after in vivo experience in a FosGFP transgenic mouse. The Journal of neuroscience : the official journal of the Society for Neuroscience *24*, 6466-6475.

Bartos, M., and Elgueta, C. (2012). Functional characteristics of parvalbumin- and cholecystokinin-expressing basket cells. J Physiol-London *590*, 669-681.

Bear, M.F., and Abraham, W.C. (1996). Long-term depression in hippocampus. Annual review of neuroscience *19*, 437-462.

Bear, M.F., Connors, B.W., and Paradiso, M.A. (2007). Neuroscience, Vol 2 (Lippincott Williams & Wilkins).

Béïque, J.-C., Na, Y., Kuhl, D., Worley, P.F., and Huganir, R.L. (2011). Arc-dependent synapse-specific homeostatic plasticity. Proceedings of the National Academy of Sciences *108*, 816-821.

Bell, A.J. (1999). Levels and loops: the future of artificial intelligence and neuroscience. Philosophical Transactions of the Royal Society of London Series B: Biological Sciences *354*, 2013-2020.

Bernier, B.E., Lacagnina, A.F., Ayoub, A., Shue, F., Zemelman, B.V., Krasne, F.B., and Drew, M.R. (2017). Dentate Gyrus Contributes to Retrieval as well as Encoding: Evidence from Context Fear Conditioning, Recall, and Extinction. Journal of Neuroscience *37*, 6359-6371.

Bliss, T.V., and Lømo, T. (1973). Long - lasting potentiation of synaptic transmission in the dentate area of the anaesthetized rabbit following stimulation of the perforant path. The Journal of physiology *232*, 331-356.

Bloodgood, B.L., Sharma, N., Browne, H.A., Trepman, A.Z., and Greenberg, M.E. (2013). The activity-dependent transcription factor NPAS4 regulates domain-specific inhibition. Nature *503*, 121-125.

Bonne, O., Grillon, C., Vythilingam, M., Neumeister, A., and Charney, D.S. (2004). Adaptive and maladaptive psychobiological responses to severe psychological stress: implications for the discovery of novel pharmacotherapy. Neuroscience and biobehavioral reviews *28*, 65-94.

Bozdagi, O., Tavassoli, T., and Buxbaum, J.D. (2013). Insulin-like growth factor-1 rescues synaptic and motor deficits in a mouse model of autism and developmental delay. Molecular autism *4*, 9.

Brigidi, G.S., Hayes, M.G.B., Delos Santos, N.P., Hartzell, A.L., Texari, L., Lin, P.A., Bartlett, A., Ecker, J.R., Benner, C., Heinz, S.*, et al.* (2019). Genomic Decoding of Neuronal Depolarization by Stimulus-Specific NPAS4 Heterodimers. Cell *179*, 373-391 e327.

Brown, S.M., and Bebko, J.M. (2012). Generalization, overselectivity, and discrimination in the autism phenotype: A review. Res Autism Spect Dis *6*, 733-740.

Bruce, D. (2001). Fifty years since Lashley's In search of the Engram: refutations and conjectures. Journal of the history of the neurosciences *10*, 308-318.

Burns, A., and Iliffe, S. (2009). Alzheimer's disease. BMJ *338*, b158.

Cai, D.J., Aharoni, D., Shuman, T., Shobe, J., Biane, J., Song, W., Wei, B., Veshkini, M., La-Vu, M., Lou, J.*, et al.* (2016). A shared neural ensemble links distinct contextual memories encoded close in time. Nature *534*, 115-118.

Cain, D.P., Saucier, D., Hall, J., Hargreaves, E.L., and Boon, F. (1996). Detailed behavioral analysis of water maze acquisition under APV or CNQX: Contribution of sensorimotor disturbances to drug-induced acquisition deficits. Behavioral Neuroscience *110*, 86-102.

Castillo, P.E., Younts, T.J., Chavez, A.E., and Hashimotodani, Y. (2012). Endocannabinoid Signaling and Synaptic Function. Neuron *76*, 70-81.

Chang, M.C., Park, J.M., Pelkey, K.A., Grabenstatter, H.L., Xu, D., Linden, D.J., Sutula, T.P., McBain, C.J., and Worley, P.F. (2010). Narp regulates homeostatic scaling of excitatory synapses on parvalbumin-expressing interneurons. Nature neuroscience *13*, 1090-1097.

Chawla, M.K., Guzowski, J.F., Ramirez-Amaya, V., Lipa, P., Hoffman, K.L., Marriott, L.K., Worley, P.F., McNaughton, B.L., and Barnes, C.A. (2005). Sparse, environmentally selective expression of Arc RNA in the upper blade of the rodent fascia dentata by brief spatial experience. Hippocampus *15*, 579-586.

Choi, J.H., Sim, S.E., Kim, J.I., Choi, D.I., Oh, J., Ye, S., Lee, J., Kim, T., Ko, H.G., Lim, C.S.*, et al.* (2018). Interregional synaptic maps among engram cells underlie memory formation. Science *360*, 430-435.

Cole, S.N., Morrison, C.M., Barak, O., Pauly-Takacs, K., and Conway, M.A. (2016). Amnesia and future thinking: Exploring the role of memory in the quantity and quality of episodic future thoughts. Br J Clin Psychol *55*, 206-224.

Cooke, S.F., and Bear, M.F. (2010). Visual experience induces long-term potentiation in the primary visual cortex. The Journal of neuroscience : the official journal of the Society for Neuroscience *30*, 16304-16313.

Cooke, S.F., Komorowski, R.W., Kaplan, E.S., Gavornik, J.P., and Bear, M.F. (2015). Visual recognition memory, manifested as long-term habituation, requires synaptic plasticity in V1. Nature neuroscience *18*, 262-271.

Cox, David D., and Dean, T. (2014). Neural Networks and Neuroscience-Inspired Computer Vision. Current Biology *24*, R921-R929.

Curzon, P., Rustay, N.R., and Browman, K.E. (2009). Cued and contextual fear conditioning for rodents. In Methods of Behavior Analysis in Neuroscience 2nd edition (CRC Press/Taylor & Francis).

Danielson, N.B., Turi, G.F., Ladow, M., Chavlis, S., Petrantonakis, P.C., Poirazi, P., and Losonczy, A. (2017). In Vivo Imaging of Dentate Gyrus Mossy Cells in Behaving Mice. Neuron *93*, 552-+.

de Sousa, A.F., Cowansage, K.K., Zutshi, I., Cardozo, L.M., Yoo, E.J., Leutgeb, S., and Mayford, M. (2019). Optogenetic reactivation of memory ensembles in the retrosplenial cortex induces systems consolidation. Proceedings of the National Academy of Sciences of the United States of America *116*, 8576-8581.

Debanne, D., Inglebert, Y., and Russier, M. (2019). Plasticity of intrinsic neuronal excitability. Current opinion in neurobiology *54*, 73-82.

Deng, W., Mayford, M., and Gage, F.H. (2013). Selection of distinct populations of dentate granule cells in response to inputs as a mechanism for pattern separation in mice. eLife *2*, e00312.

Denny, C.A., Kheirbek, M.A., Alba, E.L., Tanaka, K.F., Brachman, R.A., Laughman, K.B., Tomm, N.K., Turi, G.F., Losonczy, A., and Hen, R. (2014). Hippocampal memory traces are differentially modulated by experience, time, and adult neurogenesis. Neuron *83*, 189-201.

Denny, C.A., Lebois, E., and Ramirez, S. (2017). From Engrams to Pathologies of the Brain. Frontiers in neural circuits *11*.

Diehl, G.W., Hon, O.J., Leutgeb, S., and Leutgeb, J.K. (2017). Grid and Nongrid Cells in Medial Entorhinal Cortex Represent Spatial Location and Environmental Features with Complementary Coding Schemes. Neuron *94*, 83-92.e86.

Diering, G.H., Nirujogi, R.S., Roth, R.H., Worley, P.F., Pandey, A., and Huganir, R.L. (2017). Homer1a drives homeostatic scaling-down of excitatory synapses during sleep. Science *355*, 511-515.

Dimidschstein, J., Chen, Q., Tremblay, R., Rogers, S.L., Saldi, G.A., Guo, L., Xu, Q., Liu, R., Lu, C., Chu, J., *et al*. (2016). A viral strategy for targeting and manipulating interneurons across vertebrate species. Nature neuroscience.

Dudai, Y. (2004). The neurobiology of consolidations, or, how stable is the engram? Annu Rev Psychol *55*, 51-86.

Dunsmoor, J.E., and Paz, R. (2015). Fear Generalization and Anxiety: Behavioral and Neural Mechanisms. Biological psychiatry *78*, 336-343.

Dymond, S., Dunsmoor, J.E., Vervliet, B., Roche, B., and Hermans, D. (2015). Fear Generalization in Humans: Systematic Review and Implications for Anxiety Disorder Research. Behav Ther *46*, 561-582.

Eichenbaum, H. (2004). Hippocampus: cognitive processes and neural representations that underlie declarative memory. Neuron *44*, 109-120.

Eichenbaum, H. (2017). On the Integration of Space, Time, and Memory. Neuron *95*, 1007-1018.

Eichenbaum, H., Yonelinas, A.P., and Ranganath, C. (2007). The medial temporal lobe and recognition memory. Annual review of neuroscience *30*, 123-152.

Eysenck, M. (2012). Attention and arousal: Cognition and performance (Springer Science & Business Media).

Fields, R.D., Eshete, F., Stevens, B., and Itoh, K. (1997). Action potential-dependent regulation of gene expression: temporal specificity in Ca2+, cAMP-responsive element binding proteins, and mitogen-activated protein kinase signaling. Journal of Neuroscience *17*, 7252-7266.

Flavell, S.W., and Greenberg, M.E. (2008). Signaling mechanisms linking neuronal activity to gene expression and plasticity of the nervous system. Annual review of neuroscience *31*, 563-590.

Fleischmann, A., Hvalby, O., Jensen, V., Strekalova, T., Zacher, C., Layer, L.E., Kvello, A., Reschke, M., Spanagel, R., Sprengel, R., *et al*. (2003). Impaired long-term memory and NR2A-type NMDA receptor-dependent synaptic plasticity in mice lacking c-Fos in the CNS. The Journal of neuroscience : the official journal of the Society for Neuroscience *23*, 9116-9122.

Fong, M.F., Finnie, P.S., Kim, T., Thomazeau, A., Kaplan, E.S., Cooke, S.F., and Bear, M.F. (2019). Distinct Laminar Requirements for NMDA Receptors in Experience-Dependent Visual Cortical Plasticity. Cerebral cortex.

Frankland, P.W., Cestari, V., Filipkowski, R.K., McDonald, R.J., and Silva, A.J. (1998). The dorsal hippocampus is essential for context discrimination but not for contextual conditioning. Behavioral Neuroscience *112*, 863-874.

Frenkel, M.Y., Sawtell, N.B., Diogo, A.C., Yoon, B., Neve, R.L., and Bear, M.F. (2006). Instructive effect of visual experience in mouse visual cortex. Neuron *51*, 339-349.

Freund, T.F., and Buzsaki, G. (1996). Interneurons of the hippocampus. Hippocampus *6*, 347-470.

Froemke, R.C. (2015). Plasticity of Cortical Excitatory-Inhibitory Balance. Annual Review of Neuroscience, Vol 38 *38*, 195-219.

Fyhn, M., Hafting, T., Treves, A., Moser, M.B., and Moser, E.I. (2007). Hippocampal remapping and grid realignment in entorhinal cortex. Nature *446*, 190-194.

Gaiddon, C., Loeffler, J.P., and Larmet, Y. (1996). Brain-derived neurotrophic factor stimulates AP-1 and cyclic AMP-responsive element dependent transcriptional activity in central nervous system neurons. Journal of neurochemistry *66*, 2279-2286.

Garner, A.R., Rowland, D.C., Hwang, S.Y., Baumgaertel, K., Roth, B.L., Kentros, C., and Mayford, M. (2012). Generation of a synthetic memory trace. Science *335*, 1513-1516.

Ghandour, K., Ohkawa, N., Fung, C.C.A., Asai, H., Saitoh, Y., Takekawa, T., Okubo-Suzuki, R., Soya, S., Nishizono, H., Matsuo, M., *et al*. (2019). Orchestrated ensemble activities constitute a hippocampal memory engram. Nature communications *10*, 2637.

Ghirlanda, S., and Enquist, M. (2003). A century of generalization. Anim Behav *66*, 15-36.

Ginty, D.D., Bonni, A., and Greenberg, M.E. (1994). Nerve Growth-Factor Activates a Ras-Dependent Protein-Kinase That Stimulates C-Fos Transcription Phosphorylation of Creb. Cell *77*, 713-725.

Gluck, M.A., Mercado, E., and Myers, C.E. (2016). Learning and memory (Worth Publishers).

Gonzalez, W.G., Zhang, H., Harutyunyan, A., and Lois, C. (2019). Persistence of neuronal representations through time and damage in the hippocampus. Science *365*, 821-825.

GoodSmith, D., Chen, X.J., Wang, C., Kim, S.H., Song, H.J., Burgalossi, A., Christian, K.M., and Knierim, J.J. (2017). Spatial Representations of Granule Cells and Mossy Cells of the Dentate Gyrus. Neuron *93*, 677-+.

Grewe, B.F., Grundemann, J., Kitch, L.J., Lecoq, J.A., Parker, J.G., Marshall, J.D., Larkin, M.C., Jercog, P.E., Grenier, F., Li, J.Z., *et al*. (2017). Neural ensemble dynamics underlying a long-term associative memory. Nature *543*, 670-+.

Griggs, R.A. (2010). Psychology: A concise introduction (Macmillan).

Grosmark, A.D., and Buzsáki, G. (2016). Diversity in neural firing dynamics supports both rigid and learned hippocampal sequences. Science *351*, 1440-1443.

Grosso, A., Santoni, G., Manassero, E., Renna, A., and Sacchetti, B. (2018). A neuronal basis for fear discrimination in the lateral amygdala. Nature communications *9*.

Gu, Y., Huang, S., Chang, M.C., Worley, P., Kirkwood, A., and Quinlan, E.M. (2013). Obligatory role for the immediate early gene NARP in critical period plasticity. Neuron *79*, 335-346.

Guenthner, C.J., Miyamichi, K., Yang, H.H., Heller, H.C., and Luo, L. (2013a). Permanent genetic access to transiently active neurons via TRAP: targeted recombination in active populations. Neuron *78*, 773-784.

Guenthner, C.J., Miyamichi, K., Yang, H.H., Heller, H.C., and Luo, L.Q. (2013b). Permanent Genetic Access to Transiently Active Neurons via TRAP: Targeted Recombination in Active Populations (vol 78, pg 773, 2013). Neuron *79*, 1257-1257.

Guo, M.-L., Xue, B., Jin, D.-Z., Liu, Z.-G., Fibuch, E.E., Mao, L.-M., and Wang, J.Q. (2012). Upregulation of Npas4 protein expression by chronic administration of amphetamine in rat nucleus accumbens in vivo. Neuroscience letters *528*, 210-214.

Guo, N.N., Soden, M.E., Herber, C., Kim, M.T., Besnard, A., Lin, P.Y., Ma, X., Cepko, C.L., Zweifel, L.S., and Sahay, A. (2018). Dentate granule cell recruitment of feedforward inhibition governs engram maintenance and remote memory generalization. Nat Med *24*, 438-+.

Guzowski, J.F., Timlin, J.A., Roysam, B., McNaughton, B.L., Worley, P.F., and Barnes, C.A. (2005). Mapping behaviorally relevant neural circuits with immediate-early gene expression. Current opinion in neurobiology *15*, 599-606.

Hainmueller, T., and Bartos, M. (2018). Parallel emergence of stable and dynamic memory engrams in the hippocampus. Nature.

Hales, J.B., Schlesiger, M.I., Leutgeb, J.K., Squire, L.R., Leutgeb, S., and Clark, R.E. (2014). Medial Entorhinal Cortex Lesions Only Partially Disrupt Hippocampal Place Cells and Hippocampus-Dependent Place Memory. Cell reports *9*, 893-901.

Hamm, J.P., and Yuste, R. (2016). Somatostatin Interneurons Control a Key Component of Mismatch Negativity in Mouse Visual Cortex. Cell reports *16*, 597-604.

Han, J.H., Kushner, S.A., Yiu, A.P., Cole, C.J., Matynia, A., Brown, R.A., Neve, R.L., Guzowski, J.F., Silva, A.J., and Josselyn, S.A. (2007). Neuronal competition and selection during memory formation. Science *316*, 457-460.

Han, J.H., Kushner, S.A., Yiu, A.P., Hsiang, H.L., Buch, T., Waisman, A., Bontempi, B., Neve, R.L., Frankland, P.W., and Josselyn, S.A. (2009). Selective erasure of a fear memory. Science *323*, 1492-1496.

Hardcastle, K., Maheswaranathan, N., Ganguli, S., and Giocomo, L.M. (2017). A Multiplexed, Heterogeneous, and Adaptive Code for Navigation in Medial Entorhinal Cortex. Neuron *94*, 375-387.e377.

Hartzell, A.L., Martyniuk, K.M., Brigidi, G.S., Heinz, D.A., Djaja, N.A., Payne, A., and Bloodgood, B.L. (2018). NPAS4 recruits CCK basket cell synapses and enhances cannabinoid-sensitive inhibition in the mouse hippocampus. eLife *7*.

Hashimotodani, Y., Nasrallah, K., Jensen, K.R., Chavez, A.E., Carrera, D., and Castillo, P.E. (2017). LTP at Hilar Mossy Cell-Dentate Granule Cell Synapses Modulates Dentate Gyrus Output by Increasing Excitation/Inhibition Balance. Neuron *95*, 928-+.

Hassabis, D., Kumaran, D., Summerfield, C., and Botvinick, M. (2017). Neuroscience-Inspired Artificial Intelligence. Neuron *95*, 245-258.

Hebb, D.O. (1949). The organization of behavior (na).

Hefft, S., and Jonas, P. (2005). Asynchronous GABA release generates long-lasting inhibition at a hippocampal interneuron-principal neuron synapse. Nature neuroscience *8*, 1319-1328.

Hennequin, G., Agnes, E.J., and Vogels, T.P. (2017). Inhibitory Plasticity: Balance, Control, and Codependence. Annual review of neuroscience *40*, 557-579.

Herry, C., Ciocchi, S., Senn, V., Demmou, L., Muller, C., and Luthi, A. (2008). Switching on and off fear by distinct neuronal circuits. Nature *454*, 600-606.

Hess, J., Angel, P., and Schorpp-Kistner, M. (2004). AP-1 subunits: quarrel and harmony among siblings. Journal of cell science *117*, 5965-5973.

Huckleberry, K.A., Ferguson, L.B., and Drew, M.R. (2016). Behavioral mechanisms of context fear generalization in mice. Learning & memory *23*, 703-709.

Hunt, S.P., Pini, A., and Evan, G. (1987). Induction of C-Fos-Like Protein in Spinal-Cord Neurons Following Sensory Stimulation. Nature *328*, 632-634.

Iaccarino, H.F., Singer, A.C., Martorell, A.J., Rudenko, A., Gao, F., Gillingham, T.Z., Mathys, H., Seo, J., Kritskiy, O., and Abdurrob, F. (2016). Gamma frequency entrainment attenuates amyloid load and modifies microglia. Nature *540*, 230-235.

Isaacson, J.S., and Scanziani, M. (2011). How Inhibition Shapes Cortical Activity. Neuron *72*, 231-243.

Jasnow, A.M., Lynch Iii, J.F., Gilman, T.L., and Riccio, D.C. (2017). Perspectives on fear generalization and its implications for emotional disorders. Journal of neuroscience research *95*, 821-835.

Jiang, X., Shen, S., Cadwell, C.R., Berens, P., Sinz, F., Ecker, A.S., Patel, S., and Tolias, A.S. (2015). Principles of connectivity among morphologically defined cell types in adult neocortex. Science *350*, aac9462.

Jinde, S., Zsiros, V., Jiang, Z., Nakao, K., Pickel, J., Kohno, K., Belforte, J.E., and Nakazawa, K. (2012). Hilar mossy cell degeneration causes transient dentate granule cell hyperexcitability and impaired pattern separation. Neuron *76*, 1189-1200.

Johnson, M.K., and Hasher, L. (1987). Human Learning and Memory. Annual review of psychology *38*, 631-668.

Johnston, S.T., Shtrahman, M., Parylak, S., Goncalves, J.T., and Gage, F.H. (2016). Paradox of pattern separation and adult neurogenesis: A dual role for new neurons balancing memory resolution and robustness. Neurobiology of learning and memory *129*, 60-68.

Jones, M.W., Errington, M.L., French, P.J., Fine, A., Bliss, T.V., Garel, S., Charnay, P., Bozon, B., Laroche, S., and Davis, S. (2001). A requirement for the immediate early gene Zif268 in the expression of late LTP and long-term memories. Nature neuroscience *4*, 289-296.

Josselyn, S.A., Kohler, S., and Frankland, P.W. (2015). Finding the engram. Nature reviews Neuroscience *16*, 521-534.

Josselyn, S.A., Kohler, S., and Frankland, P.W. (2017). Heroes of the Engram. The Journal of neuroscience : the official journal of the Society for Neuroscience *37*, 4647-4657.

Josselyn, S.A., and Tonegawa, S. (2020). Memory engrams: Recalling the past and imagining the future. Science *367*.

Jun, J.K., Miller, P., Hernández, A., Zainos, A., Lemus, L., Brody, C.D., and Romo, R. (2010). Heterogenous Population Coding of a Short-Term Memory and Decision Task. The Journal of Neuroscience *30*, 916.

Jung, M.W., and Mcnaughton, B.L. (1993). Spatial Selectivity of Unit-Activity in the Hippocampal Granular Layer. Hippocampus *3*, 165-182.

Kandel, Eric R., Dudai, Y., and Mayford, Mark R. (2014). The Molecular and Systems Biology of Memory. Cell *157*, 163-186.

Kanter, B.R., Lykken, C.M., Avesar, D., Weible, A., Dickinson, J., Dunn, B., Borgesius, N.Z., Roudi, Y., and Kentros, C.G. (2017). A Novel Mechanism for the Grid-to-Place Cell Transformation Revealed by Transgenic Depolarization of Medial Entorhinal Cortex Layer II. Neuron *93*, 1480-+.

Kaplan, E.S., Cooke, S.F., Komorowski, R.W., Chubykin, A.A., Thomazeau, A., Khibnik, L.A., Gavornik, J.P., and Bear, M.F. (2016). Contrasting roles for parvalbumin-expressing inhibitory neurons in two forms of adult visual cortical plasticity. eLife *5*.

Karlsson, M.P., and Frank, L.M. (2008). Network dynamics underlying the formation of sparse, informative representations in the hippocampus. The Journal of neuroscience : the official journal of the Society for Neuroscience *28*, 14271-14281.

Kawashima, T., Kitamura, K., Suzuki, K., Nonaka, M., Kamijo, S., Takemoto-Kimura, S., Kano, M., Okuno, H., Ohki, K., and Bito, H. (2013). Functional labeling of neurons and their projections using the synthetic activity-dependent promoter E-SARE. Nature methods *10*, 889-895.

Kawashima, T., Okuno, H., and Bito, H. (2014). A new era for functional labeling of neurons: activity-dependent promoters have come of age. Frontiers in neural circuits *8*.

Keiser, A.A., Turnbull, L.M., Darian, M.A., Feldman, D.E., Song, I., and Tronson, N.C. (2017). Sex differences in context fear generalization and recruitment of hippocampus and amygdala during retrieval. Neuropsychopharmacology : official publication of the American College of Neuropsychopharmacology *42*, 397-407.

Kheirbek, M.A., Drew, L.J., Burghardt, N.S., Costantini, D.O., Tannenholz, L., Ahmari, S.E., Zeng, H., Fenton, A.A., and Hen, R. (2013). Differential control of learning and anxiety along the dorsoventral axis of the dentate gyrus. Neuron *77*, 955-968.

Kheirbek, M.A., Klemenhagen, K.C., Sahay, A., and Hen, R. (2012a). Neurogenesis and generalization: a new approach to stratify and treat anxiety disorders. Nature neuroscience *15*, 1613-1620.

Kheirbek, M.A., Klemenhagen, K.C., Sahay, A., and Hen, R. (2012b). Neurogenesis and generalization: a new approach to stratify and treat anxiety disorders. Nat Neurosci *15*, 1613-1620.

Kim, T., Chaloner, F.A., Cooke, S.F., Harnett, M.T., and Bear, M.F. (2020). Opposing Somatic and Dendritic Expression of Stimulus-Selective Response Plasticity in Mouse Primary Visual Cortex. Frontiers in cellular neuroscience *13*.

Kim, T.K., Hemberg, M., Gray, J.M., Costa, A.M., Bear, D.M., Wu, J., Harmin, D.A., Laptewicz, M., Barbara-Haley, K., Kuersten, S.*, et al.* (2010). Widespread transcription at neuronal activity-regulated enhancers. Nature *465*, 182-187.

Kitamura, T., Sun, C., Martin, J., Kitch, L.J., Schnitzer, M.J., and Tonegawa, S. (2015). Entorhinal Cortical Ocean Cells Encode Specific Contexts and Drive Context-Specific Fear Memory. Neuron *87*, 1317-1331.

Knierim, J.J., and Neunuebel, J.P. (2016). Tracking the flow of hippocampal computation: Pattern separation, pattern completion, and attractor dynamics. Neurobiology of learning and memory *129*, 38-49.

Koch, C.E., Leinweber, B., Drengberg, B.C., Blaum, C., and Oster, H. (2017). Interaction between circadian rhythms and stress. Neurobiology of stress *6*, 57-67.

Kohwi, M., Petryniak, M.A., Long, J.E., Ekker, M., Obata, K., Yanagawa, Y., Rubenstein, J.L.R., and Alvarez-Buylla, A. (2007). A subpopulation of olfactory bulb GABAergic interneurons is derived from Emx1- and Dlx5/6-expressing progenitors. Journal of Neuroscience *27*, 6878-6891.

Korte, M., Carroll, P., Wolf, E., Brem, G., Thoenen, H., and Bonhoeffer, T. (1995). Hippocampal long-term potentiation is impaired in mice lacking brain-derived neurotrophic factor. Proceedings of the National Academy of Sciences *92*, 8856-8860.

Kuhn, H.G., DickinsonAnson, H., and Gage, F.H. (1996). Neurogenesis in the dentate gyrus of the adult rat: Age-related decrease of neuronal progenitor proliferation. Journal of Neuroscience *16*, 2027-2033.

Kuhn, M., Mertens, G., and Lonsdorf, T.B. (2016). State anxiety modulates the return of fear. International journal of psychophysiology *110*, 194-199.

Kullmann, D.M., Moreau, A.W., Bakiri, Y., and Nicholson, E. (2012). Plasticity of inhibition. Neuron *75*, 951-962.

Kumaran, D., Hassabis, D., and McClelland, J.L. (2016). What Learning Systems do Intelligent Agents Need? Complementary Learning Systems Theory Updated. Trends in cognitive sciences *20*, 512-534.

Kuzniewska, B., Nader, K., Dabrowski, M., Kaczmarek, L., and Kalita, K. (2016). Adult deletion of SRF increases epileptogenesis and decreases activity-induced gene expression. Molecular neurobiology *53*, 1478-1493.

Lashley, K.S. (1950a). In search of the engram. In Physiological mechanisms in animal behavior (Society's Symposium IV) (Oxford, England: Academic Press), pp. 454-482.

Lashley, K.S. (1950b). In search of the engram.

Lee, S.H., Kwan, A.C., Zhang, S., Phoumthipphavong, V., Flannery, J.G., Masmanidis, S.C., Taniguchi, H., Huang, Z.J., Zhang, F., Boyden, E.S., *et al*. (2012). Activation of specific interneurons improves V1 feature selectivity and visual perception. Nature *488*, 379-383.

Leutgeb, J.K., Leutgeb, S., Moser, M.B., and Moser, E.I. (2007). Pattern separation in the dentate gyrus and CA3 of the hippocampus. Science *315*, 961-966.

Lim, S., and Goldman, M.S. (2013). Balanced cortical microcircuitry for maintaining information in working memory. Nature neuroscience *16*, 1306-U1196.

Lin, Y., Bloodgood, B.L., Hauser, J.L., Lapan, A.D., Koon, A.C., Kim, T.K., Hu, L.S., Malik, A.N., and Greenberg, M.E. (2008). Activity-dependent regulation of inhibitory synapse development by Npas4. Nature *455*, 1198-1204.

Litwin-Kumar, A., and Doiron, B. (2014). Formation and maintenance of neuronal assemblies through synaptic plasticity. Nature communications *5*.

Liu, X., Ramirez, S., Pang, P.T., Puryear, C.B., Govindarajan, A., Deisseroth, K., and Tonegawa, S. (2012). Optogenetic stimulation of a hippocampal engram activates fear memory recall. Nature *484*, 381-385.

Liu, X., Ramirez, S., and Tonegawa, S. (2014). Inception of a false memory by optogenetic manipulation of a hippocampal memory engram. Philosophical transactions of the Royal Society of London Series B, Biological sciences *369*, 20130142.

Lonergan, M.E., Gafford, G.M., Jarome, T.J., and Helmstetter, F.J. (2010). Time-dependent expression of Arc and zif268 after acquisition of fear conditioning. Neural plasticity *2010*, 139891.

Lovett-Barron, M., Kaifosh, P., Kheirbek, M.A., Danielson, N., Zaremba, J.D., Reardon, T.R., Turi, G.F., Hen, R., Zemelman, B.V., and Losonczy, A. (2014). Dendritic inhibition in the hippocampus supports fear learning. Science *343*, 857-863.

Lynch, J., Cullen, P.K., Jasnow, A.M., and Riccio, D.C. (2013). Sex differences in the generalization of fear as a function of retention intervals. Learning & memory *20*, 628-632.

Lynch, M.A. (2004). Long-term potentiation and memory. Physiol Rev *84*, 87-136.

Macek, T.A., Winder, D.G., Gereau, R.W., Ladd, C.O., and Conn, P.J. (1996). Differential involvement of group II and group III mGluRs as autoreceptors at lateral and medial perforant path synapses. Journal of neurophysiology *76*, 3798-3806.

Mahan, A.L., and Ressler, K.J. (2012). Fear conditioning, synaptic plasticity and the amygdala: implications for posttraumatic stress disorder. Trends in neurosciences *35*, 24-35.

Malik, A.N., Vierbuchen, T., Hemberg, M., Rubin, A.A., Ling, E., Couch, C.H., Stroud, H., Spiegel, I., Farh, K.K., Harmin, D.A., *et al*. (2014). Genome-wide identification and characterization of functional neuronal activity-dependent enhancers. Nature neuroscience *17*, 1330-1339.

Mallory, C.S., and Giocomo, L.M. (2018). Heterogeneity in hippocampal place coding. Current opinion in neurobiology *49*, 158-167.

Marblestone, A.H., Wayne, G., and Kording, K.P. (2016). Toward an Integration of Deep Learning and Neuroscience. Frontiers in computational neuroscience *10*.

Mardinly, A.R., Spiegel, I., Patrizi, A., Centofante, E., Bazinet, J.E., Tzeng, C.P., Mandel-Brehm, C., Harmin, D.A., Adesnik, H., Fagiolini, M., *et al*. (2016). Sensory experience regulates cortical inhibition by inducing IGF1 in VIP neurons. Nature *531*, 371-375.

Marr, D. (1982). Vision: A computational investigation into the human representation and processing of visual information.

Martin, S.J., Grimwood, P.D., and Morris, R.G. (2000). Synaptic plasticity and memory: an evaluation of the hypothesis. Annual review of neuroscience *23*, 649-711.

Mayford, M. (2014). The search for a hippocampal engram. Philosophical transactions of the Royal Society of London Series B, Biological sciences *369*, 20130161.

McHugh, T.J., Jones, M.W., Quinn, J.J., Balthasar, N., Coppari, R., Elmquist, J.K., Lowell, B.B., Fanselow, M.S., Wilson, M.A., and Tonegawa, S. (2007). Dentate gyrus NMDA receptors mediate rapid pattern separation in the hippocampal network. Science *317*, 94-99.

Meeter, M., Murre, J., and Talamini, L. (2004). Mode shifting between storage and recall based on novelty detection in oscillating hippocampal circuits. Hippocampus *14*, 722-741.

Meiri, N., and Rosenblum, K. (1998). Lateral ventricle injection of the protein synthesis inhibitor anisomycin impairs long-term memory in a spatial memory task. Brain research *789*, 48-55.

Mejias, J.F., and Longtin, A. (2012). Optimal heterogeneity for coding in spiking neural networks. Physical review letters *108*, 228102.

Meyers, E.M., Freedman, D.J., Kreiman, G., Miller, E.K., and Poggio, T. (2008). Dynamic population coding of category information in inferior temporal and prefrontal cortex. Journal of neurophysiology *100*, 1407-1419.

Miao, C.L., Cao, Q.C., Ito, H.T., Yamahachi, H., Witter, M.P., Moser, M.B., and Moser, E.I. (2015). Hippocampal Remapping after Partial Inactivation of the Medial Entorhinal Cortex. Neuron *88*, 590-603.

Miao, Q.L., Yao, L., Rasch, M.J., Ye, Q., Li, X., and Zhang, X.H. (2016). Selective Maturation of Temporal Dynamics of Intracortical Excitatory Transmission at the Critical Period Onset. Cell reports *16*, 1677-1689.

Milner, B. (1972). Disorders of learning and memory after temporal lobe lesions in man. Neurosurgery *19*, 421-446.

Mongiat, L.A., Esposito, M.S., Lombardi, G., and Schinder, A.F. (2009). Reliable Activation of Immature Neurons in the Adult Hippocampus. PloS one *4*.

Morris, R.G. (2003). Long-term potentiation and memory. Philosophical Transactions of the Royal Society of London Series B: Biological Sciences *358*, 643-647.

Morris, R.G., and Kopelman, M.D. (1986). The memory deficits in Alzheimer-type dementia: a review. The Quarterly journal of experimental psychology A, Human experimental psychology *38*, 575-602.

Moser, E.I., Kropff, E., and Moser, M.B. (2008). Place cells, grid cells, and the brain's spatial representation system. Annual review of neuroscience *31*, 69-89.

Mukherjee, D., Ignatowska-Jankowska, B.M., Itskovits, E., Gonzales, B., Turm, H., Izakson, L., Haritan, D., Bleistein, N., Cohen, C., Amit, I., *et al*. (2018). Salient experiences are represented by unique transcriptional signatures in the mouse brain. eLife *7*.

Nabavi, S., Fox, R., Proulx, C.D., Lin, J.Y., Tsien, R.Y., and Malinow, R. (2014). Engineering a memory with LTD and LTP. Nature *511*, 348-+.

Nadim, F., and Bucher, D. (2014). Neuromodulation of neurons and synapses. Current opinion in neurobiology *29*, 48-56.

Nairne, J.S., and Pandeirada, J.N. (2016). Adaptive memory: The evolutionary significance of survival processing. Perspectives on Psychological Science *11*, 496-511.

Nakashiba, T., Cushman, J.D., Pelkey, K.A., Renaudineau, S., Buhl, D.L., McHugh, T.J., Rodriguez Barrera, V., Chittajallu, R., Iwamoto, K.S., McBain, C.J., *et al*. (2012). Young dentate granule cells mediate pattern separation, whereas old granule cells facilitate pattern completion. Cell *149*, 188-201.

Nakazawa, K., McHugh, T.J., Wilson, M.A., and Tonegawa, S. (2004). NMDA receptors, place cells and hippocampal spatial memory. Nature reviews Neuroscience *5*, 361-372.

Neunuebel, J.P., and Knierim, J.J. (2012). Spatial firing correlates of physiologically distinct cell types of the rat dentate gyrus. The Journal of neuroscience : the official journal of the Society for Neuroscience *32*, 3848-3858.

Nonaka, A., Toyoda, T., Miura, Y., Hitora-Imamura, N., Naka, M., Eguchi, M., Yamaguchi, S., Ikegaya, Y., Matsuki, N., and Nomura, H. (2014). Synaptic plasticity associated with a memory engram in the basolateral amygdala. The Journal of neuroscience : the official journal of the Society for Neuroscience *34*, 9305-9309.

Okuno, H., and Miyashita, Y. (1996). Expression of the transcription factor Zif268 in the temporal cortex of monkeys during visual paired associate learning. The European journal of neuroscience *8*, 2118-2128.

Olarte-Sánchez, C.M., Amin, E., Warburton, E.C., and Aggleton, J.P. (2015). Perirhinal cortex lesions impair tests of object recognition memory but spare novelty detection. European Journal of Neuroscience *42*, 3117-3127.

Osborne, L.C., Palmer, S.E., Lisberger, S.G., and Bialek, W. (2008). The neural basis for combinatorial coding in a cortical population response. The Journal of neuroscience : the official journal of the Society for Neuroscience *28*, 13522-13531.

Ostergaard, A.L. (1987). Episodic, semantic and procedural memory in a case of amnesia at an early age. Neuropsychologia *25*, 341-357.

Park, S., Kramer, E.E., Mercaldo, V., Rashid, A.J., Insel, N., Frankland, P.W., and Josselyn, S.A. (2016). Neuronal Allocation to a Hippocampal Engram. Neuropsychopharmacology.

Park, S., Park, J.M., Kim, S., Kim, J.A., Shepherd, J.D., Smith-Hicks, C.L., Chowdhury, S., Kaufmann, W., Kuhl, D., Ryazanov, A.G., *et al*. (2008). Elongation factor 2 and fragile X mental retardation protein control the dynamic translation of Arc/Arg3.1 essential for mGluR-LTD. Neuron *59*, 70-83.

Pavlov, P.I. (1926). Conditioned reflexes: An investigation of the physiological activity of the cerebral cortex. Annals of neurosciences *17*, 136-141.

Pearce, J.M. (1994). Similarity and Discrimination - a Selective Review and a Connectionist Model. Psychological review *101*, 587-607.

Pelkey, K.A., Chittajallu, R., Craig, M.T., Tricoire, L., Wester, J.C., and McBain, C.J. (2017). Hippocampal Gabaergic Inhibitory Interneurons. Physiol Rev *97*, 1619-1747.

Penfield, W., and Milner, B. (1958). Memory deficit produced by bilateral lesions in the hippocampal zone. AMA Archives of Neurology & Psychiatry *79*, 475-497.

Penke, Z., Morice, E., Veyrac, A., Gros, A., Chagneau, C., LeBlanc, P., Samson, N., Baumgartel, K., Mansuy, I.M., Davis, S., *et al*. (2014). Zif268/Egr1 gain of function facilitates hippocampal

synaptic plasticity and long-term spatial recognition memory. Philosophical transactions of the Royal Society of London Series B, Biological sciences *369*, 20130159.

Petersen, R.P., Moradpour, F., Eadie, B.D., Shin, J.D., Kannangara, T.S., Delaney, K.R., and Christie, B.R. (2013). Electrophysiological Identification of Medial and Lateral Perforant Path Inputs to the Dentate Gyrus. Neuroscience *252*, 154-168.

Pfeffer, C.K., Xue, M., He, M., Huang, Z.J., and Scanziani, M. (2013). Inhibition of inhibition in visual cortex: the logic of connections between molecularly distinct interneurons. Nature neuroscience *16*, 1068-1076.

Pignatelli, M., Ryan, T.J., Roy, D.S., Lovett, C., Smith, L.M., Muralidhar, S., and Tonegawa, S. (2018). Engram Cell Excitability State Determines the Efficacy of Memory Retrieval. Neuron.

Potter, G.B., Petryniak, M.A., Shevchenko, E., McKinsey, G.L., Ekker, M., and Rubenstein, J.L. (2009). Generation of Cre-transgenic mice using Dlx1/Dlx2 enhancers and their characterization in GABAergic interneurons. Molecular and cellular neurosciences *40*, 167-186.

Poulos, A.M., Mehta, N., Lu, B., Amir, D., Livingston, B., Santarelli, A., Zhuravka, I., and Fanselow, M.S. (2016). Conditioning-and time-dependent increases in context fear and generalization. Learning & memory *23*, 379-385.

Radulovic, J., Blank, T., Nijholt, I., Kammermeier, J., and Spiess, J. (2000). In vivo NMDA/dopamine interaction resulting in Fos production in the limbic system and basal ganglia of the mouse brain. Mol Brain Res *75*, 271-280.

Ramamoorthi, K., Fropf, R., Belfort, G.M., Fitzmaurice, H.L., McKinney, R.M., Neve, R.L., Otto, T., and Lin, Y. (2011). Npas4 regulates a transcriptional program in CA3 required for contextual memory formation. Science *334*, 1669-1675.

Ramaswami, M. (2014). Network plasticity in adaptive filtering and behavioral habituation. Neuron *82*, 1216-1229.

Reijmers, L.G., Perkins, B.L., Matsuo, N., and Mayford, M. (2007). Localization of a stable neural correlate of associative memory. Science *317*, 1230-1233.

Renier, N., Adams, E.L., Kirst, C., Wu, Z.H., Azevedo, R., Kohl, J., Autry, A.E., Kadiri, L., Venkataraju, K.U., Zhou, Y.*, et al*. (2016). Mapping of Brain Activity by Automated Volume Analysis of Immediate Early Genes. Cell *165*, 1789-1802.

Richards, B.A., Lillicrap, T.P., Beaudoin, P., Bengio, Y., Bogacz, R., Christensen, A., Clopath, C., Costa, R.P., de Berker, A., Ganguli, S.*, et al*. (2019). A deep learning framework for neuroscience. Nature neuroscience *22*, 1761-1770.

Richter, F.R., Cooper, R.A., Bays, P.M., and Simons, J.S. (2016). Distinct neural mechanisms underlie the success, precision, and vividness of episodic memory. eLife *5*.

Robinson, M.D., Watkins, E.R., and Harmon-Jones, E. (2013). Handbook of cognition and emotion (Guilford Press).

Roth, B.L. (2016). DREADDs for Neuroscientists. Neuron *89*, 683-694.

Roy, D.S., Arons, A., Mitchell, T.I., Pignatelli, M., Ryan, T.J., and Tonegawa, S. (2016). Memory retrieval by activating engram cells in mouse models of early Alzheimer's disease. Nature *531*, 508-512.

Rozeske, R.R., Jercog, D., Karalis, N., Chaudun, F., Khoder, S., Girard, D., Winke, N., and Herry, C. (2018). Prefrontal-Periaqueductal Gray-Projecting Neurons Mediate Context Fear Discrimination. Neuron *97*, 898-+.

Rubin, R.D., Watson, P.D., Duff, M.C., and Cohen, N.J. (2014). The role of the hippocampus in flexible cognition and social behavior. Front Hum Neurosci *8*, 742.

Rudy, J.W., Huff, N.C., and Matus-Amat, P. (2004). Understanding contextual fear conditioning: insights from a two-process model. Neuroscience and biobehavioral reviews *28*, 675-685.

Ruediger, S., Vittori, C., Bednarek, E., Genoud, C., Strata, P., Sacchetti, B., and Caroni, P. (2011). Learning-related feedforward inhibitory connectivity growth required for memory precision. Nature *473*, 514-518.

Ryan, T.J., Roy, D.S., Pignatelli, M., Arons, A., and Tonegawa, S. (2015). Engram cells retain memory under retrograde amnesia. Science *348*, 1007-1013.

Sadanandappa, M.K., Blanco Redondo, B., Michels, B., Rodrigues, V., Gerber, B., VijayRaghavan, K., Buchner, E., and Ramaswami, M. (2013). Synapsin function in GABA-ergic interneurons is required for short-term olfactory habituation. The Journal of neuroscience : the official journal of the Society for Neuroscience *33*, 16576-16585.

Schafe, G.E., and LeDoux, J.E. (2000). Memory consolidation of auditory pavlovian fear conditioning requires protein synthesis and protein kinase A in the amygdala. Journal of Neuroscience *20*, RC96-RC96.

Scharfman, H.E., and Myers, C.E. (2013). Hilar mossy cells of the dentate gyrus: a historical perspective. Frontiers in neural circuits *6*.

Scoville, W.B., and Milner, B. (1957). Loss of recent memory after bilateral hippocampal lesions. Journal of neurology, neurosurgery, and psychiatry *20*, 11.

Sehgal, M., Song, C., Ehlers, V.L., and Moyer Jr, J.R. (2013). Learning to learn–intrinsic plasticity as a metaplasticity mechanism for memory formation. Neurobiology of learning and memory *105*, 186-199.

Semon, R.W. (1921). The mneme (G. Allen & Unwin Limited).

Senzai, Y., and Buzsaki, G. (2017). Physiological Properties and Behavioral Correlates of Hippocampal Granule Cells and Mossy Cells. Neuron *93*, 691-+.

Shepherd, J.D., and Bear, M.F. (2011). New views of Arc, a master regulator of synaptic plasticity. Nature neuroscience *14*, 279-284.

Shepherd, J.D., Rumbaugh, G., Wu, J., Chowdhury, S., Plath, N., Kuhl, D., Huganir, R.L., and Worley, P.F. (2006). Arc/Arg3.1 mediates homeostatic synaptic scaling of AMPA receptors. Neuron *52*, 475-484.

Sherwood, L. (2015). Human physiology: from cells to systems (Cengage learning).

Simpson, J.N., and Mcginty, J.F. (1994). Forskolin Increases Phosphorylated-Creb and Fos Immunoreactivity in Rat Striatum. Neuroreport *5*, 1213-1216.

Sørensen, A.T., Cooper, Y.A., Baratta, M.V., Weng, F.-J., Zhang, Y., Ramamoorthi, K., Fropf, R., LaVerriere, E., Xue, J., Young, A.*, et al*. (2016). A robust activity marking system for exploring active neuronal ensembles. eLife *5*, e13918.

Souchay, C., and Moulin, C.J. (2009). Memory and consciousness in Alzheimer's disease. Curr Alzheimer Res *6*, 186-195.

Spiegel, I., Mardinly, A.R., Gabel, H.W., Bazinet, J.E., Couch, C.H., Tzeng, C.P., Harmin, D.A., and Greenberg, M.E. (2014). Npas4 regulates excitatory-inhibitory balance within neural circuits through cell-type-specific gene programs. Cell *157*, 1216-1229.

Squire, L.R. (2009a). The legacy of patient HM for neuroscience. Neuron *61*, 6-9.

Squire, L.R. (2009b). Memory and Brain Systems: 1969–2009. The Journal of Neuroscience *29*, 12711-12716.

Squire, L.R., and Zola, S.M. (1998). Episodic memory, semantic memory, and amnesia. Hippocampus *8*, 205-211.

Staddon, J.E.R. (2016). Adaptive behavior and learning (Cambridge University Press).

Stefanelli, T., Bertollini, C., Luscher, C., Muller, D., and Mendez, P. (2016). Hippocampal Somatostatin Interneurons Control the Size of Neuronal Memory Ensembles. Neuron *89*, 1074-1085.

Stone, S.S.D., Teixeira, C.M., Zaslavsky, K., Wheeler, A.L., Martinez-Canabal, A., Wang, A.H., Sakaguchi, M., Lozano, A.M., and Frankland, P.W. (2011). Functional convergence of developmentally and adult-generated granule cells in dentate gyrus circuits supporting hippocampus-dependent memory. Hippocampus *21*, 1348-1362.

Sun, X., Bernstein, M.J., Meng, M., Rao, S., Sørensen, A.T., Yao, L., Zhang, X., Anikeeva, P.O., and Lin, Y. (2020). Functionally Distinct Neuronal Ensembles within the Memory Engram. Cell.

Sun, X., and Lin, Y. (2016). Npas4: Linking Neuronal Activity to Memory. Trends in neurosciences *39*, 264-275.

Suvrathan, A., and Raymond, J.L. (2018). Depressed by Learning—Heterogeneity of the Plasticity Rules at Parallel Fiber Synapses onto Purkinje Cells. The Cerebellum *17*, 747-755.

Tanaka, K.Z., He, H.S., Tomar, A., Niisato, K., Huang, A.J.Y., and McHugh, T.J. (2018). The hippocampal engram maps experience but not place. Science *361*, 392-397.

Tanaka, K.Z., and McHugh, T.J. (2018a). The Hippocampal Engram as a Memory Index. Journal of experimental neuroscience *12*, 1179069518815942.

Tanaka, K.Z., and McHugh, T.J. (2018b). The Hippocampal Engram as a Memory Index. Journal of experimental neuroscience *12*, 1179069518815942.

Tanaka, K.Z., Pevzner, A., Hamidi, A.B., Nakazawa, Y., Graham, J., and Wiltgen, B.J. (2014). Cortical representations are reinstated by the hippocampus during memory retrieval. Neuron *84*, 347-354.

Taniguchi, H., He, M., Wu, P., Kim, S., Paik, R., Sugino, K., Kvitsani, D., Fu, Y., Lu, J., Lin, Y., *et al*. (2011). A Resource of Cre Driver Lines for Genetic Targeting of GABAergic Neurons in Cerebral Cortex. Neuron *71*, 995-1013.

Taniguchi, M., Carreira, M.B., Cooper, Y.A., Bobadilla, A.-C., Heinsbroek, J.A., Koike, N., Larson, E.B., Balmuth, E.A., Hughes, B.W., and Penrod, R.D. (2017). HDAC5 and its target gene, Npas4, function in the nucleus accumbens to regulate cocaine-conditioned behaviors. Neuron *96*, 130-144. e136.

Temme, S.J., Bell, R.Z., Pahumi, R., and Murphy, G.G. (2014). Comparison of inbred mouse substrains reveals segregation of maladaptive fear phenotypes. Frontiers in behavioral neuroscience *8*, 282.

Thompson, R.F. (1986). The neurobiology of learning and memory. Science *233*, 941-947.

Thompson, R.F. (2005). In search of memory traces. Annual review of psychology *56*, 1-23.

Tonegawa, S., Liu, X., Ramirez, S., and Redondo, R. (2015a). Memory Engram Cells Have Come of Age. Neuron *87*, 918-931.

Tonegawa, S., Pignatelli, M., Roy, D.S., and Ryan, T.J. (2015b). Memory engram storage and retrieval. Current opinion in neurobiology *35*, 101-109.

Treves, A., and Rolls, E.T. (1994). Computational Analysis of the Role of the Hippocampus in Memory. Hippocampus *4*, 374-391.

Tsou, K., Mackie, K., Sanudo-Pena, M.C., and Walker, J.M. (1999). Cannabinoid CB1 receptors are localized primarily on cholecystokinin-containing gabaergic interneurons in the rat hippocampal formation. Neuroscience *93*, 969-975.

Tulving, E. (1985). Memory and consciousness. Canadian Psychology/Psychologie canadienne *26*, 1-12.

Turi, G.F., Li, W.-K., Chavlis, S., Pandi, I., O'Hare, J., Priestley, J.B., Grosmark, A.D., Liao, Z., Ladow, M., Zhang, J.F., *et al*. (2019). Vasoactive Intestinal Polypeptide-Expressing Interneurons in the Hippocampus Support Goal-Oriented Spatial Learning. Neuron *101*, 1150-1165.e1158.

Turrigiano, G.G., and Nelson, S.B. (2004). Homeostatic plasticity in the developing nervous system. Nature reviews Neuroscience *5*, 97-107.

Tyssowski, K.M., DeStefino, N.R., Cho, J.H., Dunn, C.J., Poston, R.G., Carty, C.E., Jones, R.D., Chang, S.M., Romeo, P., Wurzelmann, M.K., *et al*. (2018). Different Neuronal Activity Patterns Induce Different Gene Expression Programs. Neuron *98*, 530-546 e511.

van Dijk, M.T., and Fenton, A.A. (2018). On How the Dentate Gyrus Contributes to Memory Discrimination. Neuron *98*, 832-+.

Vetere, G., Kenney, J.W., Tran, L.M., Xia, F., Steadman, P.E., Parkinson, J., Josselyn, S.A., and Frankland, P.W. (2017). Chemogenetic Interrogation of a Brain-wide Fear Memory Network in Mice. Neuron *94*, 363-374.e364.

Vogels, T.P., Sprekeler, H., Zenke, F., Clopath, C., and Gerstner, W. (2011). Inhibitory Plasticity Balances Excitation and Inhibition in Sensory Pathways and Memory Networks. Science *334*, 1569-1573.

Wang, K.H., Majewska, A., Schummers, J., Farley, B., Hu, C., Sur, M., and Tonegawa, S. (2006). In vivo two-photon imaging reveals a role of arc in enhancing orientation specificity in visual cortex. Cell *126*, 389-402.

Warburton, E.C., and Brown, M.W. (2015). Neural circuitry for rat recognition memory. Behavioural brain research *285*, 131-139.

Waung, M.W., Pfeiffer, B.E., Nosyreva, E.D., Ronesi, J.A., and Huber, K.M. (2008). Rapid translation of Arc/Arg3.1 selectively mediates mGluR-dependent LTD through persistent increases in AMPAR endocytosis rate. Neuron *59*, 84-97.

Weng, F.-J., Garcia, R.I., Lutzu, S., Alviña, K., Zhang, Y., Dushko, M., Ku, T., Zemoura, K., Rich, D., Garcia-Dominguez, D., *et al*. (2018). Npas4 Is a Critical Regulator of Learning-Induced Plasticity at Mossy Fiber-CA3 Synapses during Contextual Memory Formation. Neuron *97*, 1137-1152.e1135.

Whitlock, J.R., Heynen, A.J., Shuler, M.G., and Bear, M.F. (2006). Learning induces long-term potentiation in the hippocampus. Science *313*, 1093-1097.

Wilson, D.I.G., Watanabe, S., Milner, H., and Ainge, J.A. (2013). Lateral entorhinal cortex is necessary for associative but not nonassociative recognition memory. Hippocampus *23*, 1280-1290.

Wiltgen, B.J., and Silva, A.J. (2007). Memory for context becomes less specific with time. Learning & memory *14*, 313-317.

Witter, M.P. (2007). The perforant path: projections from the entorhinal cortex to the dentate gyrus. Prog Brain Res *163*, 43-61.

Xie, H., Liu, Y., Zhu, Y.Z., Ding, X.L., Yang, Y.H., and Guan, J.S. (2014). In vivo imaging of immediate early gene expression reveals layer-specific memory traces in the mammalian brain. Proceedings of the National Academy of Sciences of the United States of America *111*, 2788-2793.

Xu, W., and Sudhof, T.C. (2013). A neural circuit for memory specificity and generalization. Science *339*, 1290-1295.

Xue, M., Atallah, B.V., and Scanziani, M. (2014a). Equalizing excitation-inhibition ratios across visual cortical neurons. Nature *511*, 596-600.

Xue, M.S., Atallah, B.V., and Scanziani, M. (2014b). Equalizing excitation-inhibition ratios across visual cortical neurons. Nature *511*, 596-+.

Yiu, A.P., Mercaldo, V., Yan, C., Richards, B., Rashid, A.J., Hsiang, H.L., Pressey, J., Mahadevan, V., Tran, M.M., Kushner, S.A., *et al*. (2014). Neurons are recruited to a memory trace based on relative neuronal excitability immediately before training. Neuron *83*, 722-735.

Yokose, J., Okubo-Suzuki, R., Nomoto, M., Ohkawa, N., Nishizono, H., Suzuki, A., Matsuo, M., Tsujimura, S., Takahashi, Y., Nagase, M., *et al*. (2017). Overlapping memory trace indispensable for linking, but not recalling, individual memories. Science *355*, 398-403.

Yun, J., Koike, H., Ibi, D., Toth, E., Mizoguchi, H., Nitta, A., Yoneyama, M., Ogita, K., Yoneda, Y., Nabeshima, T., *et al*. (2010). Chronic restraint stress impairs neurogenesis and hippocampus-dependent fear memory in mice: possible involvement of a brain-specific transcription factor Npas4. Journal of neurochemistry *114*, 1840-1851.

Zhao, R., Grunke, S.D., Keralapurath, M.M., Yetman, M.J., Lam, A., Lee, T.C., Sousounis, K., Jiang, Y.Y., Swing, D.A., Tessarollo, L., *et al*. (2016). Impaired Recall of Positional Memory following Chemogenetic Disruption of Place Field Stability. Cell reports *16*, 793-804.

Zhou, Y., Won, J., Karlsson, M.G., Zhou, M., Rogerson, T., Balaji, J., Neve, R., Poirazi, P., and Silva, A.J. (2009). CREB regulates excitability and the allocation of memory to subsets of neurons in the amygdala. Nature neuroscience *12*, 1438-1443.

Zhou, Y., Zhu, H., Liu, Z., Chen, X., Su, X., Ma, C., Tian, Z., Huang, B., Yan, E., Liu, X., *et al*. (2019). A ventral CA1 to nucleus accumbens core engram circuit mediates conditioned place preference for cocaine. Nature neuroscience *22*, 1986-1999.

* Part of this article (Chapter 2&3) is published in Sun, X., Bernstein, M.J., Meng, M., Rao, S., Sørensen, A.T., Yao, L., Zhang, X., Anikeeva, P.O., and Lin, Y. (2020). Functionally Distinct Neuronal Ensembles within the Memory Engram. Cell.